

**A Bubble-Particle Interaction Model for Flotation
Combining Hydrodynamic and Surface Forces**

by

Brian Keith Schimmoller


Thesis submitted to the Faculty of the
Virginia Polytechnic Institute and State University
in partial fulfillment of the requirements for the degree of

Master of Science


in

Mining and Minerals Engineering

APPROVED:



G.H. Luttrell, Chairman



R.-H. Yoon



G.T. Adel

May, 1992

Blacksburg, Virginia

C.2

LD

5655

V855

1992

S335

C.2

A Bubble-Particle Interaction Model for Flotation Combining Hydrodynamic and Surface Forces

by

Brian Keith Schimmoller

Committee Chairman: Dr. G.H. Luttrell
Mining and Minerals Engineering

(ABSTRACT)

It is generally recognized that the recovery of particles from a flotation pulp is controlled by (i) the flotation rate constant and (ii) the residence time distribution of the particles. In the present work, theoretical and experimental analyses have been carried out to develop methods for predicting these parameters from first principles considerations.

In order to predict the flotation rate constant, a bubble-particle interaction model has been developed using a dynamic force balance to determine the trajectory of a particle as it approaches a rising air bubble. The trajectory has been used to determine the probability of bubble-particle attachment, from which the flotation rate constant can be readily obtained. The model is unique in that it simultaneously considers the effects of hydrodynamic and surface forces on the interaction between bubbles and particles. Model predictions have been shown to be in good agreement with results from bubble-particle attachment experiments for narrowly-sized coal and silica samples.

In the present work, the residence time distribution of particles in column

flotation has been examined by conducting experimental tracer tests. These tests have been performed with two tracer materials to characterize mixing for both the liquid and the solids in a single system. The measured residence time distributions have shown that the assumption of equating liquid and solids residence time distributions is inappropriate, except for very small and low density particles. At larger sizes and higher densities, the correction formula advocated by Dobby and Finch (1985) has been shown to adequately predict the solids residence time.

ACKNOWLEDGEMENTS

Numerous people have made this effort possible. First of all, the author would like to thank his advisor, Dr. Gerald H. Luttrell, whose enthusiasm and knowledge fueled this research from the beginning. Deepest appreciation also goes to the other members of the committee, Dr. Roe-Hoan Yoon and Dr. Gregory T. Adel, for their confidence, guidance, and inspiration during the course of the work. Sincere gratitude is expressed to Dr. Michael J. Mankosa for his help with the tracer tests and mixing studies.

More than a few words of thanks are reserved for everyone at the 'Road' - past and present, upstairs and downstairs - for their friendship, assistance, and encouragement over the past two years. Without their presence, both this research and my sanity would have suffered. The author would like to acknowledge his fellow graduate students at Holden Hall as well, who were always armed with a helpful suggestion and a welcome smile during my frequent visits.

My family also deserves special recognition, for their continued role in fostering my academic development and career preparation. Finally, dearest thanks are given to my fiancée, Debbie, for her unwavering faith, support, and love - we made it, Deb.

TABLE OF CONTENTS

Chapter 1 Introduction	1
1.1 General	1
1.2 Literature Review	7
1.3 Research Objectives	9
1.4 Report Organization	11
1.5 References	13
Chapter 2 Bubble-Particle Interaction Model	15
2.1 Introduction	15
2.2 Literature Review	16
2.3 Research Objectives	27
2.4 Model Development	28
2.4.1 Hydrodynamics	31
2.4.2 Surface Forces	39
2.4.3 Force Balance	44
2.5 Simulation Results	49
2.5.1 Model Validity	49
2.5.2 Effect of Model Parameters	54
a) Effect of Particle Size	54

b) Effect of Bubble Size	56
c) Effect of Particle Density	58
d) Effect of Particle Charge	58
e) Effect of Structural Constant	60
2.6 Experimental	65
2.6.1 Samples	65
2.6.2 Reagents	65
2.6.3 Procedure	66
2.6.4 Calculation of Probability of Collection	69
2.6.5 Experimental Results and Comparison with Model Predictions	71
2.6.6 Regions of Flotation	81
2.7 Conclusions	83
2.8 References	86
 Chapter 3 Mixing Characterization	 92
3.1 Introduction	92
3.2 Literature Review	93
3.3 Research Objectives	97
3.4 Experimental	98
3.4.1 Samples	98
3.4.2 Reagents	98

3.4.3 Equipment	99
3.4.4 Procedure	101
3.5 Data Analysis	102
3.6 Results and Discussion	105
3.7 Flotation Performance	114
3.8 Conclusions	123
3.9 References	125
Chapter 4 Conclusions	128
Chapter 5 Recommendations for Future Work	132
APPENDIX I	136
VITA	144

LIST OF FIGURES

	Page
Figure 2.1 Coordinate system used to characterize bubble-particle interaction	30
Figure 2.2 Schematic of hydrodynamic and surface forces involved in bubble-particle interaction	32
Figure 2.3 Relationship between the film thinning resistance factor, β , and dimensionless distance, h/r_p	38
Figure 2.4 Simulation results for various force combinations	52
Figure 2.5 Simulation results illustrating the effect of particle size on bubble-particle interaction	55
Figure 2.6 Simulation results illustrating the effect of bubble size on bubble-particle interaction	57
Figure 2.7 Simulation results illustrating the effect of particle density on bubble-particle interaction	59
Figure 2.8 Simulation results illustrating the effect of particle zeta potential on bubble-particle interaction for $C = -1.8 \text{ mJ/m}^2$	61
Figure 2.9 Simulation results illustrating the effect of particle zeta potential on bubble-particle interaction for $C = -1.0 \text{ mJ/m}^2$	62
Figure 2.10 Simulation results illustrating the effect of the structural constant on bubble-particle interaction	64
Figure 2.11 Schematic of apparatus used for bubble-particle attachment experiments	67
Figure 2.12 Simulation results for 100 x 150 mesh coal sample used in bubble-particle attachment experiments	75

Figure 2.13	Simulation results for 200 x 270 mesh coal sample used in bubble-particle attachment experiments	76
Figure 2.14	Simulation results for 250 x 270 mesh silica sample used in bubble-particle attachment experiments	78
Figure 2.15	Simulation results for 325 x 400 mesh silica sample used in bubble-particle attachment experiments	79
Figure 2.16	Comparison between experimental and theoretical values for the probability of particle collection	80
Figure 2.17	Contour plot of equilibrium film thickness showing viable regions of flotation as a function of the structural constant and the particle zeta potential	82
Figure 3.1	Schematic of experimental apparatus used for determining solid and liquid residence time distributions in a flotation column . . .	100
Figure 3.2	Liquid residence time distribution as constructed from time-stamped conductivity values	103
Figure 3.3	Solids residence time distribution for 48 x 65 mesh silica size fraction from tailings discharge sample collection weights	104
Figure 3.4	Normalized liquid and solid residence time distributions for 48 x 65 mesh coal sample	106
Figure 3.5	Normalized liquid and solid residence time distributions for 48 x 65 mesh silica sample	107
Figure 3.6	Normalized liquid and solid residence time distributions for 250 x 270 mesh coal sample	109
Figure 3.7	Normalized liquid and solid residence time distributions for 250 x 270 mesh silica sample	110
Figure 3.8	Relationship between Peclet number and particle size for coal and silica samples	111

Figure 3.9 Relationship between residence time and particle size for coal and silica samples 113

Figure 3.10 Comparison between experimental and theoretical solids residence time for silica 115

Figure 3.11 Comparison between experimental and theoretical solids residence time for coal 116

Figure 3.12 Relationship between recovery and $k\tau$ as a function of the mixing conditions 121

LIST OF TABLES

	Page
Table 1.1 Land use in the United States in 1980 (Cameron, 1980)	4
Table 2.1 Values of P_c as calculated from various equations for a $10\ \mu\text{m}$ particle and $300\ \mu\text{m}$ bubble	21
Table 2.2 Dimensionless stream function as a function of flow conditions . . .	35
Table 2.3 Results of bubble-particle attachment experiments	72
Table 2.4 Material characteristics of coal and silica samples used in bubble-particle attachment experiments	74

LIST OF SYMBOLS

- a - Constant
- a - Particle acceleration
- A - Constant
- A_{11} - Hamaker constant of bubble
- A_{22} - Hamaker constant of particle
- A_{33} - Hamaker constant of water
- A_{132} - Composite Hamaker constant
- B_1, B_2 - Constant expressions used in calculation of F_e
- c - Particle concentration
- C - Structural constant
- C - Tracer concentration
- D_b - Bubble diameter
- D_c - Cell diameter
- d_p - Particle diameter
- D_0 - Decay length
- E - Energy barrier
- E - Liquid axial dispersion coefficient
- f - Retardation factor
- F_b - Buoyancy force
- F_d - Dispersion force

- F_e - Electrostatic force
- F_g - Gravitational force
- F_{gb} - Gravitational and buoyancy forces expressed as a single term
- F_p - Streamline pressing force
- F_r - Film thinning resistance force
- F_s - Structural force
- F_t - Total bubble-particle interaction force
- F_t^{rad} - Total bubble-particle interaction force in radial direction
- F_t^{tan} - Total bubble-particle interaction force in tangential direction
- g - Acceleration due to gravity
- h - Film thickness between bubble and particle
- h_c - Critical film thickness
- k - Boltzmann's constant
- k - Flotation rate constant
- l - Recovery zone length
- L - Cell length
- l' - Effective recovery zone length
- m - Particle mass
- m - Constant
- n - Constant
- N_b - Number of bubbles

- N_p - Number of particles
- $N_{p/b}$ - Number of particles collected per bubble
- p - Parameter for calculating retardation factor
- P - Probability of particle collection by a bubble
- P_a - Probability of bubble-particle adhesion
- P_c - Probability of bubble-particle collision
- P_d - Probability of bubble-particle detachment
- P_g - Probability of gravitational collision
- P_i - Probability of interceptional collision
- P_{exp} - Experimental probability of particle collection by a bubble
- P_{th} - Theoretical probability of particle collection by a bubble
- Pe - Peclet number
- Pe_l - Peclet number of the liquid
- Pe_s - Peclet number of the solids
- Q - Volumetric air flow rate
- r_p - Particle radius
- R - Recovery
- R - Radial distance between bubble and particle centers
- R_b - Bubble radius
- R_c - Critical starting distance from bubble centerline
- R_0 - Initial particle starting distance from bubble centerline

R_{new} - New radial position of particle
 R_{old} - Old radial position of particle
 Re - Reynolds number
 t - Time
 t' - Effective bubble rise time
 T - Absolute temperature
 u_i - Interstitial liquid velocity
 u_s - Particle settling velocity
 u_{sp} - Particle settling velocity corrected for volume percent solids
 U_b - Bubble rise velocity
 U_b' - Effective bubble rise velocity
 U_i - Streamline velocity in i^{th} direction
 U_{ip} - Particle velocity in i^{th} direction
 U_r - Streamline velocity in radial direction
 U_t - Streamline velocity in tangential direction
 U_{rp} - Particle velocity in radial direction
 U_{tp} - Particle velocity in tangential direction
 V_b - Volume of bubble
 V_c - Cell volume
 V_g - Superficial gas velocity
 V_l - Liquid flow velocity

- x - Distance along cell length
- X - R/R_b
- β - Film thinning resistance factor
- ϵ - Dielectric constant
- ϵ - Air hold-up
- κ - Debye reciprocal length
- λ - Parameter for calculating retardation factor
- ϕ - Volume percent solids
- ρ_f - Fluid density
- ρ_p - Particle density
- Ψ - Stream function
- ψ_b - Surface potential of bubble
- ψ_p - Surface potential of particle
- τ - Mean residence time
- τ_c - Contact time
- τ_i - Induction time
- τ_l - Liquid residence time
- τ_s - Solids residence time
- θ - Angle between bubble centerline and particle
- θ_c - Closest streamline approach angle
- θ_n - Maximum angle of contact

θ_{new} - New angle between bubble centerline and particle

θ_{old} - Old angle between bubble centerline and particle

ζ_{b} - Zeta potential of bubble

ζ_{p} - Zeta potential of particle

Chapter 1 Introduction

1.1 General

Froth flotation is a physico-chemical separation process extensively used today in a wide variety of processing plants around the world. Its success is founded in the selective chemical pretreatment of the feed material to a flotation cell, which renders a certain portion of the feedstock hydrophobic (water-hating), leaving the remaining portion hydrophilic (water-loving). The particles which have become hydrophobic are then able to attach to buoyant air bubbles and "float" away from the hydrophilic particles in suspension. The particle-laden bubbles are collected from the top of the cell as product, and the hydrophilic particles are discarded as tailings.

The first known applications of froth flotation were in the early 1900's for the processing of zinc ores (Hoover, 1912). Previous technologies, namely bulk-oil flotation and skin flotation, had also taken advantage of the hydrophobic/hydrophilic nature of certain materials. Bulk-oil flotation, however, suffered from excessive oil consumption, and skin flotation was confined to the treatment of coarse particles. It was not until the first decade of the 20th century that investigators discovered the benefits associated with utilizing rising air bubbles as the transport media for hydrophobic particles (Froment, 1902; Sulman and Picard, 1903; Sulman, Picard,

and Ballot, 1905). Required oil dosages were reduced, and a wider size range of material was able to be processed effectively.

Immediate widespread use of froth flotation was hampered by its restricted applicability. Only a few systems existed where the mating of oil and air with the feed material effected an efficient separation. Many other systems did not respond favorably to oil treatment, with the valuable component remaining hydrophilic, precluding flotation. Beginning in the 1920's, however, researchers began to develop chemicals specifically designed to render substances hydrophobic. These surface active reagents, called collectors, revolutionized the flotation industry. The high performance, high throughput advantages of froth flotation could now be applied to any number of systems.

Industrial flotation installations can now be found virtually everywhere, processing a vast array of materials: coal, graphite, kaolin clays, phosphate, potash, copper, molybdenum, lead, zinc, lithium, feldspar, mica, tin, tungsten, titanium, vermiculite, sericite, gold, silver, lanthanides, barite, antimony, etc. (Engineering and Mining Journal International Directory of Mining, 1991; Ives, 1982). This tremendous diversity is a revealing indication of the versatility froth flotation offers the processing community. With the continued depletion of high grade ores, and the scientific advances into the fundamentals governing flotation, it is no wonder froth flotation has attained such a prominent position in the minerals industry. In fact, it is estimated that over two billion tons of ore, representing over one hundred different

minerals, are processed annually by flotation worldwide (Schulze, 1983). In the United States alone, four to five hundred million tons of ore and raw coal are subjected to flotation each year (Mineral Industry Survey, 1987).

Froth flotation technology has also come to the forefront because of recent environmental concerns. Despite the fact that mining ventures occupy but a small fraction of the total United States land mass (Table 1.1), less than 1%, powerful environmental lobbies have formed to voice their opposition to what they consider an evil, destructive entity. Permitting has become more difficult than the actual mining and processing, and legislation has threatened to cripple certain mining districts. The Clean Air Act severely restricts industrial emissions of various forms of pollution, including sulfur compounds, nitrogen compounds, and particulate matter. Emission reduction is a complex problem with many potential solutions, one of which is the production of cleaner burning fuels. For coal-powered plants, froth flotation, and column flotation in particular, can be used for this purpose.

Column flotation, developed in Canada in the 1960's, is markedly different from conventional cell flotation. The basic premise is the same, but the flotation environment has been radically restructured. The flow is no longer cocurrent, but countercurrent, with a rising stream of bubbles contacting a settling flow of feed particles. The hydrophobic particles attach to the air bubbles and are carried to a froth layer, while the hydrophilic particles remain in suspension and exit the bottom of the column as tailings. The unique feature of flotation columns is in the treatment

Table 1.1 Land Use in the United States, 1980 (Cameron, 1986)

Land Use	Millions of Acres
Agriculture	1589.0
Wildlife refuge system	88.7
National Park system	77.0
Urban and built-up areas	68.7
Forest Service wilderness	25.1
Highways	21.5
Mining	5.7
Airports	4.0
Railroads	3.0
Other	388.1
Total	2270.8

of the froth. A wash water spray is positioned in the froth zone to wash hydraulically entrained particles back into the pulp. This cleaning action results in an improved product grade as compared to conventional flotation.

Column flotation is gaining increased popularity in industry. Advantages over conventional flotation include reduced floor space requirements, fewer moving parts, higher throughput per unit, improved efficiency (single-pass cleaning), and lower operating costs (Moon, 1982). Coupled with fine bubble generators, flotation columns are also extremely effective at recovering fine particles from a given circuit. For fine coal flotation, columns can produce a superclean product by rejecting the liberated mineral matter through the use of the wash water addition (Yoon et al., 1989).

Although columns are mechanically simpler than conventional cells, they are still subject to the same elementary principles governing flotation. Bubble-particle attachment is required, followed by transfer into the froth zone, and subsequent removal from the overflow lip as product. The differences between columns and conventional cells are design, operating, and performance considerations; improved fundamental understanding of flotation would be beneficial to *both* types of units.

Flotation, in and of itself, is quite complicated. Numerous physical and chemical variables are known to impact the success of a given flotation application. Traditionally, obtaining the optimum operating conditions has been a nonscientific procedure, relying on trial and error. Gradually, however, processing engineers have

come to realize that fundamental understanding of the flotation process will lead to more effective control schemes. This, in turn, will equate with better flotation performance, and a more successful mining operation.

The basic step in flotation - the attachment of a hydrophobic particle to an air bubble - has been the focus of numerous researcher investigations for the past fifty years. Important discoveries have been made, but many uncertainties still exist. Accurate characterization of bubble-particle attachment, both qualitatively and quantitatively, remains essential for the development of a comprehensive theoretical flotation model. Such a model, relating flotation performance to its fundamental constituents, would be invaluable to the processing engineer. Alternate circuit designs could be tested, optimum conditions readily defined, and effective control strategies easily implemented.

In the past, too many operations simply applied historical flotation principles with little regard for the actual mechanisms involved and the changing physical and chemical characteristics of the material being treated. This indifference resulted in stagnation; reliance on dated technology and limited understanding allowed continued operation, but with no substantial improvement. Today, this trend is quickly turning the other way. Research is being coupled with industry to forge a symbiotic relationship. One of the primary duties of research in this partnership is the development of fundamental models to fully describe a given process. Flotation modeling, and the modeling of bubble-particle attachment in particular, is the subject

of the present work.

1.2 Literature Review

In flotation applications, the operational goal is commonly the attainment of maximum recovery at an acceptable grade. The determination of the most appropriate strategy for achieving a high recovery is often difficult because of the numerous variables which are known to impact flotation performance. Three parameters are consistently cited as playing key roles in assessing recovery. These are the flotation rate constant, k , the residence time, τ , and the Peclet number, Pe , which characterizes the degree of axial mixing in a flotation cell. Levenspiel (1972) has incorporated these variables into a general expression for calculating recovery, R , in an axially dispersed system:

$$R = 1 - \frac{4a \exp\left(\frac{Pe}{2}\right)}{(1+a)^2 \exp\left[\left(\frac{a}{2}\right)Pe\right] - (1-a)^2 \exp\left[\left(\frac{-a}{2}\right)Pe\right]} \quad [1.1]$$

where:

$$a = \sqrt{1 + \frac{4k\tau}{Pe}} \quad [1.2]$$

Equation [1.1] represents the recovery for a flotation column operating under mixing conditions intermediate between perfectly-mixed ($Pe = 0$) and plug-flow ($Pe = \infty$).

The rate constant defines the rate at which flotation occurs. It is dependent on both the material properties and the flotation cell conditions. Luttrell et al. (1988) have shown that k can be expressed as:

$$k = \frac{3P}{2D_b} V_g \quad [1.3]$$

where P is the probability of particle capture, D_b is the bubble diameter, and V_g is the superficial gas velocity. The latter two factors are determined by the operating conditions. The probability of particle capture, on the other hand, is a complicated function of numerous variables related to the system hydrodynamics and surface chemistry (Yoon, 1991). P is often considered to consist of three independent probabilistic values, as indicated by the following equation (Sutherland, 1948):

$$P = P_c P_a (1 - P_d) \quad [1.4]$$

where P_c is the probability of bubble-particle collision, P_a is the probability of adhesion, and P_d is the probability of detachment. Extensive research has been conducted into these separate subprocesses and their effects on P . Several equations for P_c , P_a , and P_d have been proposed, relating to various physical and chemical parameters. Which of these equations are the correct ones, if any, remains unknown.

The residence time and Peclet number, characterizing the mixing in a flotation unit, are also known to impact recovery. The residence time indicates how long solid particles are present in the cell, engaged in bubble-particle interactions. Therefore,

this parameter places constraints on the physical size of the flotation cell, providing a basis for scale-up. Commonly, engineers have simply relied on the liquid residence time for predictions and scale-up, ignoring the possibility that the solids may exhibit a shorter residence time because of their finite weight. Dobby and Finch (1985) have proposed a correction equation for the solids residence time, τ_s , as a function of the liquid residence time, τ_l :

$$\tau_s = \tau_l \left[\frac{u_l}{u_l + u_s} \right] \quad [1.5]$$

where u_l is the interstitial liquid velocity and u_s is the particle settling velocity. This equation has not been validated experimentally, however.

The Peclet number, Pe , defines the degree of axial mixing in a reactor. A low value of Pe indicates well-mixed conditions, while a high Pe corresponds to plug-flow conditions. Several investigators (Rice et al., 1974; Dobby and Finch, 1985; Kho and Sohn, 1989) have demonstrated the equality of the solid and liquid Peclet numbers for fine particles. The validity of this equality is questionable at larger particle sizes and densities, however. Also, Mankosa (1990) has utilized a dimensionless analysis to develop an expression for the Peclet number in terms of the column geometry and operating conditions. Unfortunately, the equation was derived from liquid residence time distributions, and may not be applicable to the solids in a flotation system.

1.3 Research Objectives

The primary objective of the present work is the development of a flotation model, founded on first principles, which can predict recovery for a given set of conditions. Historically, this has been a difficult task, due to limited understanding of the numerous subprocesses involved in flotation. The present work addresses this problem by analyzing flotation behavior outside of the framework imposed by these subprocesses. The bubble-particle interaction is examined as a single entity by concentrating simply on the motion of a particle around a bubble.

Flotation performance is most commonly assessed in terms of the recovery, R , of a certain mineral or component. As shown in Equation [1.1], recovery is a function of three main variables, i.e., k , τ , and Pe . Despite the extensive amount of literature related to these parameters, they are still not completely understood. The probability of particle collection, P , used to determine k , demands more attention, particularly by considering *all* of the forces known to affect the capture mechanism. The mixing parameters also deserve additional research. The validity of the equations describing τ and Pe need further validation over a wider particle size range.

The present investigation has been divided into two main parts. In the first section, the rate constant for flotation will be studied indirectly by conducting a fundamental analysis of bubble-particle interaction. A dynamic force-balance will be utilized that incorporates both hydrodynamic and surface forces into a bubble-particle

interaction model. The probability of particle collection obtained with this model will provide information from which the first-order rate constant for flotation can be determined. Also, bubble-particle attachment tests will be performed and compared to model predictions in order to assess the validity of the model.

The second section of this report will be concerned with characterization of the mixing in a flotation column. Solid and liquid residence time distributions will be acquired from tracer tests for two different materials as a function of particle size. The degree of axial mixing and residence time can then be determined for both the liquid and the solids. The results will allow conclusions to be drawn concerning the relationship between the liquid and solid mixing parameters. This is important because scale-up criteria and operating conditions will be erroneous if improper values are employed.

Finally, the results of these two sections will be considered in light of their impact on recovery, as alluded to in Equation [1.1].

1.4 Report Organization

Because of the relatively independent nature of each of the topics in this report, they will be presented as separate, stand-alone chapters. The formats, though not identical, share a similar skeleton. Each chapter consists of an introduction, a literature review, an experimental section, results and discussion, and conclusions.

Chapter 2 focuses on the development of the bubble-particle interaction

model. The structure of the model is described in detail, and sample computer simulations are discussed. The effects of various physical and chemical variables on the probability of particle collection are theoretically evaluated with the model and compared to literature results. Experimentally determined values for the probability of collection are shown to correlate well with model predictions. From the model results, favorable regions of flotation are identified as a function of various variables.

Chapter 3 deals with mixing characterization, in terms of the Peclet number and the residence time. Mixing parameters for both the liquid and the solids in a flotation column are found by using different tracers concurrently: a potassium chloride solution for the liquid, and a hydrophilic size fraction for the solids. The resulting residence time distributions provide important information concerning the equality of liquid and solid mixing parameters.

Chapter 3 also outlines the procedure that would be used to construct an overall flotation model. The results of the mixing studies are integrated with the bubble-particle interaction model developed in chapter 2 to provide a method for estimating flotation recovery. Such a model, founded on the first principles discussed in chapter 2, would be particularly beneficial for performance predictions, control purposes, scale-up, and optimization.

1.5 References

- Cameron, E.N., 1986, *At the Crossroads: The Mineral Problems of the United States*, John Wiley and Sons, New York, N.Y.
- Dobby, G.S., and Finch, J.A., "Mixing Characterization of Industrial Flotation Columns," *Chemical Engineering Science*, Volume 40, Number 7, p. 1061.
- E & MJ International Directory of Mining*, 1991, Maclean Hunter Publishing Co., Chicago, IL.
- Hoover, T.J., 1912, "Concentrating Ores by Flotation," *Mining Magazine*, London.
- Froment, 1902
 - Sulman and Picard, 1903
 - Sulman, Picard, and Ballot, 1905
- Kho, C.J., and Sohn, H.J., "Column Flotation of Talc," *International Journal of Mineral Processing*, Volume 27, p. 157.
- Kitchener, J.A., 1984, "The Froth Flotation Process: Past, Present, and Future - In Brief," in *The Scientific Basis of Flotation*, K.J. Ives, editor, Martinus Nijhoff Publishers, Boston, MA, p. 3.
- Levenspiel, O., 1972, *Chemical Reaction Engineering*, John Wiley & Sons, Inc., New York, N.Y.
- Luttrell, G.H., Adel, G.T., and Yoon, R.-H., 1988, "Hydrodynamics and Mathematical Modeling of Fine Coal Flotation," *Proceedings, XVI International Mineral Processing Congress*, E. Forssberg, editor, Elsevier, Amsterdam, p. 1791.
- Mankosa, M.J., Adel, G.T., Luttrell, G.H., and Yoon, R.-H., 1987, "Model-Based Design of Column Flotation," *Proceedings, The Mathematical Modeling of Metals Processing Operations, Extractive and Process Metallurgy Fall Meeting, AIME*, New York, p. 219.
- Mankosa, M.J., 1990, *Ph.D. Dissertation*, Virginia Polytechnic Institute and State University, Blacksburg, VA.
- Mineral Industry Survey, 1987, "Froth Flotation in the United States, 1985," U.S. Department of the Interior, Bureau of Mines, Washington, D.C.

Moon, K.S., 1982, *Counter Current Column Flotation Machine*, Project ERP-4.3.03.02, Energy Research Program, Mineral Sciences Laboratories, CANMET, Ottawa.

Rice, R.G., Oliver, A.D., Newman, J.P., and Wiles, R.J., 1974, "Reduced Dispersion Using Baffles in Column Flotation," *Powder Technology*, Volume 10, p. 201.

Schulze, H.J., 1983, *Physico-chemical Elementary Processes in Flotation*, Elsevier, New York, N.Y.

Sutherland, K.L., 1948, "Physical Chemistry of flotation XI. Kinetics of the Flotation Process," *Journal of Physical Chemistry*, Volume 52, p. 394.

Yoon, R.-H., "Hydrodynamic and Surface Forces in Bubble-Particle Interactions," *Aufbereitungs Technik*, Volume 32, Number 9, p. 474.

Yoon, R.-H., Luttrell, G.H., Adel, G.T., and Mankosa, M.J., 1989, "Recent Advances in Fine Coal Flotation," in *Advances in Coal and Mineral Processing Using Flotation*, S. Chander and R.R. Klimpel, editors, SME, Inc., Littleton, CO.

Chapter 2 Bubble-Particle Interaction Model

2.1 Introduction

The ultimate aim of process modeling is the development of fundamental models for the accurate prediction of a given system's response to input conditions. Achievement of this goal has been particularly difficult for froth flotation because of the various subprocesses involved. Integrating bubble-particle attachment, bubble-particle detachment, froth transfer, froth dropback, etc., into a contiguous whole is a complicated matter. Considerable research has been conducted into these phenomena, but until each of these subprocesses is fully understood, a comprehensive phenomenological model for flotation will remain unattainable.

Perhaps the most important of the subprocesses in flotation is the attachment of particle to bubble. Beginning with Sutherland's work in 1948, numerous investigators have attempted to quantify this event. Their efforts, though providing increased insight into bubble-particle interaction, have failed to produce a unified process model. Therefore, it may be necessary to approach bubble-particle interaction from an alternate vantage point in order to formulate a fundamental model capable of accurate flotation performance prediction.

2.2 Literature Review

The modeling of flotation has had a relatively brief, but eventful history. Early research (Gaudin, 1932; Schuhmann, 1942; Gaudin et al., 1942) focused on assessing flotation performance and evaluating the effects of certain physical parameters. Numerous studies were also conducted during this time analyzing the nature and behavior of the many different reagents (collectors, frothers, activators, depressants, pH modifiers) employed in flotation practice.

Sutherland (1948) developed the first truly theoretical approach into the investigation of flotation by considering the capture mechanism of a single particle by a single rising air bubble. He adapted Gaudin's (1932) probabilistic model to his analysis, equating the overall probability of particle capture, P , to the product of three independent probabilistic events: collision, adhesion, and detachment. The probability equation is expressed as:

$$P = P_c P_a (1 - P_d) \quad [2.1]$$

where P_c is the probability of collision, P_a is the probability of adhesion, and P_d is the probability of particle detachment. For fine size particles, detachment is likely to be negligible, and P is equal to the product of just P_c and P_a .

The collision process between a bubble and particle has long been considered a hydrodynamic event. As a result, numerous fundamental analyses that make use of the principles of fluid mechanics have been conducted to quantify the collision

process. Sutherland was the first to do this, deriving the following expression for P_c :

$$P_c = 3 \left(\frac{d_p}{D_b} \right) \quad [2.2]$$

where d_p and D_b are the particle and bubble diameters, respectively. This derivation was based on potential (inviscid) flow conditions, and is applicable only for very large Reynolds numbers (Re).

Gaudin (1957) investigated the opposite flow regime, i.e., creeping flow, and derived an expression for P_c based on Stokes flow conditions:

$$P_c = \frac{3}{2} \left(\frac{d_p}{D_b} \right)^2 \quad [2.3]$$

Since Stokes flow corresponds to low Reynolds numbers, this relationship is strictly valid only for extremely small bubbles. Equation [2.3] may be applicable to certain column flotation circuits, if quiescent conditions and small bubbles prevail.

In their analyses, Sutherland and Gaudin operated on the premise that the particle trajectory could be equated with the fluid flow. The motion of the particle was dictated solely by the motion of the fluid field it was traveling with. Furthermore, gravitational and inertial effects were ignored.

Flint and Howarth (1971) incorporated a relative acceleration component into their collision model. Expanding on previous work studying collision probabilities for raindrops and dust particles (Pearcey and Hill, 1957; Hocking, 1960; Fonda and

Herne, 1960; Shafrir and Neiburger, 1964), Flint and Howarth calculated particle trajectories for Stokes flow and potential flow conditions. The important conclusion to be drawn from their work is that for fine particles, the limiting collision probability is the same for both Stokes and potential flows.

Reay and Ratcliff (1973) conducted a similar analysis of collision probability, but as applied to effluent treatment, where both particle and bubble size are small. Stokes flow conditions can then be used, relatively easily and accurately. The authors demonstrated the effects of bubble and particle size on P_c , concluding that P_c would theoretically be increased using smaller bubbles and larger particles, as has been proven experimentally. Furthermore, an important distinction concerning the probability of collision was proposed, separating P_c into gravitational (P_g) and interceptional (P_i) components. Gravitational collision occurs because of particle deviation from the liquid streamlines due to the particle's settling velocity. Interceptional collision occurs when the particle moves with the liquid streamlines and collides because of finite geometrical constraints. Reay and Ratcliff derived an explicit expression for P_g , and also showed that P_i was directly proportional to the square of the particle diameter and inversely proportional to the square of the bubble diameter.

The collision models outlined above are informative, but restrictive, because they were derived from either Stokes flow or potential flow conditions. For most flotation applications, the Reynolds number is intermediate between these two

extremes. Recognizing this fact, Weber and Paddock (1983) and Luttrell (1986) have each proposed expressions for the probability of collision for intermediate conditions. Weber and Paddock utilized Masliyah (1970) and Woo's (1971) numerical solutions to the Navier-Stokes equations at higher Reynolds numbers ($0.2 \leq Re \leq 400$) to develop an expression for P_i :

$$P_i = \frac{3}{2} \left(\frac{d_p}{D_b} \right)^2 \left[1 + \frac{(3/16) Re}{1 + 0.249 Re^{0.56}} \right] \quad [2.4]$$

Equation [2.4] was the first expression which was able to predict particle collision probability over a wide range of bubble sizes.

Luttrell analyzed the intermediate case from a more theoretical viewpoint. A stream function applicable to intermediate Re was developed by combining the stream functions for Stokes flow and potential flow. The probability of collision by interception could then be calculated, giving:

$$P_i = \left[\frac{3}{2} + \frac{4 Re^{0.72}}{15} \right] \left(\frac{d_p}{D_b} \right)^2 \quad [2.5]$$

For the collection of very fine particles, P_i is essentially equal to P_c because the P_g term becomes negligible.

Jiang and Holtham (1986) have developed a theoretical model of collision between a particle and a bubble applicable to intermediate Re , but the model also includes the inertia force. A fourth-order Runge-Kutta numerical technique was used

to solve the equations of motion. They found the relationship between P_c , d_p , and D_b to be:

$$P_c = A \left(\frac{d_p}{D_b} \right)^n \quad [2.6]$$

where A and n are functions of Re . For bubbles of diameter between 280 and 860 μm , n is essentially constant at 2 and A varies between 6 and 12. Jiang and Holtham did not develop a generalized equation for P_c , preferring instead to tabulate expressions for P_c for different values of d_p and D_b .

A comparison between the various models for collision probability is presented in Table 2.1 for a 10 μm particle and 300 μm bubble. The equations proposed by Weber and Paddock and by Luttrell predict quite similar values for P_c , with both considerably larger than the Stokes flow value because the 300 μm bubble corresponds to intermediate conditions. The higher value of P_c found using Jiang and Holtham's equation may be due to several factors. First of all, Jiang and Holtham did not derive an expression exactly for this particle size and bubble size; the value shown in Table 2.1 was calculated from the expression for the most similar conditions. Secondly, the inclusion of inertia in their model may contribute to a higher value of P_c . The potential flow prediction of P_c is grossly out of line. The reason for this is that a 300 μm bubble ($Re \approx 8$) produces flow patterns far removed from potential flow.

Table 2.1 Values of P_c as calculated from various equations for a 10-um diameter particle and 300-um bubble.

Equation Source	Probability of Collision, P_c
Stokes flow	0.00167
Weber and Paddock	0.00308
Luttrell	0.00301
Jiang and Holtham	0.00609
Potential flow	0.10000

It should be obvious that collision between particle and bubble does not guarantee attachment and subsequent flotation. Adhesion, whereby the particle establishes three-phase contact with the bubble, must be considered as well. It is the differences in P_a , the probability of adhesion, between two species which forms the foundation for the selective separation involved in flotation.

Adhesion was initially addressed by Derjaguin and Kussakov (1939), who introduced the concept of a "disjoining pressure" acting between two surfaces. When they pressed an air bubble against a hydrophilic plate of glass submerged in water, the liquid film thinned to a given thickness and then resisted further thinning. This resistance was termed the "disjoining pressure."

Derjaguin and Dukhin (1961) offered a more rigorous definition of the events leading to flotation. Particles must pass through three distinct stages prior to flotation:

- 1) Particle approach to bubble surface;
- 2) Particle passage through a diffuse electrical boundary layer; and
- 3) Thinning and rupture of the disjoining film.

Stage 1 is a function of the system hydrodynamics, as shown in the previous discussion concerning collision. The latter two stages, conversely, depend on the surface forces acting between the bubble and particle. The magnitude of these surface forces will dictate the fate of the disjoining film, i.e., whether or not it will rupture and permit attachment.

For nearly forty years, the classical DLVO theory of colloid stability has been used to describe the stability of thin films between two species. Aqueous colloidal suspensions, where only electrostatic and dispersion forces are present, have been successfully modeled with the DLVO theory. The total interaction force, F_t , is given by:

$$F_t = F_e + F_d \quad [2.7]$$

where F_e and F_d are the electrostatic and dispersion forces. The combined effect of the repulsive electrostatic force and the attractive dispersion force produces a net interaction force which exhibits characteristics similar to observed experimental results for colloidal systems.

More recently, however, numerous systems have been found which cannot be adequately explained by considering only F_e and F_d (Christenson, 1988; Churaev and Derjaguin, 1985; Claesson, 1987; Xu and Yoon, 1989; Laskowski and Kitchener, 1969). Claesson (1987) performed direct force measurements between mica surfaces and found both repulsive and attractive forces not accounted for by the classical DLVO theory. Xu and Yoon (1989) performed coagulation experiments on coal and methylated silica samples, and discovered that, while the classical DLVO theory was applicable to weakly hydrophobic solids, it failed for strongly hydrophobic materials. Laskowski and Kitchener (1969), studying a solid/liquid/gas system, measured substantial contact angles despite the fact that the electrostatic and dispersion forces

were repulsive. These findings suggested a third force which must operate in certain situations. Structural forces, which can be either attractive or repulsive, are believed to be responsible for the observed experimental anomalies.

In light of this additional interaction, the total interaction force can now be expressed as:

$$F_t = F_e + F_d + F_s \quad [2.8]$$

where F_s is the structural force. The relative magnitudes of each of these forces will determine the stability of the intervening film between two species. Since adhesion requires the rupture of this film, P_a is directly dependent on F_t .

Quantifying P_a for a bubble-particle system has been a challenging task. Commonly, induction time, τ_i , and contact (or sliding) time, τ_c , have been employed to assess adhesion in flotation. The induction time is the time required for the film between the bubble and particle to thin and rupture. The contact time is the amount of time in which the particle is sliding over the bubble surface. If the contact time is greater than the induction time ($\tau_c > \tau_i$), adhesion will occur. Induction time, then, provides an indication of the floatability of a given species. Particles with a short induction time are easily floated, while particles with higher values of τ_i exhibit poor flotation characteristics.

Considerable effort has been expended analyzing the mechanisms and behavior of τ_i and τ_c . Research into induction time has focused on relating τ_i to the

flotation rate and examining the effects of various variables on τ_i , such as temperature, collector addition, pH, frother concentration, etc. (Eigeles and Volova, 1960; Dobby and Finch, 1987; Yordan and Yoon, 1990; Laskowski, 1989). Sliding time has been modeled using several different methods, including sliding (Sutherland, 1948; Dobby and Finch, 1986), vibration (Philippoff, 1952), distortion (Evans, 1954), and distortion with motion (Ye and Miller, 1988).

Several investigators have developed equations for P_a based on the induction time and other physical parameters (Finch and Dobby, 1990; Luttrell and Yoon, 1988; Laskowski, 1989). Finch and Dobby (1990) defined the probability of adhesion as the fraction of particles that are in contact with the bubble longer than the induction time. Using relationships for the closest streamline approach angle (θ_c) and the maximum angle of contact (θ_n), the following expression was derived:

$$P_a = \frac{\sin^2 \theta_n}{\sin^2 \theta_c} \quad [2.9]$$

where θ_n is a function of the particle velocity, particle and bubble sizes, and induction time. Luttrell and Yoon (1988) conducted a more theoretical hydrodynamic analysis of adhesion, based on the intermediate stream function, and found P_a to be:

$$P_a = \sin^2 \left[2 \arctan \exp \left(\frac{-(45 + 8 Re^{0.72}) U_b \tau_i}{30 R_b \left(\frac{R_b}{r_p} + 1 \right)} \right) \right] \quad [2.10]$$

The validity of this expression was confirmed by performing microflotation tests with particles large enough so that P_c could be assumed equal to one. Equations [2.9] and [2.10] both conform to a probabilistic definition, since P_a can only take on values between zero and one.

An alternate way of analyzing bubble-particle adhesion is by considering the energy barrier which develops due to the interaction of the surface forces. The particle must possess sufficient kinetic energy to overcome this barrier, at which point the film spontaneously ruptures and adhesion occurs. Recently, Yoon (1991) has incorporated this concept into an Arrhenius-type equation for P_a :

$$P_a = \exp \left(\frac{-E}{kT} \right) \quad [2.11]$$

where E is the energy barrier, k is the Boltzmann constant, and T is the absolute temperature. The point where film rupture occurs corresponds to the position of the top of the energy barrier, and is called the critical film thickness (h_c). If the particle can thin the film separating it from the bubble to a thickness of less than h_c , adhesion will take place. Research has found h_c to be a function of the hydrophobicity of the solid, generally falling between 70 and 150 nm (Hernandez, 1989).

The work summarized above has greatly increased fundamental understanding

of bubble-particle collision and adhesion. Tremendous strides have also been made towards accurate quantification of these flotation subprocesses. Dobby and Finch (1987) have drawn from these efforts to develop a particle collection model for flotation. Their model adequately simulates bubble-particle interaction, correctly predicting optimums in recovery as a function of bubble and particle size, and defining trends between the probability of particle collection and other physical variables. The empirical/theoretical methodology Dobby and Finch employed, however, hampers its fundamental soundness. A complete, first principles model describing flotation is still lacking.

2.3 Research Objectives

The inability of previous investigators to derive a workable flotation model founded on fundamental principles may stem from a common conceptual flaw. Their work was based on the separation of the individual elements involved in bubble-particle interaction, i.e., collision was treated independently from adhesion, and vice versa. Separate expressions have been developed governing collision and adhesion, and different factors have been cited as affecting their behavior, hydrodynamics impacting collision and surface chemistry determining adhesion. The reason for this dissociation is primarily one of convenience; it is far easier to investigate a process by resolving it into independent components. However, such partitioning is inherently restrictive since it prohibits any interactive effects between collision and

adhesion. A solution which obviates the need for separate representation of collision and adhesion would be fundamentally more sound.

Towards this end, bubble-particle attachment has been investigated as an integral whole. Collision and adhesion were not considered as individual entities in formulating the model, but as intermediate phases of the attachment process. The motion of the particle has been analyzed strictly by studying the relevant forces influencing its trajectory. It is believed that this approach suffers from fewer constraints than models based on collision/adhesion separation, and will therefore produce a model more synonymous with actual flotation behavior.

2.4 Model Development

Ever since Isaac Newton's teachings entered the mainstream of scientific thought, the analysis of motion has been conducted primarily from a "force accounting" foundation. The various forces which could possibly impact motion in a given system are identified and cumulated, in terms of direction and magnitude. The overall force produced is then what determines the resulting motion of the system. This simple force balance procedure can be applied to any system, regardless of complexity, provided expressions for the acting forces are available.

Bubble-particle attachment provides a formidable challenge for force balance methodology. The structural framework remains simple, but the individual components complicate the analysis. Numerous forces influence the motion of a

particle around a bubble. These forces have completely different natures, some being related to the hydrodynamics of the system, others linked to the surface chemistry of the interacting species. Furthermore, the range of action of these forces varies - the magnitude of the forces being a function of the relative position of bubble and particle. Despite these disparities, a fundamental force balance offers the most valid representation of bubble-particle attachment.

The geometry and coordinate system involved in bubble-particle interaction is illustrated in Figure 2.1. Cylindrical coordinates, derived through the center of the bubble, are chosen for mathematical convenience. The bubble is taken to be stationary, with the settling particles flowing past at a speed equal to the relative velocity between the bubble and particle. Bubble and particle are assumed to behave as rigid spheres (Clift, Grace, and Weber, 1978; Davis, Hansen, and Sullivan, 1980).

The liquid flow around the bubble can be represented by an infinite series of streamlines. These streamlines can be mathematically expressed as stream functions (ψ), which depend on flow conditions and obstacle characteristics. The effect of the streamlines on the motion of a particle is a function of particle size. Smaller particles, lacking considerable inertia, are carried with the streamlines; larger particles, with greater inertia, are able to deviate from the streamline trajectory.

The particle position at any point is defined in terms of R , the distance between bubble and particle centers, and θ , the angle between the bubble centerline and the particle. R and θ indicate the radial and tangential positions of the particle,

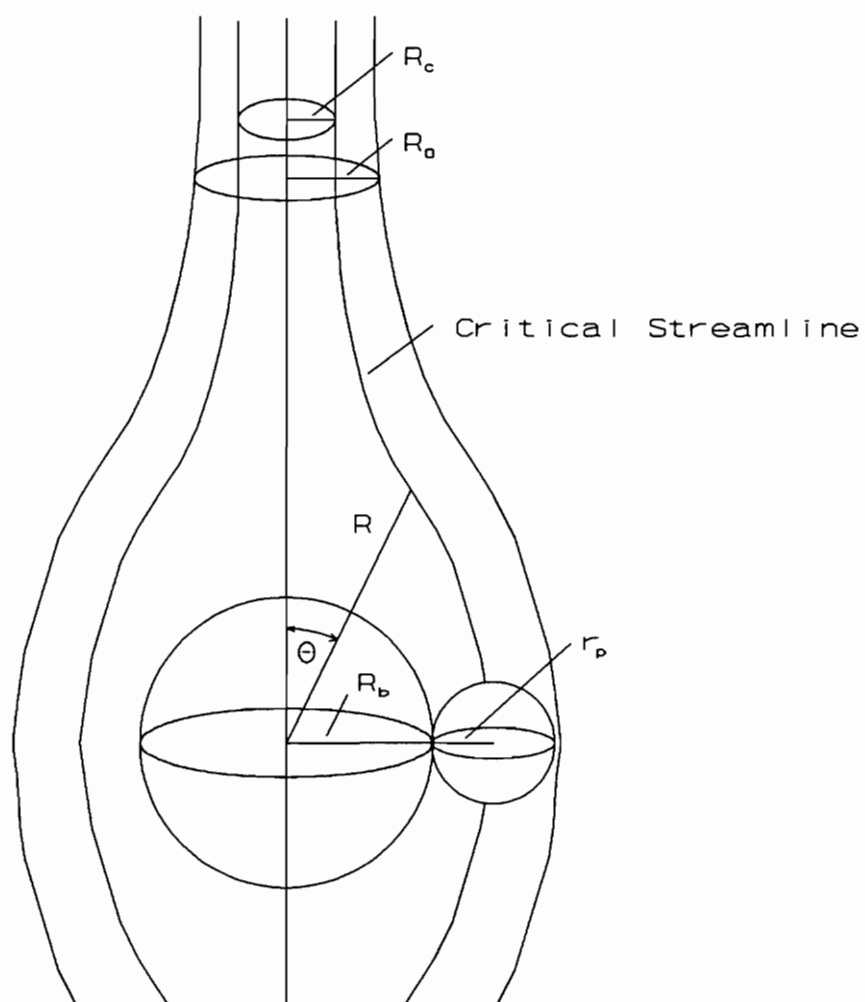


Figure 2.1 Coordinate system used to characterize bubble-particle interaction.

respectively. By determining R and θ at each moment in time, the trajectory of the particle around the bubble can be constructed.

The relevant forces in bubble-particle interaction are depicted in Figure 2.2, along with the nature of each force - either attractive or repulsive. The forces to be considered are the gravitational force (F_g), the buoyancy force (F_b), the streamline pressing force (F_p), the film thinning resistance force (F_r), the electrostatic force (F_e), the dispersion force (F_d), and the structural force (F_s). In order to better understand their impact on bubble-particle interaction, the origin of each of these forces will briefly be discussed.

2.4.1 Hydrodynamics

Hydrodynamic forces include gravity (F_g), buoyancy (F_b), the streamline pressing force (F_p), and the film thinning resistance force (F_r). Inertia has been neglected to simplify the solution. Inclusion of inertia into bubble-particle attachment models has received little theoretical attention, primarily because of the mathematical difficulty quantifying its effect. Recently, however, Plate (1989) has derived an expression for inertial collision efficiency based on work by Schuch and Löffler (1978), Herne (1960), and Flint and Howarth (1971). Schulze (1989) incorporated Plate's equation into his discourse on hydrodynamics and demonstrated the importance inertia plays in bubble-particle interaction, especially as compared to interception and gravitational effects. The omission of inertia from the model

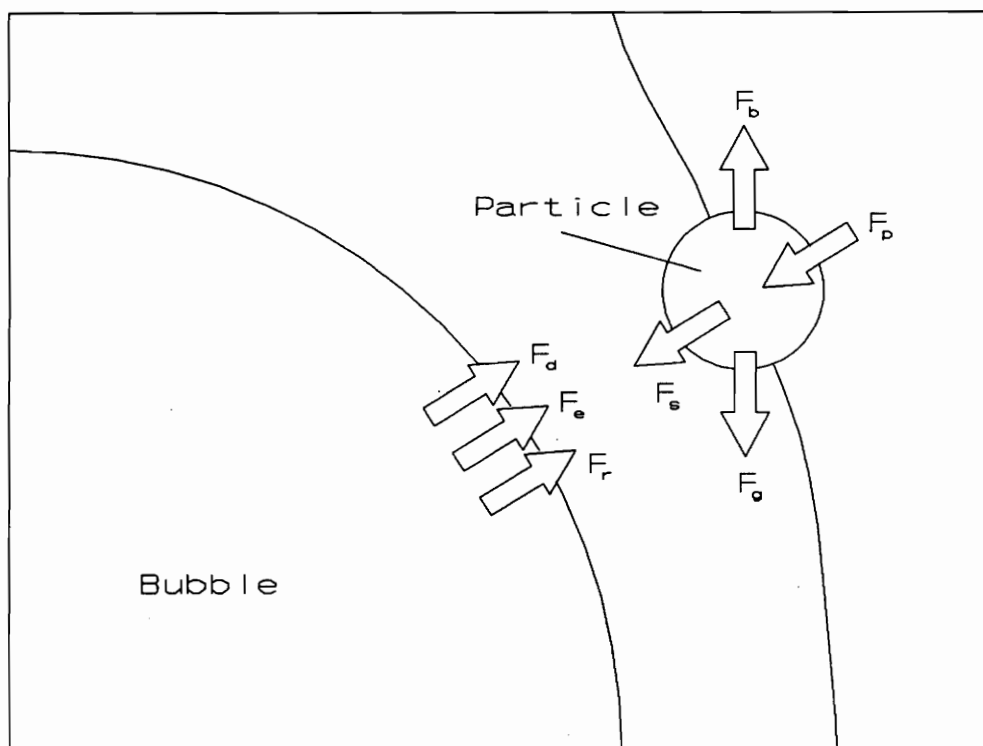


Figure 2.2 Schematic of hydrodynamic and surface forces involved in bubble-particle interaction.

proposed here is a weakness, but informative knowledge can still be gleaned from the model. It is postulated here that the film thinning resistance force may effectively offset the attractive inertia force, thereby dampening the tremendous influence Schulze reported. Additional research is required to investigate this possibility.

The gravity and buoyancy forces can be combined into a single term, denoted F_{gb} , and is expressed as:

$$F_{gb} = \frac{4}{3} \pi r_p^3 (\rho_p - \rho_f) g \quad [2.12]$$

where r_p is the radius of the particle, ρ_p and ρ_f are the densities of the particle and fluid, respectively, and g is the acceleration due to gravity. This force acts in the vertical direction, and will be oriented downward as long as $\rho_p > \rho_f$.

The streamline pressing force (F_p) arises due to the motion of the fluid streamlines around the bubble. The momentum possessed by the liquid as it skirts the bubble is imparted to the particle, resulting in a pressing force. The equation for F_p is given by:

$$F_p = 6 \pi \mu r_p U_i \quad [2.13]$$

where μ is the fluid viscosity and U_i is the streamline velocity in either the radial or tangential direction. The streamline velocity is determined from the stream function corresponding to the system flow conditions. Numerous stream functions have been

derived, some theoretically and others based on the analysis of particle trajectories (Kawaguti, 1955; Masliyah and Epstein, 1972; Seeley et al., 1975; Plate, 1989). With regard to flotation, stream functions representing the gamut of flow conditions are considered (Table 2.2): Stokes flow (low Re), potential flow (high Re), and intermediate flow (intermediate Re).

Gaudin (1957) and Sutherland (1948) investigated bubble-particle interaction for low and high Reynolds number applications, respectively, and derived expressions for the probability of collision, P_c . Most flotation, however, utilizes medium-size bubbles (100-1000 μm), which are representative of intermediate flow conditions. Luttrell (1986) has combined the stream functions for Stokes and potential flow into a single generalized expression for ψ at intermediate Re:

$$\psi = U_b R_b^2 \sin^2\theta \left[\frac{1}{2}X^2 - \frac{3}{4}X + \frac{1}{4X} + \frac{Re^{0.72}}{15} \left(\frac{1}{X^2} - \frac{1}{X} + X - 1 \right) \right] \quad [2.14]$$

where U_b is the bubble rise velocity and $X = R/R_b$. This equation reduces to Stokes stream function as Re approaches zero and approximates the potential flow stream function at large Re.

The radial and tangential velocities required for the pressing force are derived from the following well-known expressions for axisymmetric flow around a rigid sphere:

$$U_{rad} = \frac{1}{R^2 \sin\theta} \frac{d\psi}{d\theta} \quad [2.15]$$

Table 2.2 Dimensionless stream function as a function of flow conditions.

Flow Conditions	Dimensionless Stream Function
Stokes	$\left(\frac{1}{2} X^2 - \frac{3}{4} X + \frac{1}{4X}\right) \sin^2 \theta$
Intermediate	$\left[\frac{1}{2} X^2 - \frac{3}{4} X + \frac{1}{4X} + \frac{Re^{0.72}}{15} \left(\frac{1}{X^2} - \frac{1}{X} + X - 1\right)\right] \sin^2 \theta$
Potential	$\left(\frac{1}{2} X^2 - \frac{1}{2X}\right) \sin^2 \theta$

$$U_{\tan} = \frac{1}{R \sin \theta} \frac{d\psi}{dR} \quad [2.16]$$

Inserting equation [2.14] into equations [2.15] and [2.16] results in:

$$U_{rad} = U_b \cos \theta \left[1 - \frac{3}{2X} + \frac{1}{2X^3} + \frac{2Re^{0.72}}{15} \left(\frac{1}{X^4} - \frac{1}{X^3} + \frac{1}{X} - \frac{1}{X^2} \right) \right] \quad [2.17]$$

$$U_{\tan} = U_b \sin \theta \left[1 - \frac{3}{4X} - \frac{1}{4X^3} + \frac{Re^{0.72}}{15} \left(\frac{1}{X^3} - \frac{2}{X^4} + \frac{1}{X} \right) \right] \quad [2.18]$$

The film thinning resistance force, F_r is derived from lubrication theory, and accounts for the increased repulsive force that develops as the intervening film between the bubble and particle thins. The form of the film thinning resistance force is similar to that of the streamline pressing force:

$$F_r = 6\pi \mu r_p U_{ip} \beta \quad [2.19]$$

where U_{ip} is the particle velocity in the radial or tangential direction, and β is a correction factor dependent on separation distance. As the film thickness between bubble and particle diminishes, β increases.

The value of β is a matter of some dispute. Taylor (1925) derived the following linear relationship from Reynolds lubrication theory:

$$\beta = \frac{h}{r_p} \quad [2.20]$$

where h is the film thickness between two interacting species. This relationship,

however, was derived for a sphere approaching a flat plate, and is valid only at very small distances.

Brenner (1964) and Maude (1961) independently obtained an improved expression for β that is valid at greater separation distances. Unfortunately, their calculations were based on a flat plate collector assumption as well, and are not applicable to bubble-particle interaction.

Goren and O'Neill (1971) investigated spheres approaching spherical and cylindrical collectors, and concluded that the β term was substantially smaller than the reported values for a flat plate. The relationship between β and h/r_p is shown in Figure 2.3 for all three investigations. The logarithmic scale employed emphasizes the dramatic increase in β with decreasing h .

In a recent publication, Luttrell and Yoon (1992) have included Goren and O'Neill's expression into their analysis of the hydrodynamic interaction between a bubble and a particle in flotation. The importance of the corrected film thinning resistance force was demonstrated by equating F_r to the streamline pressing force, F_p , and comparing the resulting velocities. The particle velocity was retarded to a much greater extent than the fluid streamline velocity. This condition had a pronounced effect on the bubble-particle interaction by altering the trajectory of the particle.

The film thinning resistance force is commonly disregarded by most investigators studying bubble-particle hydrodynamics, who apparently assume it is

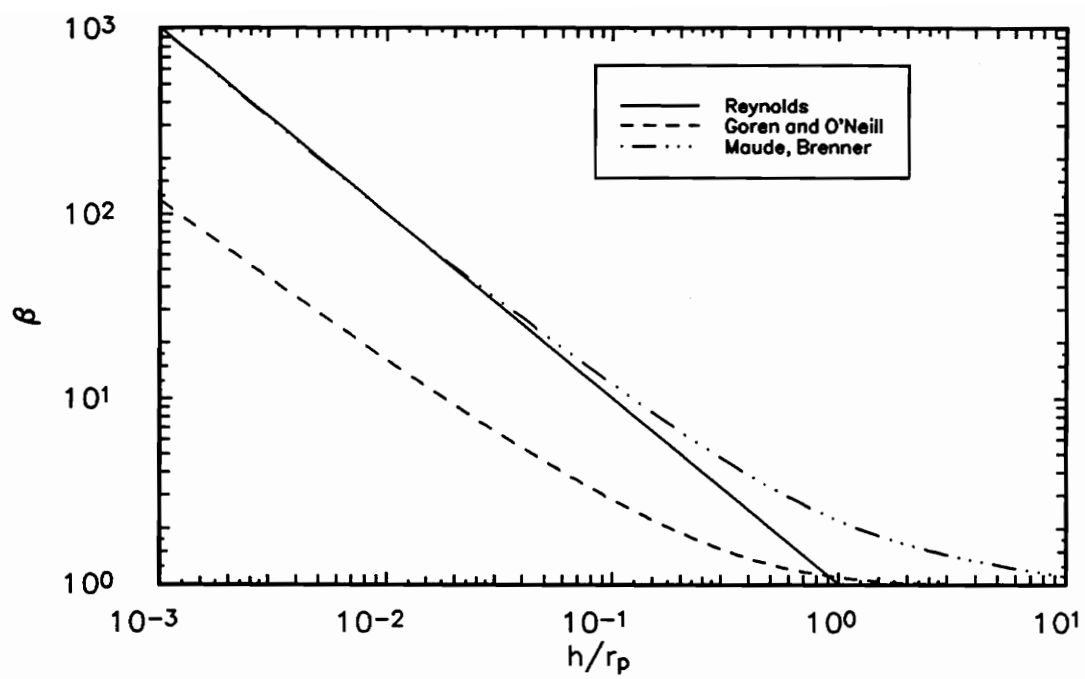


Figure 2.3 Relationship between film thinning resistance factor, β , and dimensionless distance, h/r_p (after Luttrell, 1986).

negligible, are unaware of its existence, or who believe it is accounted for elsewhere. A closer look at Figure 2.3, however, reveals the impact F_r can have. For a $20\ \mu\text{m}$ particle, for example, the β term begins to increase considerably at $h/r_p = 0.1$, which corresponds to a film thickness of 2000 nm. This is still fairly far from the bubble surface; surface forces have no influence yet. The β term will continue to increase as the film thickness decreases, exerting a significant effect on F_r and resisting the particle's approach.

2.4.2 *Surface Forces*

Expressions for the surface forces are based on the extended DLVO theory, in order to incorporate the structural interaction. The three forces that must be considered are the electrostatic force (F_e), dispersion forces (F_d), and the structural force (F_s). The signs of these forces may vary, but for bubble-particle interaction, the first two are commonly repulsive, while the last is attractive (for a hydrophobic material).

The electrostatic force (F_e) develops due to the interaction between the electrical double layers of the bubble and the particle. Overlap between the double layers gives rise to attraction or repulsion, depending on their relative signs. If the double layers are of opposite charge, the effect is a net attraction, which assists in thinning the film between the bubble and particle. When the double layers are of like charge, however, the resulting repulsion acts to resist film thinning. The

magnitude of the electrostatic force is a function of the double layer characteristics. Hogg, Healy, and Fuerstenau (1966) derived an expression for F_e applicable to two interacting spheres of unlike charge:

$$F_e = \frac{2B_1\kappa[e^{-2\kappa h} - B_2e^{-\kappa h}]}{1 - e^{-2\kappa h}} \quad [2.21]$$

where B_1 and B_2 are given by:

$$B_1 = \frac{\epsilon r_p R_b (\psi_p^2 + \psi_b^2)}{4(r_p + R_b)} \quad [2.22]$$

$$B_2 = \frac{2\psi_p\psi_b}{(\psi_p^2 + \psi_b^2)} \quad [2.23]$$

κ is the Debye reciprocal length, ψ_p and ψ_b are the surface potentials of the particle and bubble, respectively, and ϵ is the dielectric constant. The surface potentials arise due to a build-up of charge at the bubble-water and particle-water interfaces. One of several mechanisms may be responsible for this charging, including unequal distribution of lattice-forming ions, dissociation of surface groups, preferential adsorption, and substitution of crystal ions. The mechanism that is predominant in a given situation is dependent on the material characteristics. To avoid the difficulties associated with evaluating surface charge, zeta potentials (ζ_p and ζ_b) will be used in place of surface potentials. Zeta potentials are determined from the

electrical mobility of the species under investigation, and are relatively easy to measure experimentally.

Dispersion forces come about due to the van der Waals forces which operate between nonpolar atoms and molecules. Much of the initial research into dispersion forces was conducted by London (1937), who employed quantum mechanics to quantify the interaction energy between two atoms or molecules. Hamaker (1937) extended these concepts into the macroscopic regime and showed that, despite their atomic nature, dispersion forces could be significant between two macroscopic bodies.

The Hamaker constant is used to characterize the dispersion component between two macroscopic objects interacting in a third medium. The combined Hamaker constant is denoted by A_{132} and can be calculated from:

$$A_{132} = (\sqrt{A_{11}} - \sqrt{A_{33}})(\sqrt{A_{22}} - \sqrt{A_{33}}) \quad [2.24]$$

where A_{11} and A_{22} represent the Hamaker constants for the two objects (bubble and particle) and A_{33} is the Hamaker constant for the medium (water), as measured in a vacuum. The form of this equation demonstrates the possibility for both attractive and repulsive dispersion components. An attractive component ($A_{132} > 0$) results if the individual Hamaker constants for the two objects are either both greater than or less than the medium's Hamaker constant. When the Hamaker constant of the medium is between that of the two bodies, however, a repulsive dispersion component ($A_{132} < 0$) is produced. For flotation, where the particle and bubble

represent the two interacting species, and water is the medium, the dispersion component is generally repulsive. The Hamaker constant for water is less than that of the particle, but is greater than that of the air bubble (for which the Hamaker constant is assumed to be zero), resulting in a negative combined Hamaker constant. The assumption of a zero Hamaker constant for the air bubble may not be accurate in all instances, but should be applicable for minimal surfactant adsorption.

The magnitude of the dispersion force, F_d , between two species in a third medium, is determined from the following expression (Schenkel and Kitchener, 1960):

$$F_d = \frac{A_{132} r_p R_b f}{6h^2(r_p + R_b)} \quad [2.25]$$

where f is a factor included to account for the retardation effect. It is apparent that the sign of A_{132} will dictate the attractive or repulsive nature of the dispersion force.

The retardation factor, f , is given by the following:

$$f = -\frac{2\pi}{\lambda} \frac{1.77}{(1 + 1.77p)^2} \quad 0 \leq p \leq 0.57 \quad [2.26]$$

$$= \frac{2\pi}{\lambda} \left[-\frac{2.45}{p^2} + \frac{4.34}{15p^3} - \frac{1.77}{35p^4} \right] \quad 0.5 \leq p \leq \infty \quad [2.27]$$

where p and λ are experimentally measured parameters.

The origin of the structural force, F_s , is still not completely understood, but

its inclusion into the DLVO theory is now generally accepted as necessary to explain certain phenomena. The work by Israelachvili and Pashley (1982), who first directly measured F_s with the surface force apparatus, sparked renewed interest into structural forces. Extensive research over the past ten to fifteen years has done much to elucidate the theoretical backbone of structural forces and affirm their importance. With the surface force apparatus, investigators now can readily delve into the realm of molecular interaction and offer hypotheses concerning various microscopic happenings, including surface forces.

The theoretical foundation for F_s cited most often today is based on interaction between the modified liquid layers of the particle and bubble boundary surfaces. Around hydrophilic solids, a strong hydration layer is present, and the water molecules exhibit a well ordered structure. Considerable energy is therefore required to remove the water film, corresponding to a repulsive structural force. For hydrophobic solids, on the other hand, the water molecules are not as constrained, and can be more readily removed. An attractive structural force defines this situation.

Whatever its molecular origin, the mathematical description of F_s is a long range force with exponential decay (Yoon, 1991):

$$F_s = -\frac{Cr_p R_b}{(r_p + R_b)} e^{-\frac{h}{D_0}} \quad [2.28]$$

where C is the structural constant and D_0 is the decay length. If C is positive, F_s is negative, resulting in a repulsive force. The structural force in this case is often called a hydration force. When C is negative, an attractive force results, commonly termed a hydrophobic force. Values for C and D_0 are not universal constants, but adjustable parameters specific to a given material and system. Experimental determination of C and D_0 is very difficult, prompting attempts to calculate their values from other measurements (Hernandez, 1989; Xu and Yoon, 1990). Xu and Yoon recently developed an expression for C , as a function of the nondispersion component of the work of adhesion (W_a^{nd}) of water on solids. This expression was based on coagulation experiments of coal and methylated silica, however, and may not be applicable to all systems. Obviously, continued fundamental research into structural forces is imperative.

2.4.3 Force Balance

Equipped with the expressions for each of the relevant forces, it is now possible to incorporate them into an overall force balance. The general form for any force balance is given by:

$$\Sigma F = ma \quad [2.29]$$

where m and a represent the mass and acceleration of the species under investigation. Since inertia is being neglected, the acceleration term is zero, leaving:

$$\Sigma F = 0 \quad [2.30]$$

For bubble-particle interaction, in symbolic terms, this can be expressed as:

$$F_t = F_e + F_d + F_s + F_p + F_r + F_{gb} = 0 \quad [2.31]$$

where F_t is a vector representation of the resultant force acting between the bubble and the particle. To facilitate analysis for the chosen cylindrical coordinate system, the force on the particle can be resolved into its radial and tangential components, F_t^{rad} and F_t^{tan} . The position of the particle at any point will then be determined using these components in force balance equations.

The force equilibrium equation in the radial direction is given by:

$$F_t^{\text{rad}} = F_e + F_d + F_s + F_p + F_r + F_{gb} \cos\theta = 0 \quad [2.32]$$

Substituting the expressions for each of the forces yields the following equation:

$$\begin{aligned}
& \frac{2P\kappa[\exp(-2\kappa h) - Q\exp(-\kappa h)]}{1 - \exp(-2\kappa h)} + \\
& \frac{r_p R_b A_{132} f}{6h^2(r_p + R_b)} - \\
& \frac{Cr_p R_b}{(r_p + R_b)} \exp\left(\frac{-h}{D_0}\right) + \\
& 6\pi\mu r_p U_r - 6\pi\mu r_p U_{rp} \beta + \\
& \frac{4}{3}\pi r_p^3 (\rho_p - \rho_f) g \cos(\theta) = 0
\end{aligned} \tag{2.33}$$

This equation defines the net force which governs the film thickness, h , between the particle and bubble. If the net force is positive, or attractive, the film thins; if the net force is negative, or repulsive, the film thickness increases as the particle moves away from the bubble. The only unknown in Equation [2.33] is U_{rp} , the radial velocity of the particle around the bubble. Solving for U_{rp} gives:

$$U_{rp} = \frac{1}{6\pi\mu r_p \beta} \left(\frac{\frac{2P\kappa[\exp(-2\kappa h) - Q\exp(-\kappa h)]}{1 - \exp(-2\kappa h)} + \frac{r_p R_b A_{132} f}{6h^2(r_p + R_b)} - \frac{Cr_p R_b}{(r_p + R_b)} \exp\left(\frac{-h}{D_0}\right)}{6\pi\mu r_p U_r + \frac{4}{3}\pi r_p^3 (\rho_p - \rho_f) g \cos\theta} \right) \tag{2.34}$$

Once U_{rp} is known, the new radial position of the particle, R_{new} , can be estimated from the following equation, provided the time interval is small:

$$R_{new} = R_{old} - U_{rp} \Delta t \tag{2.35}$$

where R_{old} is the old radial position and Δt is the time interval. The effect of the radial velocity of the particle is directly analogous to the radial component of the

total force, F_t^{rad} . As long as U_{tp} is positive, R_{new} will continue to decrease, indicating a thinning film. When U_{tp} goes negative, R_{new} increases and the particle is beginning to move away from the bubble surface.

In the tangential direction, the force balance is given by:

$$6\pi\mu r_p U_t - 6\pi\mu r_p U_{\text{tp}} + \frac{4}{3}\pi r_p^3(\rho_p - \rho_f)g\sin\theta = 0 \quad [2.36]$$

There are no contributions from the surface force expressions in the tangential direction because they were derived in the radial direction. Here the only unknown is U_{tp} , the tangential particle velocity. Solving Equation [2.36] for U_{tp} yields:

$$U_{\text{tp}} = U_t + \frac{2}{9\mu} r_p^2(\rho_p - \rho_f)g\sin\theta \quad [2.37]$$

The velocity of the particle in the tangential direction, then, is the sum of the tangential streamline velocity and the tangential component of the particle's settling velocity. To calculate the new angle, θ_{new} , between the bubble and particle, the following formula is used:

$$\theta_{\text{new}} = \theta_{\text{old}} + \frac{U_{\text{tp}} \Delta t}{R} \quad [2.38]$$

If U_{tp} is positive, θ_{new} will increase, meaning that the particle is sweeping around the bubble.

A computer program incorporating the procedure outlined above has been written. For a given set of initial conditions, the program will determine the closest

distance between the particle and bubble surface. This closest approach distance is called the equilibrium film thickness (EFT). The program is a numerical simulation technique, similar to that of Luttrell (1986), which constructs a particle trajectory based on the acting hydrodynamic and surface forces.

To run a simulation using the model, the particle is started far enough ahead of the bubble so that it is not affected by the streamline curvature or hydrodynamic resistance. Based on numerical techniques used by others studying bubble-particle interaction (Jiang and Holtham, 1986; Luttrell, 1986), an initial starting distance of twenty bubble radii was chosen. The particle must also be offset from the bubble centerline to prevent the program from a division by zero error. (It is assumed that any particle beginning on the bubble centerline will collide with it in a quiescent environment.) The initial offset distance from the bubble centerline is denoted R_0 .

For each time step, the radial and tangential velocities of the particle are calculated from Equations [2.34] and [2.37] and used to determine the new values for R and θ . In this way, the trajectory of the particle can be obtained, and bubble-particle attachment assessed. Attachment is defined to occur when the equilibrium film thickness (EFT) goes to zero. This definition eliminates the need for separating collision from adhesion. The particle either will or will not make it to the bubble surface, depending on the interplay between the hydrodynamic and surface forces. To determine the overall probability of collection (attachment), P , the following method is employed. The simulator calculates trajectories for gradually increasing

values of R_0 . At some value of R_0 , the particle will just attach to the bubble at $\theta = 90^\circ$ (EFT = 0), defining the grazing collection streamline. All particles within the cylinder bounded by R_0 will attach to the bubble. The value of R_0 at this point is called the critical starting distance, R_c , and is used to calculate the theoretical probability of collection from:

$$P = \left(\frac{R_c}{r_p + R_b} \right)^2 \quad [2.39]$$

This equation is equivalent to defining P as the fraction of particles ahead of the bubble that are actually collected by it.

A listing of the simulation program, written in TurboBasic, is included in Appendix I.

2.5 Simulation Results

2.5.1 Model Validity

The computer simulator was used to conduct a theoretical investigation into bubble-particle interaction. Hydrodynamic and surface chemistry parameters could easily be changed in the program, facilitating evaluation of their effects on particle collection.

The first set of simulations was designed to test the validity of the model and examine some general relationships concerning bubble-particle interaction.

Conditions representative of Stokes flow were input into the computer program. The particle size was set to $5\ \mu\text{m}$ and the bubble size to $100\ \mu\text{m}$, which corresponds to a Reynolds number of 0.78, near the limit of Stokes flow. The surface force parameters were assigned the following values, based on measurements for a Pittsburgh No. 8 coal sample at pH 7: $\zeta_p = -35\ \text{mV}$ (*Development of the Selective Coagulation Process*, 1990), $\zeta_b = -37\ \text{mV}$ (Hernandez, 1989), $A_{132} = -1.4 \times 10^{-20}\ \text{J}$ (*Development of the Selective Coagulation Process*, 1990), $C = -1.8\ \text{mJ/m}^2$ (Xu, 1990), and $D_0 = 10.3\ \text{nm}$ (Xu, 1990). The structural constant and decay length values were selected based on work by Xu (1990), who used the extended DLVO theory to calculate C and D_0 at the critical film thickness for hydrophobic silica samples. Exact values of C and D_0 for the coal sample were unknown, so an assumption was made that the structural constant and decay length for the hydrophobic silica represented the hydrophobic coal sample as well.

The results of the simulations are presented in Figure 2.4. The equilibrium film thickness (EFT) is plotted on the y-axis, versus the initial particle starting distance from the bubble centerline, R_0 , on the x-axis. The individual curves were produced by gradually increasing the value of R_0 in the simulation program. Since attachment occurs only when $\text{EFT} = 0$, the critical starting distance, R_c , used in calculating P , is the point where the curve rises from the x-axis. If the curve does not intersect the x-axis, attachment (collection) has not taken place.

Curve 1 was constructed by considering only the hydrodynamic forces, just as

Sutherland and Gaudin did in deriving their expressions for P_c . The film thinning resistance force, F_r , in this case, reduces to the Stokes drag force on the particle by setting $\beta = 1$. The curve shows that all particles starting within about $3.15 \mu\text{m}$ of the bubble centerline will be collected. This corresponds to a probability of collection of:

$$P = \left(\frac{R_c}{r_p + R_b} \right)^2 = \left(\frac{3.15}{2.5 + 50} \right)^2 = 0.0036 \quad [2.40]$$

Assuming the particles to be sufficiently hydrophobic that any particle that collides with the bubble attaches to it, the probability of collection can now be directly compared with Gaudin's probability of collision for Stokes flow:

$$P_c = \frac{3}{2} \left(\frac{d_p}{D_b} \right)^2 = \frac{3}{2} \left(\frac{5}{100} \right)^2 = 0.00375 \quad [2.41]$$

The close agreement between these two values is a promising indication of the validity of the model derived in this work.

Curve 2 in Figure 2.4 demonstrates the effect of the film thinning resistance force on bubble-particle interaction. Again, only hydrodynamic forces have been considered, but β is not restricted to a value of one anymore. As the ratio h/r_p decreases (according to Figure 2.3), β will rise significantly, increasing the value of F_r . This results in a dramatic change in flotation behavior. Curve 2 is shifted considerably to the left as compared to curve 1, with a concomitant decrease in the

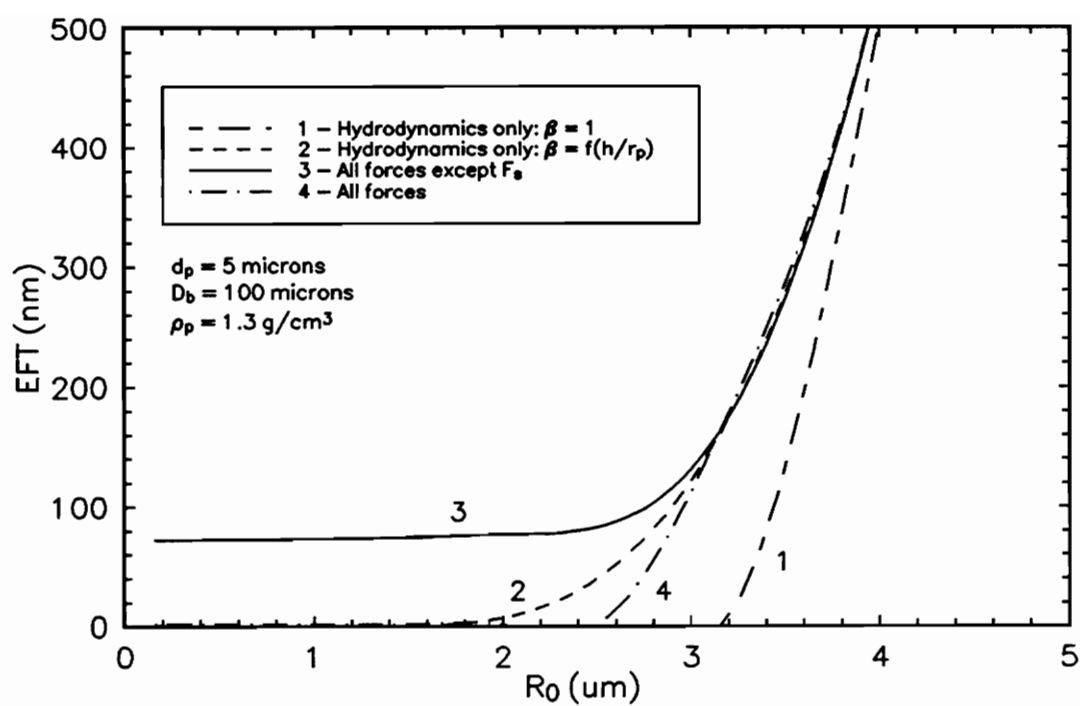


Figure 2.4 Simulation results for various force combinations.

probability of collection. Indeed, the change in R_c (down to $1.8 \mu\text{m}$) signifies a drop in P from 0.0036 to 0.0012, a factor of three. The increased film thinning resistance force at small distances requires that particles start closer to the bubble centerline in order to attach.

Curve 3 represents simulations combining the hydrodynamic forces with the forces comprising the classical DLVO theory. The particle obviously does not make it to the bubble surface, remaining about 70 nm away. This is because the repulsive electrostatic and dispersion forces resist further thinning of the intervening film between the bubble and particle, thereby prohibiting attachment. This theoretical behavior is contrary to experimental behavior, because coals with the properties described above are known to have large contact angles, conducive to flotation. Curve 3, then, is another example of the restricted applicability of the classical DLVO theory. An additional force is necessary to adequately characterize this system.

Curve 4 depicts the whole picture. Both hydrodynamic and surface forces, including the structural force, were incorporated in the model to construct this curve. The particle is now seen to attach, due to the attractive structural force, but exhibits a P value intermediate between that of curves 1 and 2. Curve 4 is to the left of curve 1 because of the increased film thinning resistance force not accounted for in curve 1. It is to the right of curve 2 because the attractive nature of F_s is able to bring particles starting further from the bubble centerline in to attach.

2.5.2 *Effect of Model Parameters*

Having confirmed the validity of the bubble-particle interaction model for Stokes flow conditions, and having explored a few implications of the model, simulations were next conducted to study the effect of certain physical and chemical variables on the probability of collection. All subsequent simulations are based on intermediate flow conditions, which more accurately define flotation applications.

a) Effect of Particle Size:

The effect of particle size on bubble-particle interaction is illustrated in Figure 2.5 for hydrophobic particles of 5, 10, and 20 μm diameter approaching a 100 μm diameter bubble. Surface force parameters were held constant. There is a gradual shift in the critical starting distance, R_c , to the right as d_p increases. The probability of collection, therefore, increases as well, from 0.0023 ($d_p = 5 \mu\text{m}$), to 0.0082 ($d_p = 10 \mu\text{m}$), to 0.0178 ($d_p = 20 \mu\text{m}$). This progression is due to the fact that larger particles, of greater weight, are able to deviate from the fluid streamlines more easily than smaller particles, resulting in a greater chance of attaching to the bubble.

The experimentally observed peak in flotation recovery with particle size (Jowett, 1980; Trahar, 1981) cannot be reproduced with the model because detachment has not been considered. There is no mechanism included to account for the fact that larger particles are more likely to become detached from the bubble (Ahmed and Jameson, 1985; Mika and Fuerstenau, 1968; Jowett, 1980). As a

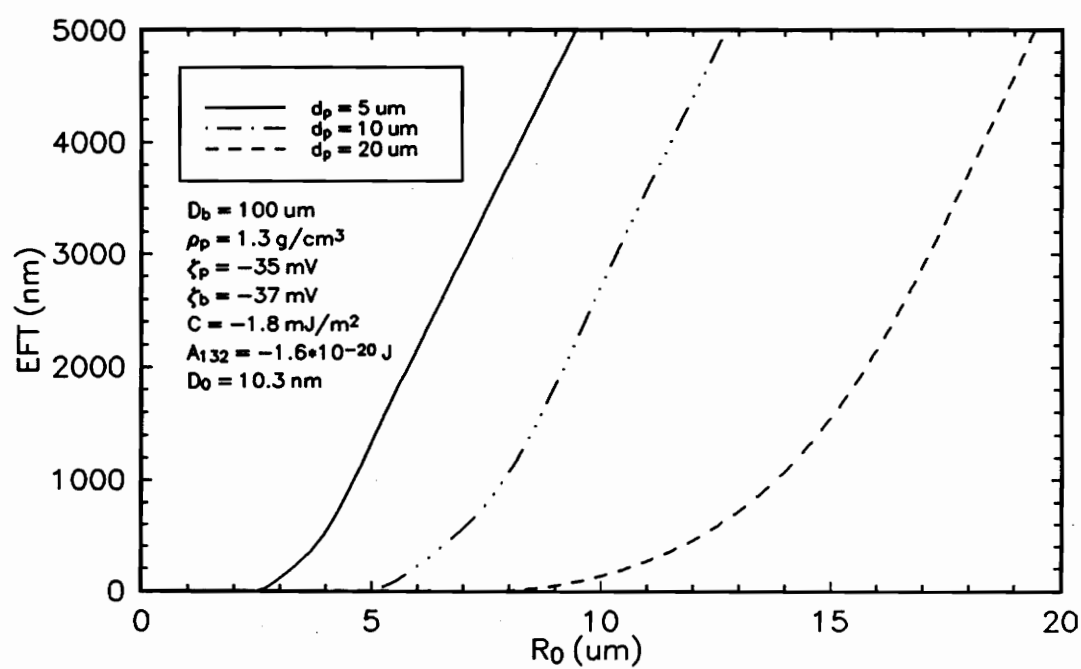


Figure 2.5 Simulation results illustrating the effect of particle size on bubble-particle interaction.

result, the probability of collection continues to increase with particle size, in accord with the simulations.

b) Effect of Bubble Size:

The increased flotation performance with small bubbles has been proven both theoretically (Flint and Howarth, 1971; Reay and Ratcliff, 1973; Jiang and Holtham, 1986) and experimentally (Anfruns and Kitchener, 1977; Yoon and Luttrell, 1986; Ahmed and Jameson, 1985). The physical reasoning behind this behavior is that, for a given volume of air, more bubbles can be produced at smaller sizes, which gives particles more chances to encounter a bubble and attach to it. Simulation results plotted in Figure 2.6 for three bubble sizes support this conclusion, although it may not appear so at first glance. The critical starting distance, R_c , remains essentially the same for all three D_b values, meaning that the numerator in Equation [2.39] for calculating P is relatively constant. As the bubble size increases, though, the denominator will increase, and the probability of particle collection will diminish.

The fact that R_c is basically unchanged for the range of bubble sizes is striking. It means that regardless of bubble size, the volume of particles swept by the bubbles is the same. The critical collection streamline does not move out proportionally with bubble size, but stays at about the same position. This outcome is powerful incentive for employing smaller bubbles in flotation. Not only do large bubbles have a lower specific surface area than smaller bubbles (at a given air rate),

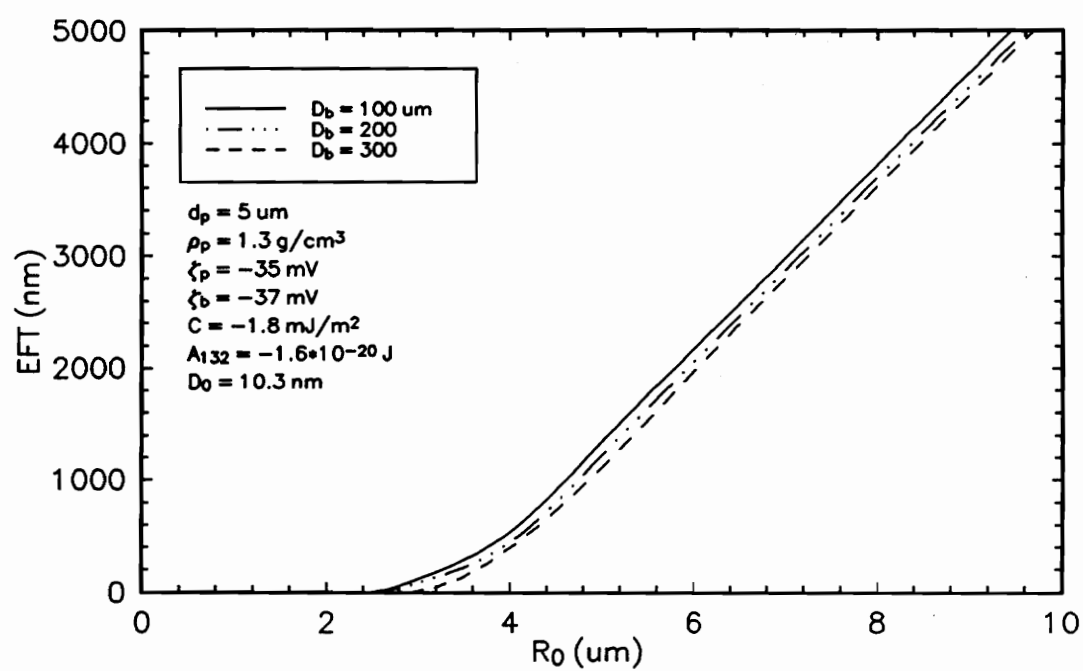


Figure 2.6 Simulation results illustrating the effect of bubble size on bubble-particle interaction.

but they also encounter no more particles.

c) Effect of Particle Density:

The effect of particle density on bubble-particle interaction has often been considered negligible, particularly for fine particles, where interceptional collision is deemed to be the dominant attachment mechanism. Figure 2.7, however, disputes this contention. The interaction between a $5\ \mu\text{m}$ particle and $100\ \mu\text{m}$ bubble at four particle densities is displayed. The curves are not widely separated, but the differences in R_c correspond to considerable differences in P . Between $\rho_p = 1.3\ \text{g/cm}^3$ and $\rho_p = 7.0\ \text{g/cm}^3$, for example, the probability of collection rises from 0.0023 to 0.0122, representing a five times greater chance of attachment. The trend demonstrated here is in excellent agreement with the particle density effect found using Dobby and Finch's model (1987).

d) Effect of Particle Charge:

Particle charge is known to influence the success of flotation to a large degree. For most applications, there is a restricted pH window within which flotation is possible (Lai and Fuerstenau, 1976; Smith and Akhtar, 1976; Fuerstenau, 1980). Outside this window, the repulsive electrostatic force prevents bubble-particle attachment, provided bubble and particle are of like charge. The results of computer simulations investigating the effect of particle charge are presented in Figures 2.8 and

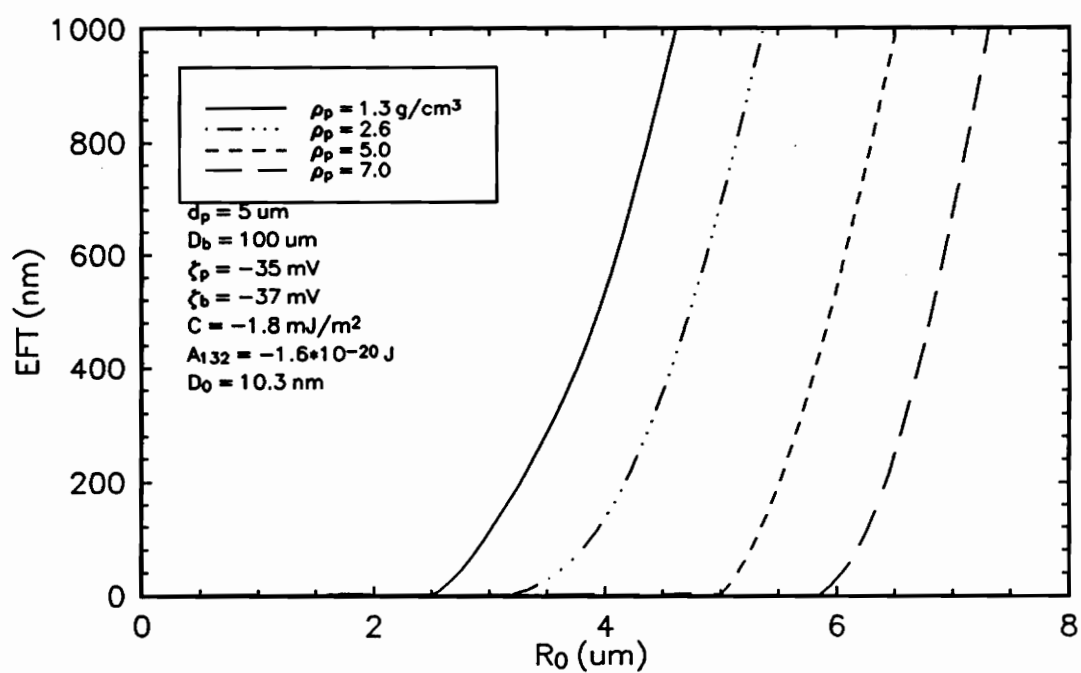


Figure 2.7 Simulation results illustrating the effect of particle density on bubble-particle interaction.

2.9. Figure 2.8 represents the interaction between a 5 μm particle and 100 μm bubble for various values of ζ_p , with $C = -1.8 \text{ mJ/m}^2$. The curves for all values of ζ_p are identical, indicating an equal probability of collection for any particle charge. A possible explanation for this behavior is that the attractive structural force ($C = -1.8 \text{ mJ/m}^2$) is so strong that the range of ζ_p studied produces an electrostatic force too weak to impede attachment. To test this hypothesis, simulations were run for the same ζ_p values, but with a weaker structural force ($C = -1.0 \text{ mJ/m}^2$). Figure 2.9 shows that the charge on the particle can now influence bubble-particle interaction. For $\zeta_p = -40 \text{ mV}$ and $\zeta_p = -50 \text{ mV}$, the electrostatic force is sufficient to prohibit attachment, since the EFT did not go to zero. The important conclusion to be drawn from Figures 2.8 and 2.9 is that flotation may be independent of pH if the particle is sufficiently hydrophobic.

e) Effect of Structural Constant:

The relationship between hydrophobicity and flotation is obvious, but not readily quantified. The more hydrophobic a particle is, the more likely it is to float, but what exactly defines hydrophobicity?. Contact angle and induction time have both been suggested and investigated as possible determinants. Contact angle values, however, provide no kinetic information concerning bubble-particle attachment, and induction time is a somewhat arbitrary experimental measurement (when does timing begin, and does 50% particle pickup correspond to τ_i). Perhaps the structural

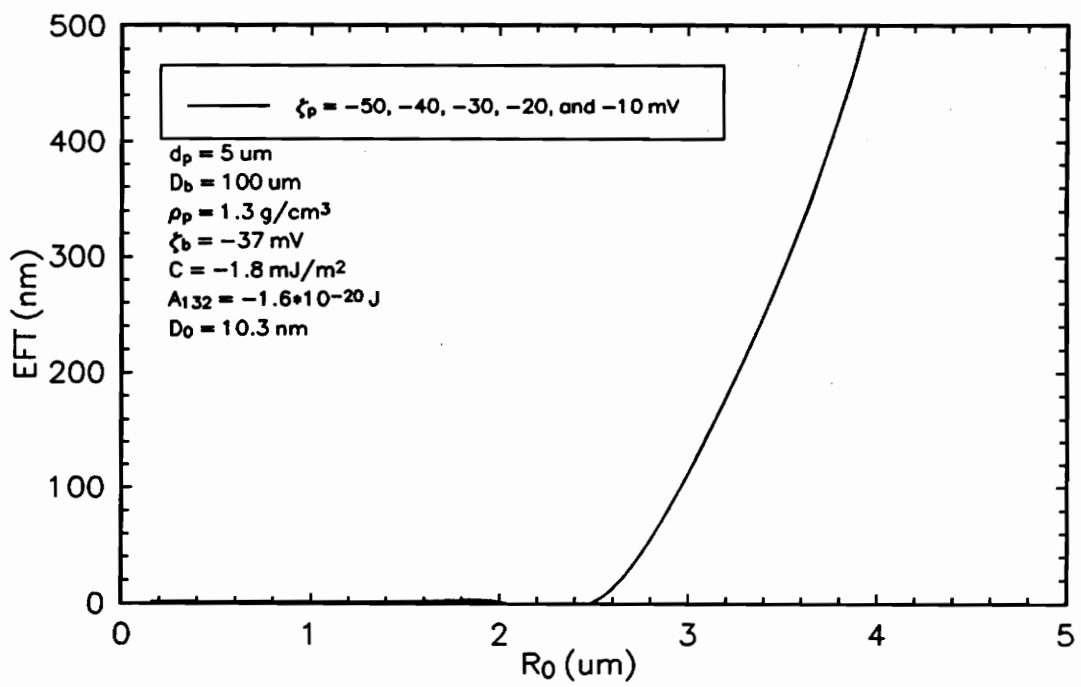


Figure 2.8 Simulation results illustrating the effect of particle charge on bubble-particle interaction for $C = -1.8 \text{ mJ/m}^2$.

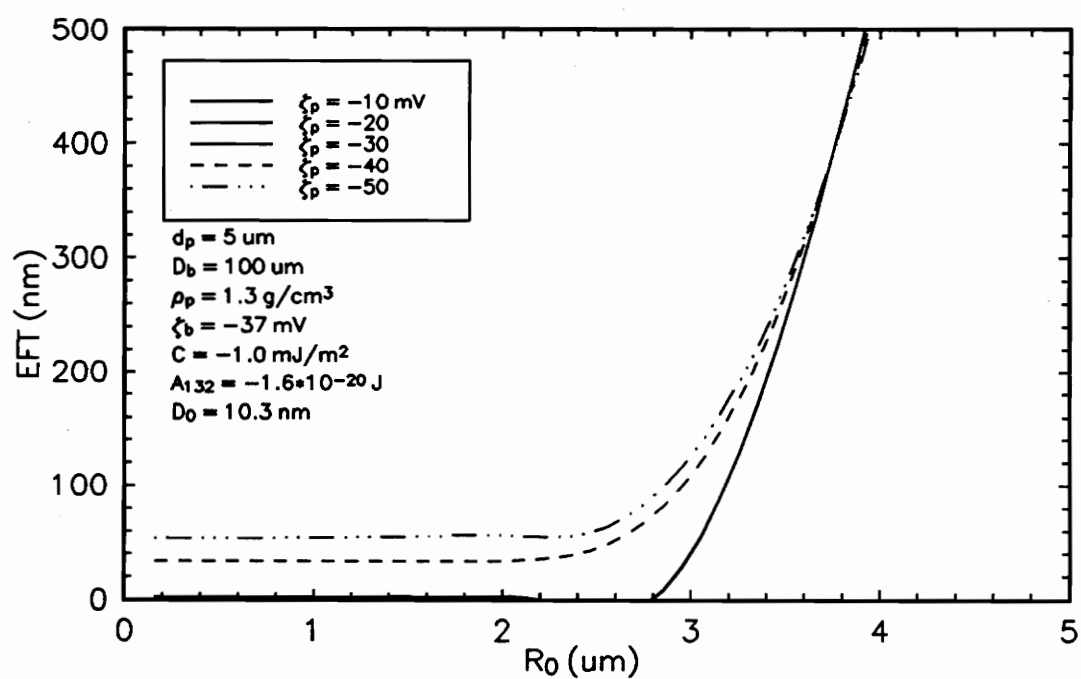


Figure 2.9 Simulation results illustrating the effect of particle charge on bubble-particle interaction for $C = -1.0 \text{ mJ/m}^2$.

constant, C , offers a more theoretical reflection of hydrophobicity (or lack thereof).

The effect of the structural constant on bubble-particle interaction is illustrated in Figure 2.10. Only for the least hydrophobic material ($C = -0.6$ and -0.2 mJ/m²) does attachment not occur: the repulsive electrostatic and dispersion forces outweigh the attractive structural force. For $C = -1.8, -1.4$, and -1.0 mJ/m², bubble-particle attachment takes place, meaning $F_s > (F_e + F_d)$. Interestingly, the probability of collection does not change for the latter three values of C . Furthermore, referring back to Figures 2.8 and 2.9, it is seen that P also does not change for various values of ζ_p . Apparently, then, the surface forces do not impact the magnitude of P . Their significance is in determining whether or not the EFT can go to zero, defining attachment. If $EFT > 0$, $P = 0$, since the particle never reaches the bubble surface. If EFT can get to zero, the value of P is a function of the hydrodynamic forces. As seen in Figures 2.5, 2.6, and 2.7, physical variables such as d_p , D_b , and ρ_p can significantly affect the probability of collection.

It seems, then, that Sutherland's original separation of collision and adhesion was justified. Computer simulations show that hydrodynamics are the controlling conditions for collision, while surface forces determine adhesion. However, this does not mean that separation is the proper analytical tool. A model which does not separate collision from adhesion, but which still predicts their independent behavior, is more sound. By using a force balance procedure, the imperfection associated with determining such vague quantities as interceptional collision probability, gravitational

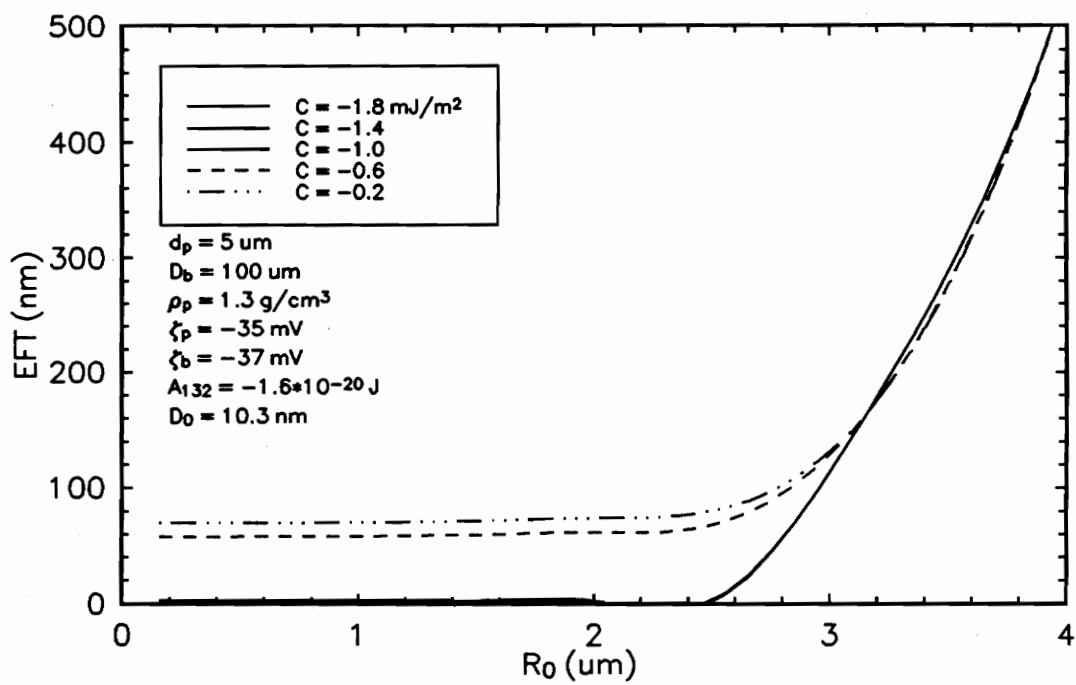


Figure 2.10 Simulation results illustrating the effect of the structural constant on bubble-particle interaction.

collision probability, sliding time, and induction time, is completely avoided.

2.6 Experimental

2.6.1 Samples

Bubble-particle attachment tests were conducted on several size fractions of coal and silica. The coal was obtained from the Pittsburgh No. 8 seam in West Virginia. A 1.3-SG float/sink with magnetite was performed to separate the coal from the waste material. After jaw crushing and hammer mill grinding, the coal was wet screened into various size fractions. Two size fractions, 100 x 150 mesh and 200 x 270 mesh, were actually employed in the flotation experiments.

The silica was acquired from Fisher Scientific Co. in 750 g lots of 250 mesh floated silica powder. Several size fractions were then produced by wet screening. The silica size fractions utilized for the tests were 250 x 270 mesh and 325 x 400 mesh. All of the samples were sealed in bags until the experiments were conducted.

2.6.2 Reagents

No reagents were used for the attachment studies of the coal. Flotation behavior was solely based on the inherent properties of the coal sample. For the silica, dodecylamine hydrochloride (DAH) was employed as a collector to render the silica hydrophobic. A fairly high concentration, 10^{-4} M DAH, was selected to insure sufficient flotation of the silica. Conditioning consisted of several minutes of

agitation, via manual stirring and an ultrasonic bath.

2.6.3 Procedure

The experimental set-up for the bubble-particle attachment studies is illustrated in Figure 2.11. The recovery zone is a 1.0-cm diameter glass tube approximately 30-cm in length. Constant liquid level is maintained with an overflow weir located in the bowl section above the recovery zone. This spillway is connected to the funnel/sump below the tube for recycle through the system. The air inlet is a high angle protrusion of the glass tube at the bottom of the recovery zone. A 0.20-mm I.D., 20° point syringe needle (purchased from Fisher Scientific Co.), attached to a syringe pump via rubber tubing, is inserted through a rubber septum covering the air inlet. Operation of the pump forces air from a 50-ml syringe through the needle, producing a steady stream of air bubbles inside the apparatus. The syringe pump permits reproducible air flow rates to be maintained for the tests.

To conduct a test, the apparatus is first filled with either a buffer solution (for the silica tests) or with distilled water (for the coal tests). A buffer solution was required for the silica tests to maintain a constant pH. The syringe pump is then turned on to begin bubble generation. In order to determine bubble size, rise times for ten bubbles over a marked 25-cm travel distance are measured and then averaged (the tailings pump is off). The coal (or silica) sample, at about 0.2% solids by volume, is subsequently added, and the tailings pump activated. The resulting

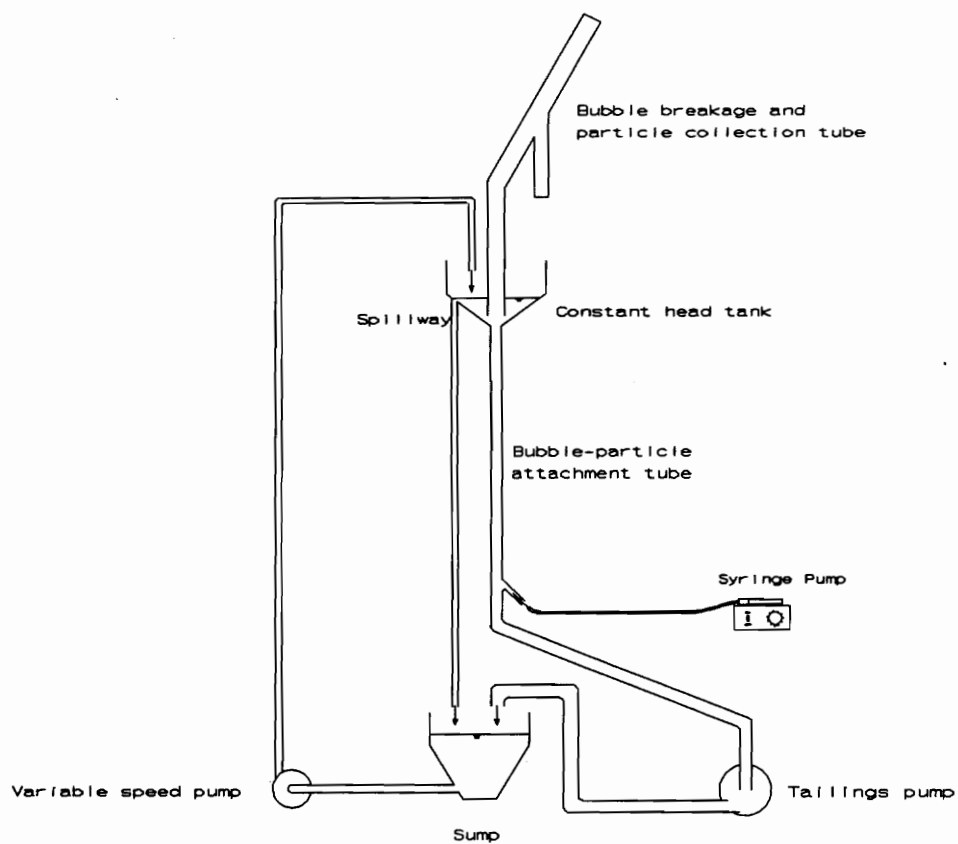


Figure 2.11 Schematic of apparatus used for bubble-particle attachment experiments.

downward fluid flow decreases the rise velocity of the bubbles, allowing a greater number of bubble-particle encounters. The system is left running for a period of time (5-10 minutes), without collecting loaded bubbles, until steady state is reached. The pH of the liquid-solid suspension is recorded.

When the experimental system has reached steady state, a water-filled collection tube is inverted and suspended over the recovery zone of the apparatus, as shown in Figure 2.11. This tube, about 1.5-cm in diameter and 50-cm in length, functions to collect particle-laden bubbles, burst these bubbles, and then capture the particles that were attached to the bubbles. Since the collection tube has a larger diameter than the apparatus, all of the rising bubbles will pass into it. The collection tube is inclined slightly from vertical to facilitate particle recovery and prevent dropback to the recovery zone.

At one or two times during the experiment, a timed sample of the column contents is taken from the tailings discharge line. (The tailings flow is assumed to be representative of the material in the cell.) From these samples, the solids concentration and tailings flow rate are determined, which will later be used to calculate the probability of collection for the test.

The experiment continues for a period of time (30 minutes) until a sufficient amount of solids have been collected to weigh. The collection tube is then removed from the apparatus and the tailings pump is turned off. The rise times of ten bubbles are again measured and averaged. The resulting value is averaged with the bubble

rise time determined at the beginning of the test to get an overall average, from which D_b can be calculated.

The contents of the collection tube are washed over a Nalgene reusable filter assembly to separate the floated solids from the liquid. The filter paper is then placed in an oven overnight to dry the collected sample. The entire apparatus is cleaned after each test.

2.6.4 Calculation of Probability of Collection

The basic formula for calculation of the experimental probability of particle collection, P , is the amount of solids collected divided by the total amount of solids encountered by the rising bubbles during the test. The first term is found by weighing the material collected on the filter paper from the collection tube. The second term is determined from the experimental conditions, and can be represented as:

$$\left[\frac{\pi}{4} D_b^2 l' \right] [N_b] [c] \quad [2.42]$$

where D_b is the bubble diameter (cm), l' is the effective recovery zone length (cm), N_b is the number of bubbles produced during the test, and c is the solids concentration in the cell (g/cm^3). The first term of Equation [2.42] is the volume swept by a single bubble during its ascent. Multiplying this by N_b gives the total volume swept during the test. Finally, multiplying by c yields the total mass of

particles encountered by the bubbles during the test.

Bubble size, as alluded to in the procedure section, is calculated based on the average measured rise time. The bubble rise velocity, U_b , is computed as the rise distance, 25-cm, divided by the average rise time. Bubble diameter, D_b , can then be calculated from the relationship derived by McCabe and Smith (1976) for a spherical particle settling under intermediate flow conditions:

$$u_t = \frac{0.153 a_e^{0.71} d_p^{1.14} (\rho_p - \rho)^{0.71}}{\rho^{0.27} \mu^{0.43}} \quad [2.43]$$

where a_e is the particle acceleration, d_p is the particle diameter, ρ_p and ρ are particle and fluid densities, and μ is the fluid viscosity. For the experimental conditions normally encountered during the tests, Equation [2.43] simplifies for a rising air bubble to:

$$U_b = 148 (D_b)^{1.14} \quad [2.44]$$

where U_b is in cm/sec and D_b is in cm.

The recovery zone, where bubbles encounter particles, is nominally 30-cm in length. This would also be the effective length, l' , if the tailings flow was zero. The downward fluid flow imposed by the tailings pump, however, retards the buoyant rise of the bubbles and necessitates determination of an increased effective length. To calculate l' , the bubble rise velocity is first corrected to account for the interstitial fluid velocity, u_i :

$$U_b' = U_b - u_t \quad [2.45]$$

A corrected rise time, t' , is then determined as the nominal recovery length divided by the corrected bubble rise velocity. Finally, the effective length can be found by multiplying the original bubble rise velocity and the corrected rise time together.

The number of bubbles, N_b , is calculated by dividing the volume per bubble into the total volume of air used during the test. The volume per bubble is obtained from the bubble diameter, assuming a spherical shape ($V_b = \pi D_b^3/6$). Total air volume for each test can be computed from the chosen flow rate setting for the syringe pump and the duration of the test.

Solids concentration in the experimental cell, c , is determined during the test, as explained above.

2.6.5 Experimental Results and Comparison with Model Predictions

Bubble-particle attachment tests were run for two size classes each of Pittsburgh No. 8 coal and powdered silica. Several tests were performed on each size class in order to obtain an average value for the probability of collection. Results of the experiments are summarized in Table 2.3. The average bubble size was fairly constant for each set of tests, since the same size needle and flow rate were employed.

For a given material, it is seen in Table 2.3 that the probability of collection

Table 2.3 Results of bubble-particle attachment experiments

Sample	Mean Particle Size (μm)	Average Bubble Size (μm)	Number of tests	Average value of P
100 x 150 mesh coal	123.8	907	4	0.0169
200 x 270 mesh coal	62.6	919	5	0.0072
250 x 270 mesh silica	57.8	954	5	0.0138
325 x 400 mesh silica	40.4	944	6	0.0103

increases with particle size, as predicted theoretically (Figure 2.5). Also, the density effect (Figure 2.7) is demonstrated in Table 2.3. The two silica samples both had higher experimental values of P than the 200 x 270 mesh coal sample, even though the particle size was smaller.

In order to run the simulator and compare the theoretical P with the experimental P , the material characteristics of the coal and silica samples were determined. The values used in the computer program are tabulated in Table 2.4.

The simulation results are shown in Figures 2.12-2.15 as EFT versus R_0 graphs. The simulations were performed as a function of the structural constant to determine in what ranges attachment was possible. Figure 2.12, for the 100 x 150 mesh coal sample, shows that attachment will occur only if C is less than -1.5 mJ/m^2 . The arrow represents the value of R_c corresponding to the experimental probability of collection (as found from Eq. [2.39]). If values of $C = -1.8 \text{ mJ/m}^2$ and $D_0 = 10.3 \text{ nm}$ are assumed to characterize this coal, the agreement between experiment and theory should be fairly close, i.e., the arrow should correspond to the point where the curve for $C = -1.8 \text{ mJ/m}^2$ rises from the x-axis. The dashed line to the right represents a simulation without surface forces and with $\beta = 1$ at all separation distances. The difference in R_c is substantial, again emphasizing the pronounced effect of the film thinning resistance force and the surface forces.

Figure 2.13 illustrates the experimental and simulation results for the 200 x 270 mesh coal fraction. In this case, the arrow corresponds to a value of C between

Table 2.4 Material characteristics of coal and silica samples used in bubble-particle attachment experiments.

Sample	Mean Particle Size (μm)	Particle density (g/cm^3)	Particle charge, ζ_p (mV)	Hamaker Constant, A_{132} (J)
100 x 150 mesh coal	123.8	1.30	-55	$-1.42 \cdot 10^{-20}$
200 x 270 mesh coal	62.6	1.30	-55	$-1.42 \cdot 10^{-20}$
250 x 270 mesh silica	57.8	2.65	-30	$-1.60 \cdot 10^{-20}$
325 x 400 mesh silica	40.4	2.65	-30	$-1.60 \cdot 10^{-20}$

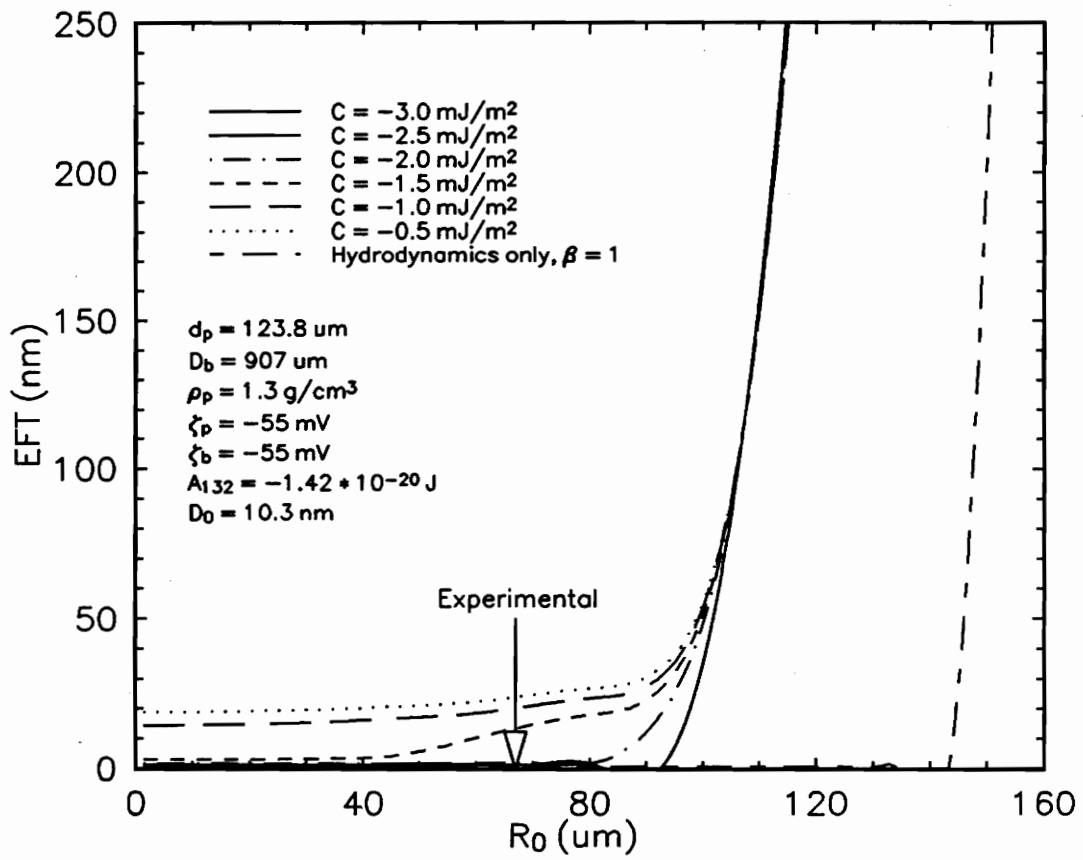


Figure 2.12 Simulation results for 100 x 150 mesh coal sample used in experiments.

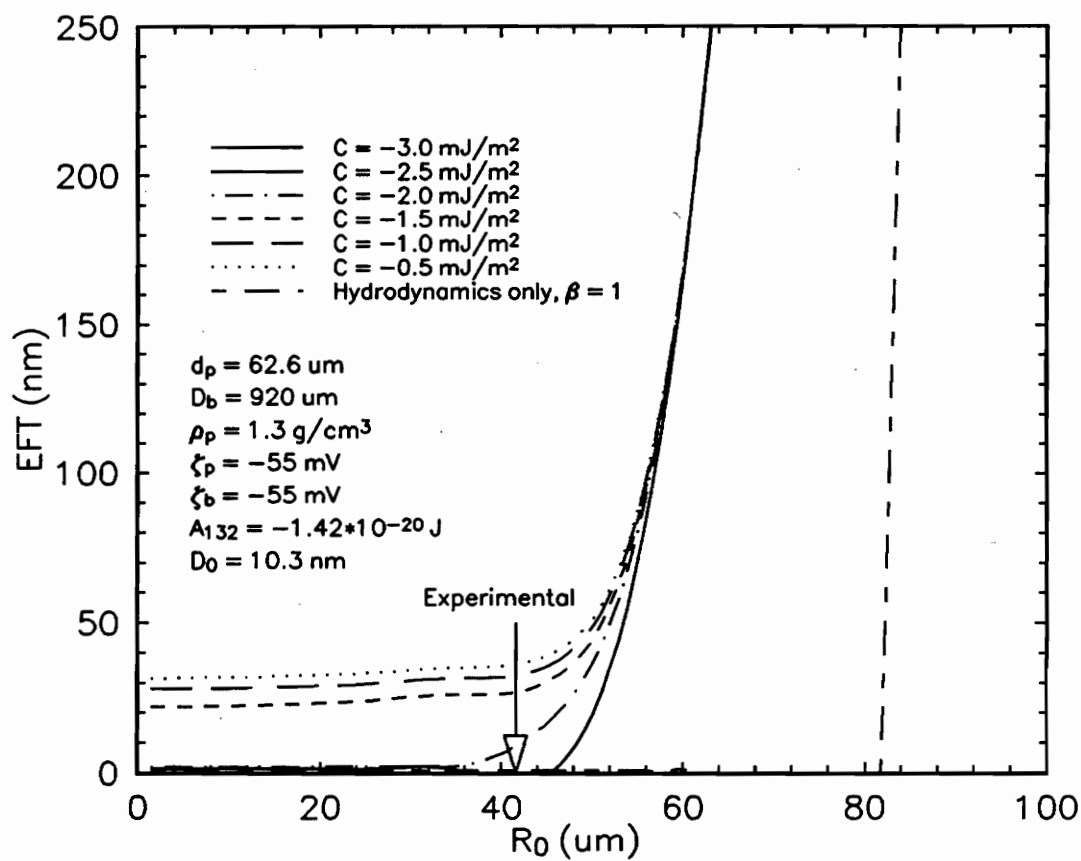


Figure 2.13 Simulation results for 200 x 270 mesh coal sample used in experiments.

-2.0 and -2.5 mJ/m². Therefore, either the finer coal sample is more hydrophobic (with a more negative C), or the experimental P value is slightly high. Since the larger size class (100 x 150 mesh) correlated so well with the model results, it is believed that the experimental P value for the 200 x 270 mesh coal sample is inflated. A lower P_{exp} would equate with a smaller value of R_c, shifting the arrow to the left, closer to where a simulation for C = -1.8 mJ/m² would be situated.

Figures 2.14 and 2.15, simulations for the two silica size fractions, are markedly different from Figures 2.12 and 2.13. The relatively small zeta potentials for the bubble and particle produce a rather weak electrostatic force which is easily overcome by the structural force at nearly all values of C. In these cases, the curve for C = -1.8 mJ/m² would be identical to the other curves for which EFT got to zero. It is seen, then, that the critical starting distances are quite similar for both the experimental and theoretical situations. The arrow is close to the point where the curves rise from the x-axis.

An overall comparison between the experimental data and the computer simulation results is presented in Figure 2.16. The experimental probability of collection (P_{exp}) is plotted versus the theoretical probability of collection (P_{th}). Ideally, this should produce a line with slope equal to one, signifying a perfect match between P_{exp} and P_{th}. The four data points shown in Figure 2.16, although not right on the line, indicate a rather good correlation between experimental results and model predictions.

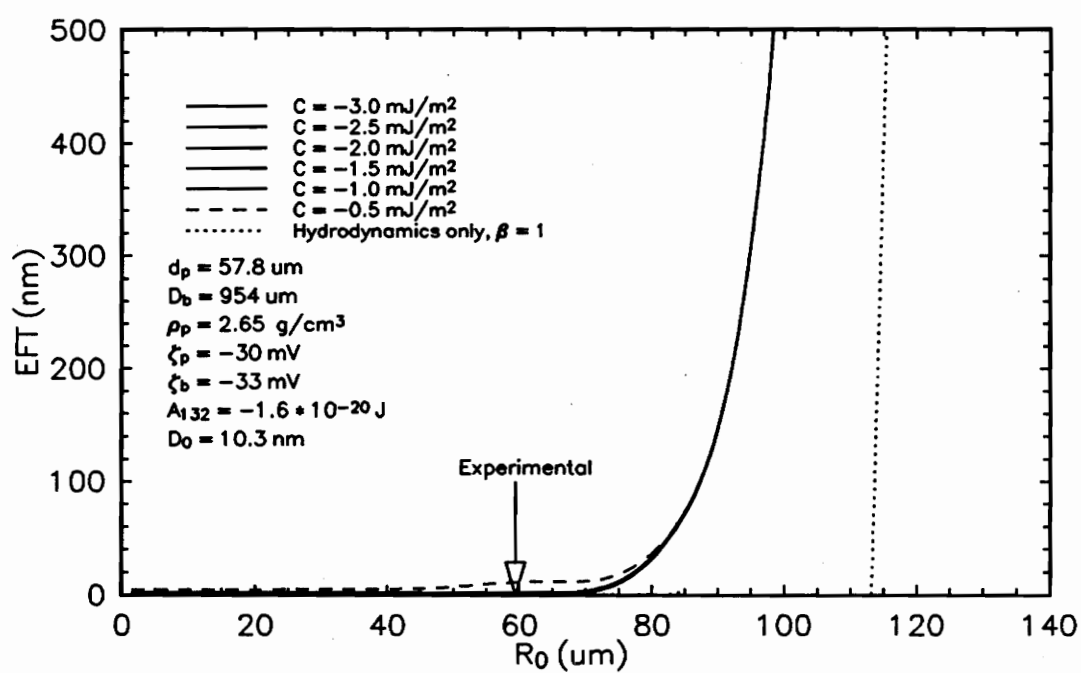


Figure 2.14 Simulation results for 250 x 270 mesh silica sample used in bubble-particle attachment experiments.

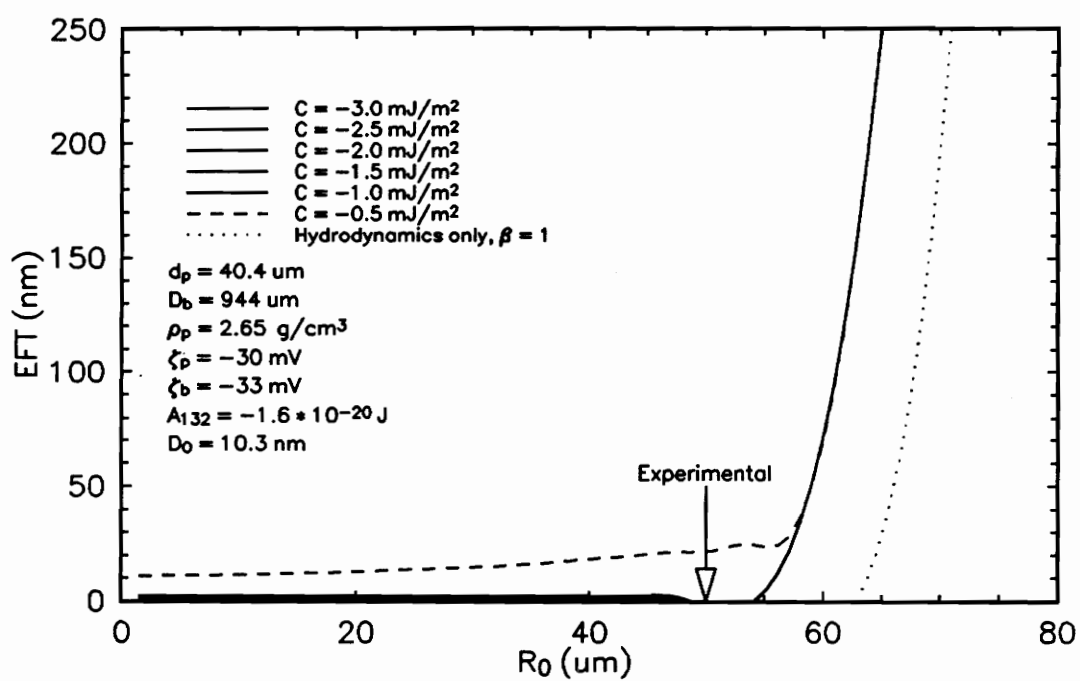


Figure 2.15 Simulation results for 325 x 400 mesh silica sample used in bubble-particle attachment experiments.

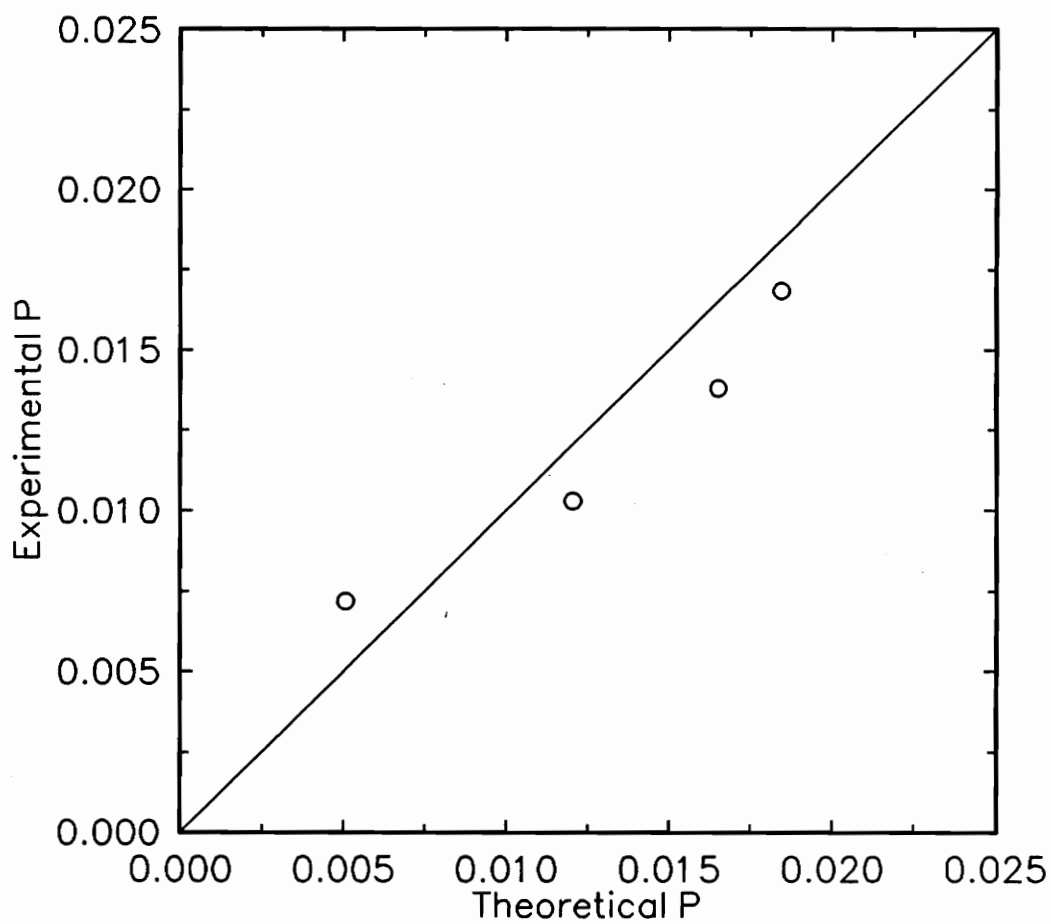


Figure 2.16 Comparison between experimental and theoretical values for the probability of particle collection.

2.6.6 Regions of flotation

As illustrated previously, the interaction model developed in this work is quite effective for predicting whether or not bubble-particle attachment is possible for a given set of initial conditions. By utilizing the computer simulator for various ranges of the model parameters, regions where flotation is viable can be identified.

Simulation results for a 10 μm diameter particle and a 100 μm diameter bubble at numerous values of C and ζ_p are depicted in Figure 2.17. The plot shows several contours, representing equilibrium film thicknesses of 0, 10, 30, and 50 nm. For any chosen combination of C and ζ_p , the EFT can be determined using Figure 2.17. The area bounded by the $\text{EFT} = 0$ contour represents the region where bubble-particle attachment, and subsequent flotation, is possible.

The general relationships exhibited in Figure 2.17 conform to theoretical expectations. It is seen that flotation becomes more likely (EFT approaching zero) as the structural constant increases negatively, indicating a more hydrophobic material, and as the particle zeta potential is reduced (towards zero), indicating a less charged surface. These factors correspond to a higher value of the attractive structural force (F_s), and a lower value of the repulsive electrostatic force (F_e), respectively. The overall effect is an increased attractive force, which enhances the chances for bubble-particle attachment.

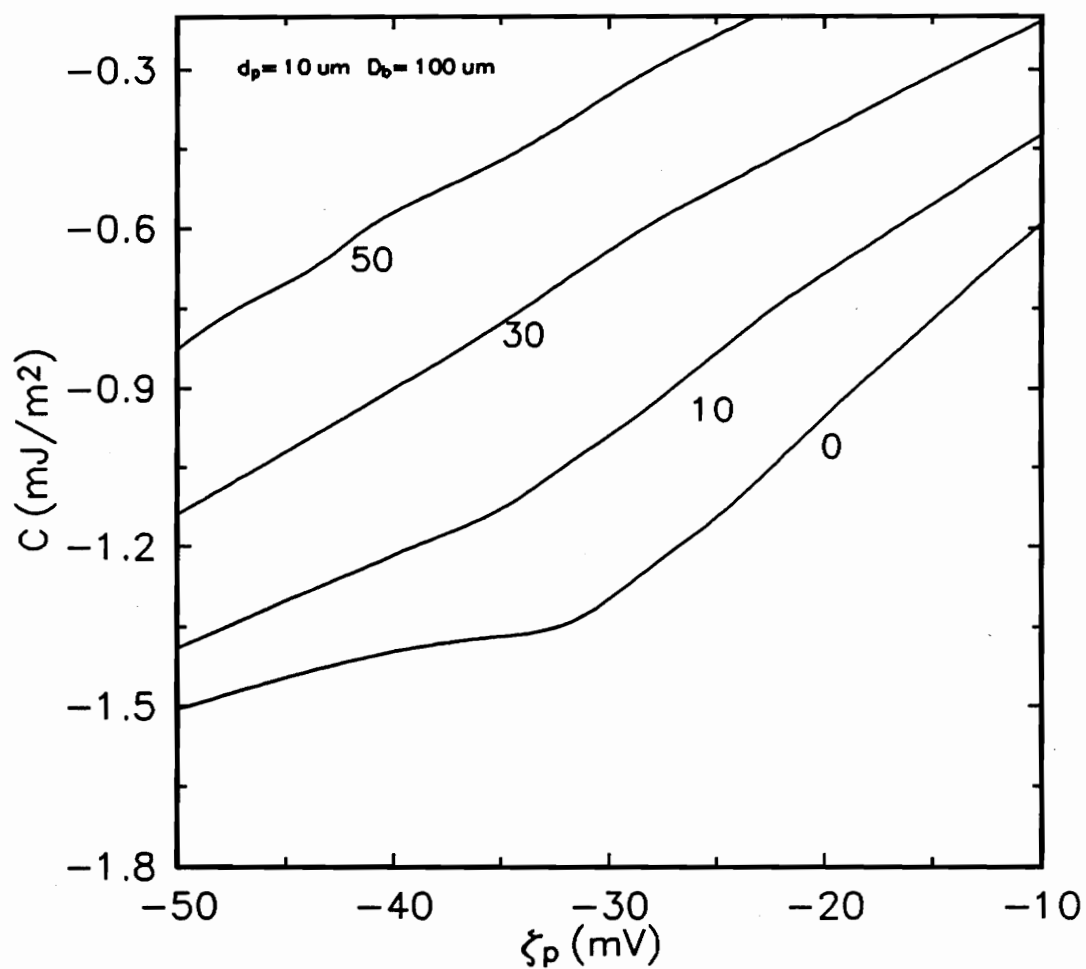


Figure 2.17 Contour plot of equilibrium film thickness showing viable regions of flotation as a function of the structural constant and the particle zeta potential.

2.7 Conclusions

1. A fundamental model for flotation has been developed which considers both the hydrodynamic and surface forces involved in the bubble-particle interaction. These forces have been studied independently in previous investigations, but the model developed herein is the first known attempt to incorporate both types of forces into a single model for flotation. Expressions for each of the forces have been included in a dynamic force balance, from which the theoretical trajectory of the particle has been constructed.
2. Using the particle trajectory determined from the force balance, the closest approach distance between the surfaces of the bubble and particle has been determined for a given set of physical and chemical conditions. This distance has been referred to as the equilibrium film thickness (EFT). Bubble-particle attachment is assumed to occur when $EFT=0$. This criterion has been used to calculate the theoretical probability of bubble-particle attachment (P). This expression defines P as the fraction of particles in the path of the rising bubble that actually become attached.
3. The simulator can be used to quickly evaluate the effects of changes in any number of relevant physical and chemical variables in flotation. Simulations have shown that an increase in the particle size or density, or a decrease in

the bubble size, resulted in a greater probability of bubble-particle attachment. The probability of attachment also increased as the particle hydrophobicity increased and as the particle charge was reduced. These improvements can be directly attributed to changes in the hydrodynamic and surface forces which control the bubble-particle interaction.

4. The benefits of using small bubbles for flotation were demonstrated using the bubble-particle interaction model. The theoretical probability of particle collection increased substantially as the bubble size was reduced. Simulations also revealed that the actual volume of pulp swept by an individual bubble is relatively independent of bubble size. For example, a 200 μm bubble has a cross-sectional area four times greater than a 100 μm bubble, but encounters the same number of particles.
5. Experimental measurements of the probability of collection were performed for coal and silica samples of various sizes. Bubble-particle attachment tests were conducted in a frothless flotation cell to directly investigate the collection process. The experimental values of P correlated well with the values of P predicted by the model.
6. The interaction model was useful for identifying regions where bubble-particle

attachment, and subsequent flotation, was possible. For example, the simulator was able to predict various combinations of C and ζ_p that would result in successful bubble-particle attachment. Similar predictions can also be made for bubble size, particle density, etc. This technique can be used to identify the optimum operating conditions for a given flotation system.

2.8 References

- Ahmed, N., and Jameson, G.J., 1985, "The Effect of Bubble Size on the Rate of Flotation of Fine Particles," *International Journal of Mineral Processing*, Volume 8, p. 289.
- Anfruns, J.F., and Kitchener, J.A., 1977, "Rate of Capture of Small Particles in Flotation," *Transactions of the Institute of Mining and Metallurgy*, Section C, Volume 86, p. C9.
- Brenner, H., 1964, "The Stokes Resistance of an Arbitrary Particle - IV. Arbitrary Fields of Flow," *Chemical Engineering Science*, Volume 19, p. 703.
- Christenson, H.K., 1988, "Non-DLVO Forces between Surfaces - Solvation and Capillary Effects," *Journal of Dispersion Science Technology*, Volume 9, p. 171.
- Churaev, N.V., and Derjaguin, B.V., 1985, "Inclusion of Structural Forces in the Theory of Stability of Colloids and Films," *Journal of Colloid and Interface Science*, Volume 103, Number 2, p. 542.
- Claesson, P.M., 1987, "Experimental Evidence for Repulsive and Attractive Forces Not Accounted for by Conventional DLVO Theory," *Progress in Colloid and Polymer Science*, Volume 74, p. 48.
- Clift, R.C., Grace, J.R., and Weber, M.E., 1978, *Bubbles, Drops, and Particles*, Academic Press, New York, N.Y.
- Davis, E.G., Hansen, J.P., and Sullivan, G.V., 1980, "Attrition Microgrinding," in *Fine Particles Processing*, Volume 1, P. Somasundaran, editor, American Institute of Mining Engineering, New York, N.Y., p. 74.
- Derjaguin, B.V., and Dukhin, S.S., 1961, "Theory of Flotation of Small and Medium Size Particles," *Transactions of the Institute of Mining and Metallurgy*, Volume 70, p. 221.
- Derjaguin, B.V., and Kussakov, M., 1939, "Anomalous Properties of Thin Polymolecular Films," *Acta Physicochimica U.S.S.R.*, Volume 10, Number 1, p. 26.

Development of the Selective Coagulation Process, Technical Progress Report, September-December 1990, Department of Energy Contract Number DE-AC22-90PC90174, R.-H. Yoon and G.H. Luttrell, Principal Investigators, Virginia Polytechnic Institute and State University, Blacksburg, VA.

Dobby, G.S., and Finch, J.A., 1986, "A Model of Particle Sliding Time for Flotation Size Bubbles," *Journal of Colloid and Interface Science*, Volume 109, Number 2, p. 493.

Dobby, G.S., and Finch, J.A., 1987, "Particle Size Dependence in Flotation Derived from a Fundamental Model of the Capture Process," *International Journal of Mineral Processing*, Volume 21, p. 241.

Eigeles, M.A., and Volova, M.L., 1960, "Kinetic Investigation of Effect of Contact Time, Temperature, and Surface Condition on the Adhesion of Bubbles to Mineral Surfaces," in *Proceedings*, Fifth International Mineral Processing Congress, Institute of Mining and Metallurgy, London, p. 271.

Evans, L.F., 1954, Bubble-Mineral Attachment in Flotation," *Industrial and Engineering Chemistry*, Volume 46, p. 2420.

Finch, J.A., and Dobby, G.S., 1990, *Column Flotation*, Pergamon Press, New York, N.Y.

Flint, L.R., and Howarth, W.J., 1971, "The Collision Efficiency of Small Particles with Spherical Air Bubbles," *Chemical Engineering Science*, Volume 26, p. 1155.

Fonda, A., and Herne, H., 1957, *Mining Research Establishment Report Number 2068*, United Kingdom National Coal Board.

Fuerstenau, D.W., 1980, "Fine Particle Flotation," in *Fine Particles Processing*, Volume 1, P. Somasundaran, editor, American Institute of Mining Engineering, New York, N.Y., p. 669.

Gaudin, A.M., 1932, *Flotation*, McGraw-Hill Book Company, New York, N.Y.

Gaudin, A.M., 1957, *Flotation*, Second Edition, McGraw-Hill Book Company, New York, N.Y.

Gaudin, A.M., Schuhmann, R., and Schlechten, A.W., "Flotation Kinetics II. The Effect of Size on the Behavior of Galena Particles," *Journal of Physical Chemistry*, Volume 46, p. 902.

Goren, S.L., and O'Neill, M.E., 1971, "On the Hydrodynamic Resistance to a Particle of a Dilute Suspension when in the Neighborhood of a Large Obstacle," *Chemical Engineering Science*, Volume 26, p. 325.

Hamaker, H.C., 1937, "The London-van der Waals Attraction between Spherical Particles," *Physica*, Volume 4, p. 1058.

Hernandez, J.L.Y., 1989, *Ph.D. Dissertation*, Virginia Polytechnic Institute and State University, Blacksburg, VA.

Herne, H., 1960, *Air and Water Pollution*, Volume 3, p. 26.

Hocking, L.M., 1960, "The Theoretical Collision Efficiency of Small Drops," *International Journal of Air Pollution*, Volume 13, p. 154.

Hogg, R., Healy, T.W., and Fuerstenau, D.W., 1966, "Mutual Coagulation of Colloidal Dispersions," *Transactions of the Faraday Society*, Volume 62, p. 1638.

Israelachvili, J., and Pashley, R., 1982, "The Hydrophobic Interaction is Long Range, Decaying Exponentially with Distance," *Nature*, Volume 300, p. 341.

Jiang, Z.W., and Holtham, P.N., 1986, "Theoretical Model of Collision between Particles and Bubbles in Flotation," *Transactions of the Institute of Mining and Metallurgy*, Volume 95, p. C187.

Jowett, A., 1980, "Formation and Disruption of Particle-Bubble Aggregates in Flotation," in *Fine Particles Processing*, Volume 1, P. Somasundaran, editor, American Institute of Mining Engineering, New York, N.Y., p. 720.

Kawaguti, M., 1955, "The Critical Reynolds Number for the Flow Past a Sphere," *Journal of the Physical Society of Japan*, Volume 10, August, p. 694.

Lai, R.W., and Fuerstenau, D.W., 1976, "Model for the Surface Charge of Oxides and Flotation Response," *Transactions AIME*, Volume 260, p. 104.

Laskowski, J., and Kitchener, J.A., 1969, "The Hydrophilic-Hydrophobic Transition on Silica," *Journal of Colloid and Interface Science*, Volume 29, Number 4, p. 670.

Laskowski, J., 1989, "Thermodynamic and Kinetic Flotation Criteria," *Mineral Processing and Extractive Metallurgy Review*, Volume 5, p. 25.

London, F., 1937, "The General Theory of Molecular Forces," *Transactions of the Faraday Society*, Volume 33, p. 8.

Luttrell, G.H., 1986, *Ph.D. Dissertation*, Virginia Polytechnic Institute and State University, Blacksburg, VA.

Luttrell, G.H., and Yoon, R.-H., 1988, "Determination of the Probability of Bubble-Particle Adhesion Using Induction Time Measurements," in *Production and Processing of Fine Particles*, A. Plumpton, editor, Pergamon Press, Toronto, p. 159.

Luttrell, G.H., and Yoon, R.-H., 1992, "A Hydrodynamic Model for Bubble-Particle Attachment," Personal Communication, Virginia Center for Coal and Mineral Processing, Blacksburg, Virginia.

Masliyah, J.H., 1970, *Ph.D. Dissertation*, University of British Columbia, Vancouver.

Masliyah, J.H., and Epstein, N., 1972, "Numerical Solution of Heat and Mass Transfer from Spheroids in Steady Axisymmetric Flow," *Progress in Heat and Mass Transfer*, Volume 6, p. 613.

Maude, A.D., 1961, *British Journal of Applied Physics*, Volume 12, p. 242.

McCabe, W.L., and Smith, J.C., 1976, *Unit Operations of Chemical Engineering*, Third Edition, McGraw-Hill Book Company, New York, N.Y., p. 155.

Mika, T.S., and Fuerstenau, D.W., 1969, "A Microscopic Model of the Flotation Process," in *Proceedings*, Eighth International Mineral Processing Congress, Leningrad, Volume II, p. C9.

Pearcey, T., and Hill, G.W., 1957, "A Theoretical Estimate of the Collection Efficiencies of Small Droplets," *Quarterly Journal of the Royal Meteorological Society*, Volume 83, p. 77.

Philippoff, W., 1952, "Some Dynamic Phenomena in Flotation," *Transactions AIME*, Volume 193, p. 386.

Plate, H., 1989, *Thesis*, Akademie der Wissenschaften der DDR, Forschungsinstitut für Aufbereitung, Freiburg, German Democratic Republic.

Reay, D, and Ratcliff, G.A., 1973, "Removal of Fine Particle from Water by Dispersed Air Flotation: Effects of Bubble Size and Particle Size on Collection Efficiency," *Canadian Journal of Chemical Engineering*, Volume 51, p. 178.

Schenkel, J.H., and Kitchener, J.A., 1960, "A Test of the Derjaguin-Verwey-Overbeek Theory with a Colloidal Suspension," *Transactions of the Faraday Society*, Volume 56, p. 161.

Schuch, G., and Löffler, F., 1978, *Verfahrenstechnik*, Mainz, Volume 12, p. 302.

Schuhmann, R., 1942, "Flotation Kinetics I. Methods for Steady-state Study of Flotation Problems," *Journal of Physical Chemistry*, Volume 46, p. 891.

Schulze, H.J., 1989, "Hydrodynamics of Bubble-Mineral Particle Collision," in *Frothing in Flotation*, J. Laskowski, editor, Gordon and Breach Science Publishers, New York, N.Y., p. 43.

Seeley, L.E., Hummel, R.L., and Smith, J.W., 1975, "Experimental Velocity Profiles in Laminar Flow Around Spheres of Intermediate Reynolds Numbers," *Journal of Fluid Mechanics*, Volume 68, Part 3, p. 591.

Shafir, U., and Neiburger, N., 1964, "Collision Efficiencies of Two Spheres Falling in a Viscous Medium," *Journal of Geophysical Research*, Volume 68, p. 4141.

Smith, R.W., and Akhtar, S., 1976, "Cationic Flotation of Oxides and Silicates," in *Flotation: A.M. Gaudin Memorial Volume*, M.C. Fuerstenau, editor, Volume 1, p. 21.

Sutherland, K.L., 1948, "Physical Chemistry of Flotation XI. Kinetics of the Flotation Process," *Journal of Physical Chemistry*, Volume 52, p. 394.

Taylor, G.I., 1925, quoted in: Hardy, W., and Bircumshaw, I., "Boundary Lubrication - Plane Surfaces and the Limitation of Amonton's Law," *Proceedings of the Royal Society*, Volume 108-A, p. 1.

Trahar, W.J., 1981, "A Rational Interpretation of the Role of Particle Size in Flotation," *International Journal of Mineral Processing*, Volume 14, p. 195.

Weber, M.E., and Paddock, D., 1983, "Interceptional and Gravitational Collision Efficiencies for Single Collectors at Intermediate Reynolds Numbers," *Journal of Colloid and Interface Science*, Volume 94, Number 2, p. 328.

Woo, S.W., 1971, *Ph.D. Dissertation*, McMaster University, Hamilton, Ontario.

Xu, Z., and Yoon, R.-H., 1989, "The Role of Hydrophobic Interactions in Coagulation," *Journal of Colloid and Interface Science*, Volume 132, Number 2, p. 532.

Xu, Z., 1990, *Ph.D. Dissertation*, Virginia Polytechnic Institute and State University, Blacksburg, VA.

Xu, Z., and Yoon, R.-H., 1990, "A Study of Hydrophobic Coagulation," *Journal of Colloid and Interface Science*, Volume 134, Number 2, p. 427.

Ye, Y., and Miller, J.D., 1988, "Bubble/Particle Contact Time in the Analysis of Coal Flotation," *Coal Preparation*, Volume 5, p. 147.

Yoon, R.-H., 1991, "Hydrodynamic and Surface Forces in Bubble-Particle Interactions," *Aufbereitungs Technik*, Volume 32, Number 9, p. 474.

Yoon, R.-H., and Luttrell, G.H., 1986, "The Effect of Bubble Size on Fine Coal Flotation," *Coal Preparation*, Volume 2, p. 179.

Yordan, J.L., and Yoon, R.-H., 1989, "Induction Time Measurements for a Coal Flotation System," Personal Communication, Virginia Center for Coal and Mineral Processing, Blacksburg, Virginia.

Chapter 3 Mixing Characterization

3.1 Introduction

The increased implementation of column flotation into mineral processing and coal preparation circuits around the world is testament to the improved efficiency this technology offers. Flotation columns, operating countercurrent with wash water, reduce the amount of nonselective entrainment into the froth, thereby enhancing product grade. Flotation columns are capable of achieving similar recoveries as conventional flotation cells, but at higher product grades. Furthermore, the relatively quiescent environment associated with column flotation enables fine air bubbles to be produced for the recovery of fine-sized particles, which are difficult to recover conventionally (Kawatra and Eisele, 1987; Reddy et al., 1988; Luttrell et al., 1988; Al Taweel and Kasireddy, 1989). The large bubbles inherent to conventional flotation are unable to capture fine particles efficiently because of hydrodynamic considerations.

Mine operators, particularly in the coal industry, have come to realize that their plants, founded on dated processing technology, often function inefficiently and discard considerable amounts of profitable product. Fines are commonly disposed of without any treatment, and the recovery devices require multiple stages to attain

prescribed grade and recovery levels. Column flotation technology can alleviate these shortcomings. However, incorporation of a flotation column into a plant circuit is not a simple process. Proper scale-up is essential to insure efficient operation and performance in the plant environment, and scale-up criteria derived with this in mind should be more useful. Several scale-up techniques have been investigated (Boutin and Wheeler, 1967; Mathieu, 1972; Deister Concentrator Company, Inc., 1989; Dobby and Finch, 1985; Luttrell et al., 1988; Mankosa et al., 1990), and three important parameters are generally identified, i.e., flotation rate constant, particle retention time, and axial mixing. Of these, the third term has received the least attention in flotation research.

3.2 Literature Review

The bulk of the previous research into the characterization of column mixing has been conducted by chemical engineers investigating bubble column reactors. Numerous practical applications exist in which representation of the mixing is important. Bubble column reactors have been successfully employed in absorption, oxidation, chlorination, and hydrogenation systems, as well as for waste water treatment, biological cell production, and coal liquefaction (Shah et al., 1982). This diversity is indicative of the widespread effectiveness of bubble column contactors. Indeed, the advent of column flotation in the 1960's was an extension of the concepts involved in bubble column reactors to the field of mineral processing.

The design and scale-up of bubble column reactors requires reasonable estimates of numerous parameters related to holdup, mass transfer, heat transfer, and mixing. A review paper by Shah et al. (1982) addresses parameter estimation in great detail. Flow regimes and bubble dynamics are investigated, and a host of nonadjustable parameters are examined, based on available literature results. Proposed relationships governing these parameters in bubble column contactors are critically evaluated, and the authors offer their recommendations. These relationships, however, may not necessarily hold for column flotation applications. Geometry and operating conditions differ widely between column flotation and bubble column contactors, highlighting the need for in-depth examination of mixing in flotation columns.

In order to examine and characterize mixing, a valid experimental technique is required. Extensive work by chemical engineers studying bubble column reactors led to the analysis of residence time distributions (RTD) for mixing quantification. Levenspiel (1972) discusses RTD analysis thoroughly in his text, describing in detail how to determine the mixing parameters from the exit age distribution (i.e., the RTD). For column flotation studies, the axial dispersion model is commonly employed:

$$E \frac{\partial^2 C}{\partial x^2} - u_1 \frac{\partial C}{\partial x} - \frac{\partial C}{\partial t} = 0 \quad [3.1]$$

where E is the liquid axial dispersion coefficient and u_1 is the interstitial liquid

velocity. Mixing can then be characterized by two values: the mean residence time, τ , and the Peclet number, $Pe = u_1 L / E$, where L is the column length.

Although the axial dispersion model has been extensively utilized with good success for mixing characterization of flotation columns (Rice et al., 1974; Rice et al., 1981; Dobby and Finch, 1985; Mankosa, 1990; Xu et al., 1991), several investigators have questioned its validity. For example, Mavros et al. (1989) and Goodall and O'Connor (1990) have developed tanks-in-series models which fit their experimental data more closely than the dispersion model. Additional work is required to resolve this controversy.

Recent research into characterization of the liquid flows in column flotation has allowed a more accurate determination of axial mixing to be made. Field and Davidson (1980), Dobby and Finch (1986) and Mankosa (1990), for example, have quantified the axial dispersion parameter in terms of the column geometry and operating conditions (gas and liquid flow rates). Accurate characterization of the mixing also allows better estimates of flotation performance to be made. Recovery can be predicted from Levenspiel's equation, which is a function of the mixing parameters, τ and Pe , and the flotation rate constant, k :

$$R = 1 - \frac{4 a \exp \left(-\frac{Pe}{2} \right)}{(1+a)^2 \exp \left[\left(\frac{a}{2} \right) Pe \right] - (1-a)^2 \exp \left[\left(-\frac{a}{2} \right) Pe \right]} \quad [3.2]$$

where:

$$a = \sqrt{\frac{1 + 4 k \tau}{Pe}} \quad [3.3]$$

Since it is recovery of the *solids* that is desired, mixing parameters of the solids should be obtained. Commonly, however, investigators have assumed the mixing parameters of the solids to be equivalent to those of the liquid. A simple liquid RTD would then be sufficient to characterize the mixing for a given system.

Dobby and Finch (1985) realized that the residence time of the solids may differ from the residence time of the liquid due to the finite size and density of the solid particles. They proposed a correction equation for τ_s given by:

$$\tau_s = \tau_l \left[\frac{u_l}{u_l + u_s} \right] \quad [3.4]$$

where τ_l is the liquid residence time, u_l is the interstitial liquid velocity, and u_s is the terminal settling velocity of the solids. If necessary, the terminal solids settling velocity can further be corrected to account for percent solids, using Richardson and Zaki's formula (1954):

$$u_{s\phi} = u_s(1 - \phi)^m \quad [3.5]$$

where $u_{s\phi}$ is the corrected settling velocity, ϕ is the volume fraction solids, and m is a constant that varies with the Reynolds number. Dobby and Finch tested their equation by conducting tracer tests on a mineral sample ($\rho_p = 5.19 \text{ g/cm}^3$) over a range of particle sizes (-100 mesh). Using fluorescein dye and solid size fractions as tracers, they found that the measured and predicted solids residence times were quite

close. However, the validity of Dobby and Finch's equation at coarser sizes and different solids densities is unknown.

3.3 Research Objectives

The major objective of the present work was to conduct RTD tests over a wide range of particle sizes and densities and compare the experimental solids residence times with Dobby and Finch's calculated values. A secondary objective was to determine whether the degree of mixing, characterized by the Peclet number, was the same for both the solids and the liquid. Rice et al. (1974), Dobby and Finch (1985), and Kho and Sohn (1989) have investigated this claim for -100 mesh material, and all concluded that $Pe_s = Pe_l$. The work presented in this chapter examines their conclusions by considering different densities and a wider particle size range.

An additional aim, relating to the overall objective of this research, was the union of the bubble-particle interaction model developed in chapter 2 with the mixing characterization studies described in this chapter. The flotation rate constant, k , obtained from the interaction model, can be combined with the values of Pe and τ through Levenspiel's equation in order to predict recovery from first principles. This achievement would represent a significant advance in the development of fundamental model describing flotation.

3.4 Experimental

3.4.1 Samples

Floated silica was obtained from Fisher Scientific Company, averaging $65\ \mu\text{m}$ in diameter. The samples were then wet screened into several size fractions, down to 400 x 500 mesh. Subsequently, the -500 mesh material was beaker decanted into a $25 \times 10\ \mu\text{m}$ size class. Narrowly-sized 5 and $10\ \mu\text{m}$ silica samples were purchased from U.S. Silica Corporation for very fine size tests.

Coal samples were from the Pittsburgh No. 8 coal seam in West Virginia. A 1.3 specific gravity float/sink with magnetite was conducted to remove any rock and heavy waste material. The floated coal was then wet screened into the same size classes as the silica. All the samples were sealed in bags to prevent contamination until the tests were performed.

3.4.2 Reagents

Dowfroth M150 (polypropylene glycol methyl ether, molecular weight = 400 g/mole), supplied by Dow Chemical Company, was used for all RTD tests. This frother has been shown to effectively stabilize bubble size and froth characteristics (Trigg, 1984).

Fisher Scientific Company provided certified ACS grade potassium chloride (KCl), a salt tracer which enabled liquid RTD construction from conductivity values. Potassium chloride has been widely incorporated in mixing studies (Rice et al., 1981;

Rice et al., 1974; Mavros et al., 1989; Kho and Sohn, 1989; Mankosa, 1990; Xu et al., 1991) because of its simplicity and handling ease. Other liquid tracers include fluorescein dye (Dobby and Finch, 1985), hydrochloric acid (Ityokumbul et al., 1988), and radioactive tracers (Field and Davidson, 1980; Goodall and O'Connor, 1991).

Aero 633 Depressant from American Cyanimid was used to depress the coal samples prior to conducting an RTD experiment with coal as the solid tracer. A flotation product was not desired because any flow split would complicate the analysis using the axial dispersion model.

3.4.3 Equipment

The complete experimental set-up is illustrated in Figure 3.1. A two-inch diameter plexiglass column with a length-to-diameter ratio of 20:1 was employed for all RTD tests. Simulated feed, a water-frother mixture ($10 \mu\text{l/liter}$), was pumped into the column with a peristaltic pump through the feed inlet located about 18 inches below the froth overflow lip. Bubbles were produced with a porous sparger connected to the laboratory air supply.

A Honeywell level controller maintained constant liquid level in the column. Based on the reading from the pressure transducer, the controller made adjustments to match its set point. A current signal was output to the pneumatic valve attached to the base of the column. The current signal was converted into a pressure value by the current-to-pressure (I/P) unit, and the pressure was then amplified by the

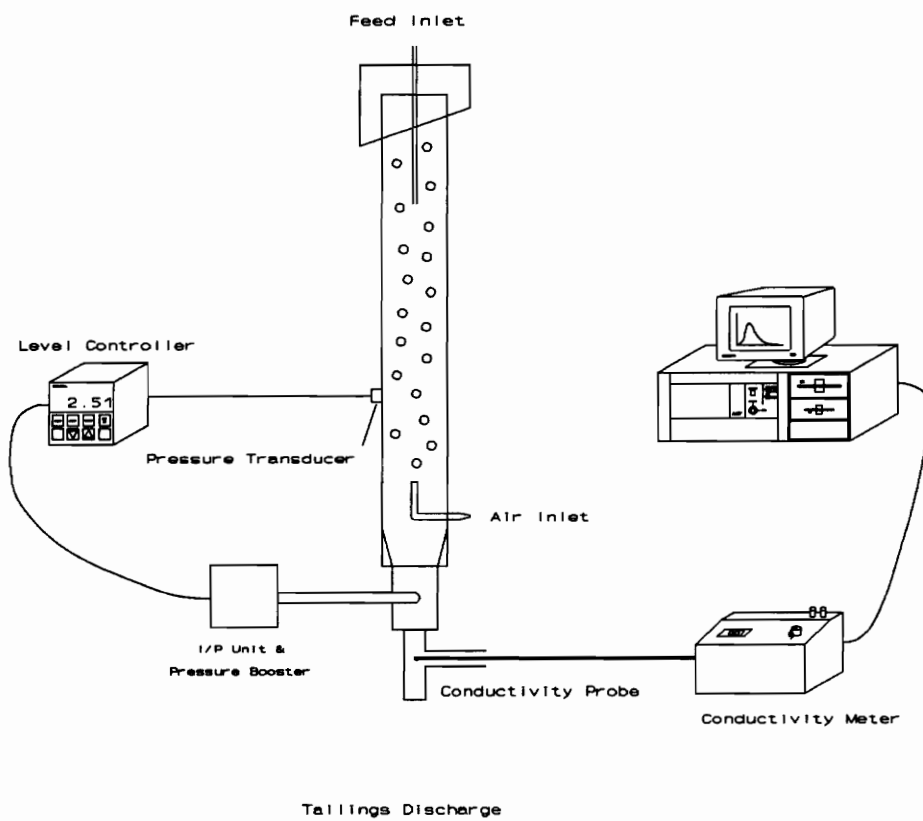


Figure 3.1 Schematic of experimental apparatus used for determining solid and liquid residence time distributions in a flotation column.

booster assembly to actuate the valve.

A plastic T connector acted as the tailings discharge line, into which a conductivity probe was inserted. The conductivity signal was transmitted to a YSI model 32 conductivity meter, where the value was displayed. The conductivity meter was interfaced with a DASH-8 data collection card and a software program on board an IBM personal computer. Sampling rates up to 10 Hz could be accommodated by the LABTECH Acquire software package utilized. Time and conductivity values were stored on disk for future analysis.

3.4.4 Procedure

To conduct an RTD test, a liquid-solid tracer mixture was injected as an idealized pulse a few inches below the overflow lip. The tracer consisted of 30 mL of 20% by weight KCl solution and 20-25 gm of a sized hydrophilic solids fraction, either silica or coal. The liquid RTD was obtained by monitoring the conductivity of the tailings discharge until the tracer had completely exited the column. Solids RTDs were constructed by collecting timed fractions of the column contents in beakers. The water was then evaporated from each beaker to obtain an accurate mass determination of solids in each time interval. From the masses collected, the RTD was produced.

Fractional air hold-up, ϵ , was measured for each test in order to determine the interstitial liquid velocity, $u_i = V_i / (1-\epsilon)$. The pressure difference between the

transducer and atmospheric pressure allowed air hold-up to be calculated.

3.5 Data Analysis

An approach similar to that of Rice et al. (1974) was utilized to analyze the data. The residence time, for either the liquid or the solids, is calculated from the moments of the residence time distribution:

$$\tau = \frac{\int C_i t_i dt}{\int C_i dt} \quad [3.6]$$

where C_i represents the concentration (or conductivity) at time t_i . Simpson's Rule is used to estimate the value of the integrals. Typical RTDs for the liquid and the solid in a given test are exhibited in Figures 3.2 and 3.3, respectively. The liquid RTD is in terms of conductivity, while the solids RTD is in terms of the amount of solid tracer collected in a given time period.

The Peclet number is determined from the time domain solution of the axial dispersion model, derived by Rice et al. (1974):

$$C(t) = \sqrt{\frac{Pe\tau}{4\pi t^3}} \exp\left[\frac{Pe}{4}\left(2 - \frac{t}{\tau} - \frac{\tau}{t}\right)\right] \quad [3.7]$$

A least squares analysis is used to determine the Peclet number which minimizes the difference between the experimental values of $C(t)$ and the theoretical values determined from Equation [3.7].

Numerous authors suggest the use of weighting factors when analyzing

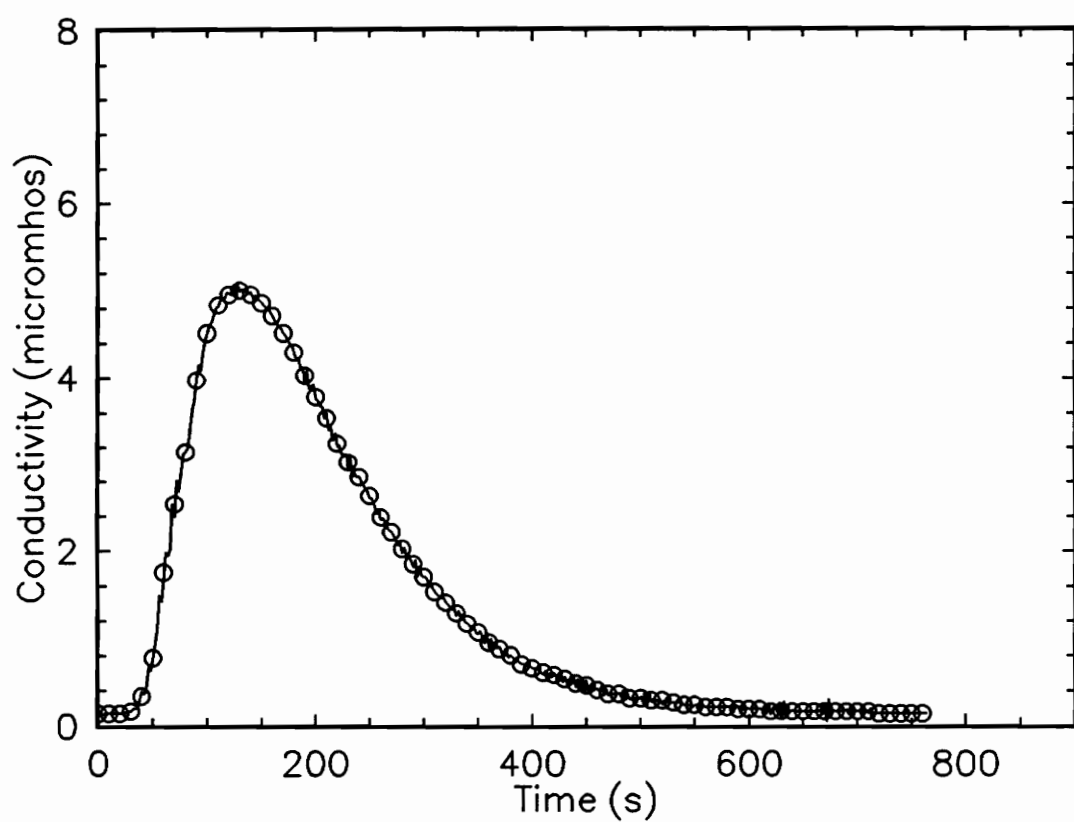


Figure 3.2 Liquid residence time distribution as constructed from time-stamped conductivity values.

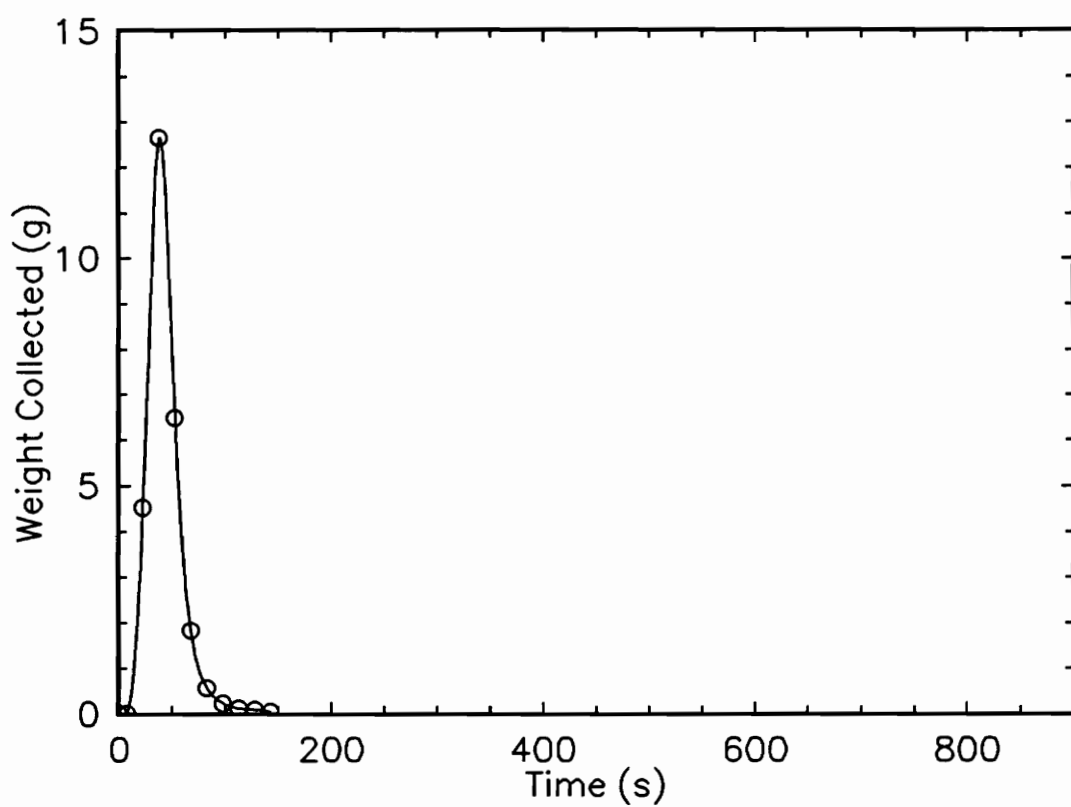


Figure 3.3 Solids residence time distribution for 48 x 65 mesh silica size fraction from tailings discharge sample collection weights.

residence time distributions (Ostergaard and Michelsen, 1969; Michelsen and Ostergaard, 1970; Rice et al., 1974; Fahim and Wakao, 1982). Their primary function is to assign less weight to the tail of the distribution, where concentration values can not be determined very accurately. In the present work, no weighting factors have been incorporated, for three reasons. First and foremost, data analysis is greatly simplified. Secondly, results from other investigators studying column flotation who employed no weighting are reasonable and consistent (Dobby and Finch, 1985; Kho and Sohn, 1989; Mankosa, 1990). Finally, there is no single weighting technique (of the many in the literature) that is widely accepted and utilized as the correct one.

3.6 Results and Discussion

The difference in residence time distributions produced by different materials is illustrated in Figures 3.4 and 3.5. Figure 3.4 shows the RTD for a coarse sample of coal (48 x 65 mesh), while Figure 3.5 depicts the RTD for a silica sample of the same size. The experimental *liquid* RTDs for the two samples are indicated by the circles, with the solid lines representing the best model fit between the data and Equation [3.6]. Little variation is apparent between coal and silica for the liquid. The liquid residence time is around 200 seconds, and the liquid Peclet number is between 6 and 7. The solids behavior is markedly different, however, as denoted by the squares and dashed line. Not only are there considerable differences between

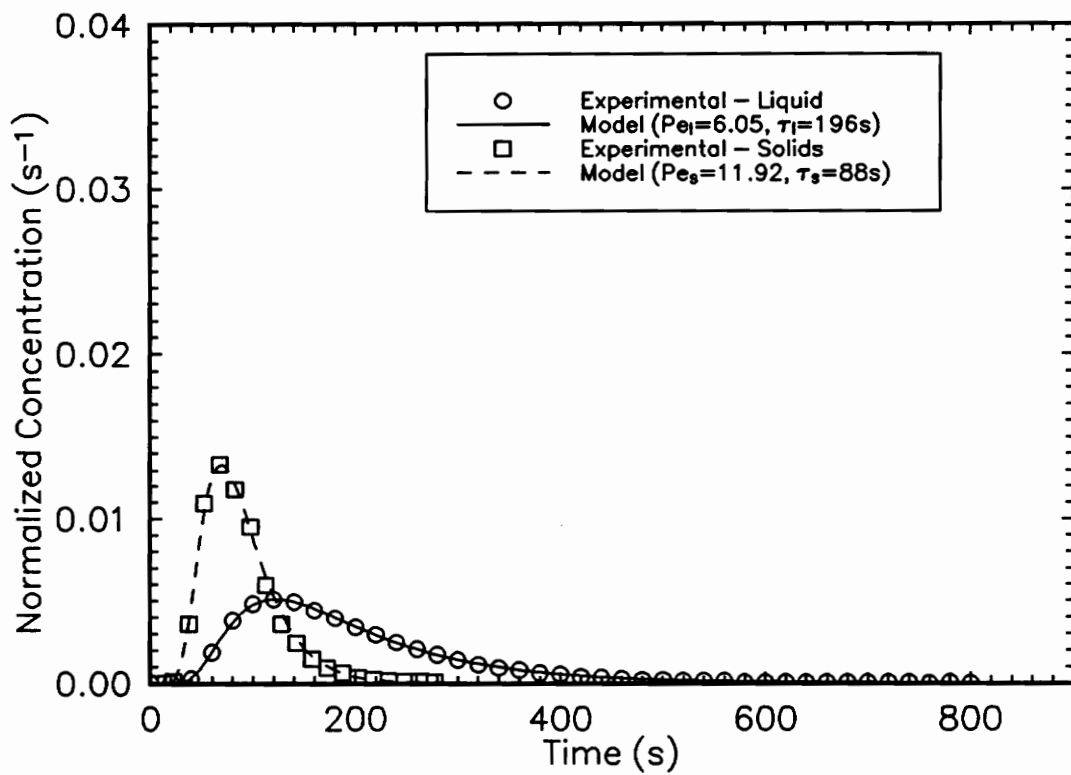


Figure 3.4 Normalized liquid and solid residence time distributions for 48 x 65 mesh coal sample.

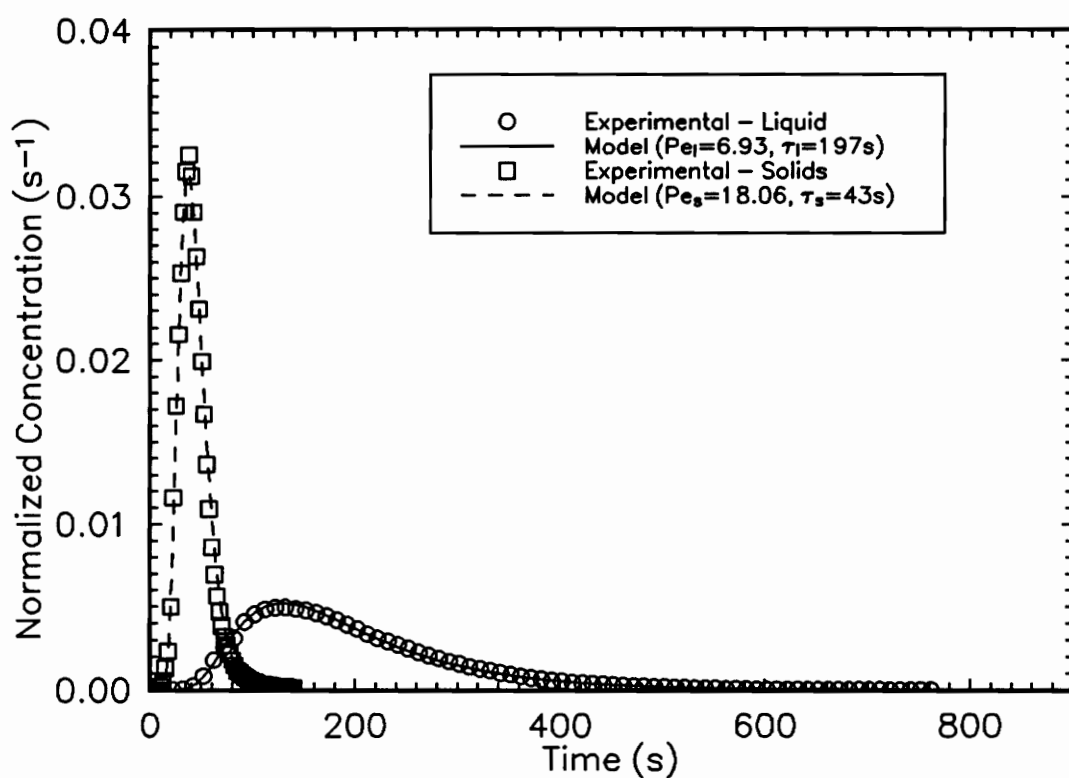


Figure 3.5 Normalized liquid and solid residence time distributions for 48 x 65 mesh silica sample.

the liquid and solids RTDs, but there is also a notable discrepancy between coal and silica. The solids residence time of the silica sample is lower than that of the coal, and the Peclet number of the silica is substantially greater, indicating a smaller degree of axial mixing.

A similar comparison between coal and silica at a smaller size (250 x 270 mesh) is shown in Figures 3.6 and 3.7. The differences between the liquid and solid RTDs for each material are minimal. It appears that the solid particles are basically following the liquid through the column, resulting in similar values for τ and Pe for the liquid and solid. The lower value of τ_s for both samples (as compared to τ_l) is due to the size and density of the solid particles, which causes them to pass through the column more quickly.

Graphical summaries of the RTD data for both materials and all sizes are presented in Figures 3.8 and 3.9. The relationship between Peclet number and particle size, d_p , is exhibited in Figure 3.8. The liquid Peclet number remains essentially constant for both the coal and silica samples. The mixing behavior of the solids, on the other hand, is much less static than that of the liquid. There is a definite correlation between Pe_s and d_p , primarily above about 150 μm . Below 150 μm , no distinct variation between Pe_s and Pe_l can be discerned. This is consistent with the experimental work cited previously for -100 mesh material, where Pe_s was shown to be the same as Pe_l .

The increase in Pe_s at larger particle sizes, denoting reduced axial mixing, is

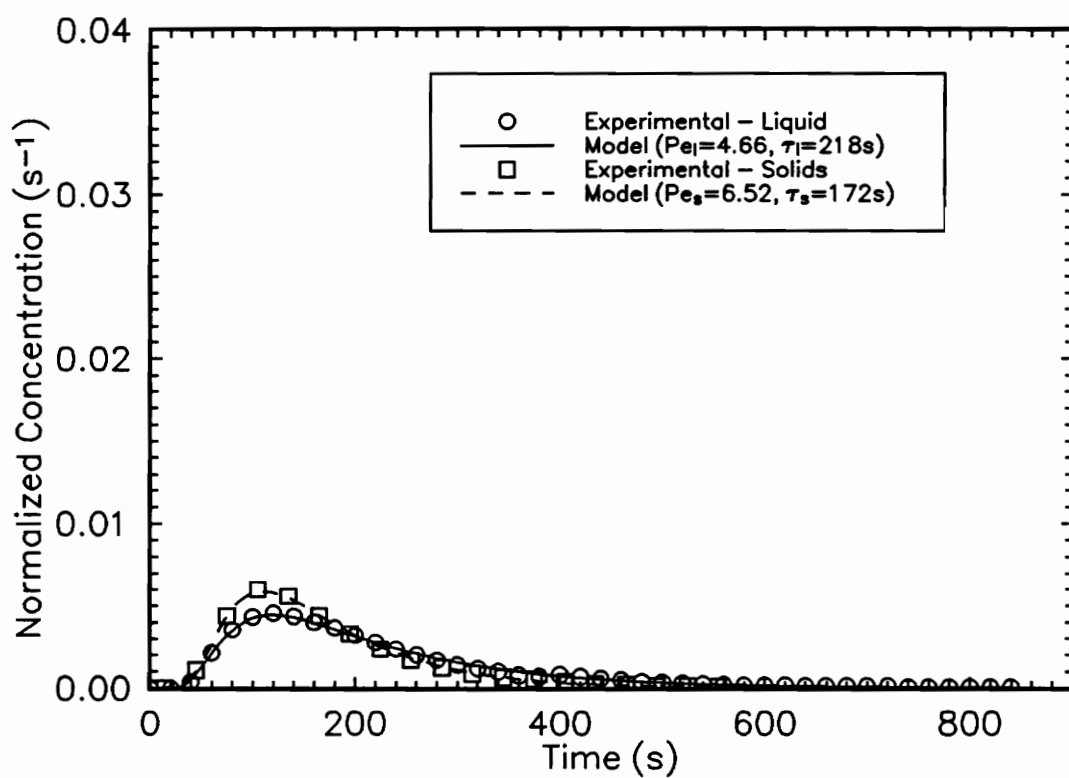


Figure 3.6 Normalized liquid and solid residence time distributions for 250 x 270 mesh coal sample.

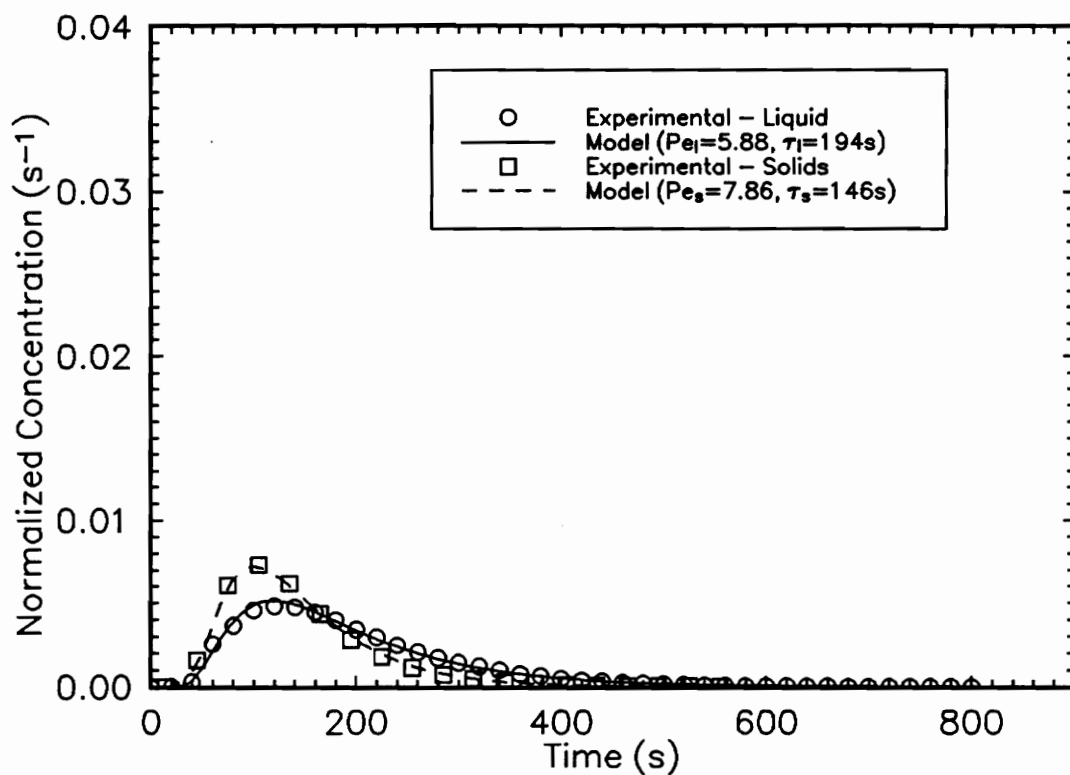


Figure 3.7 Normalized liquid and solid residence time distributions for 250 x 270 mesh silica sample.

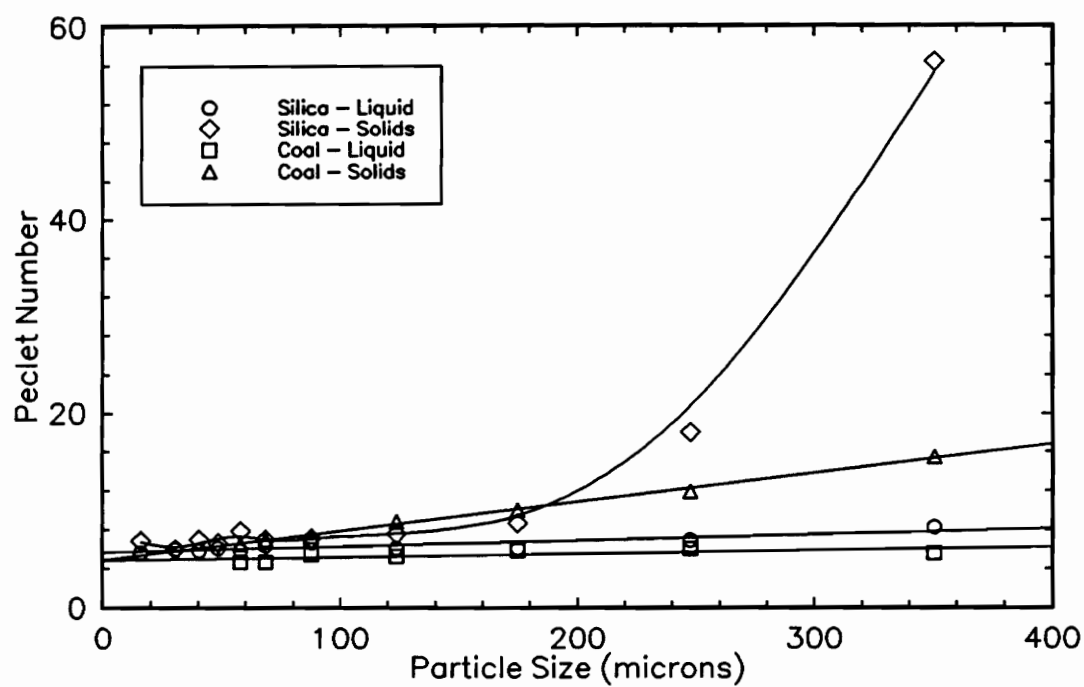


Figure 3.8 Relationship between Peclet number and particle size for coal and silica samples.

due to the increased impact of particle size and density. Large particles are less likely to exhibit characteristics similar to the liquid. The density-size effect is also adequate to rationalize the greater deviation in Pe_s exhibited by silica as compared to coal, which is half as dense. The heavier silica particles are not as likely as the coal to travel with the liquid, resulting in more plug flow conditions (higher Pe). The considerable discrepancy between Pe_s and Pe_l at large particle sizes is an important theoretical consideration, but may not have much practical utility. Since column flotation applications typically process mid to fine-size particles (leaving coarse size processing for simpler mechanical devices), assuming $Pe_s = Pe_l$ is probably valid.

Figure 3.9 depicts the relationship between residence time and particle size for the coal and silica samples. This enables evaluation of Dobby and Finch's correction formula for a wider size range and different densities. Figure 3.9 shows that liquid residence time over the entire size range is relatively constant, although τ_l for coal was usually greater than τ_l for silica. This difference is believed to be due to a slightly lower air fraction present during the coal tests, which would lead to a smaller interstitial liquid velocity and a shorter residence time. The solids residence time demonstrates a distinct dependence on d_p , with τ_s for silica showing a greater deviation from τ_l than τ_s for coal, at all sizes. This is attributed to the higher density of silica, forcing it to exit the column more quickly.

For comparison purposes, the *experimental* conditions were used to calculate the *theoretical* solids residence time from Dobby and Finch's equation (Equation

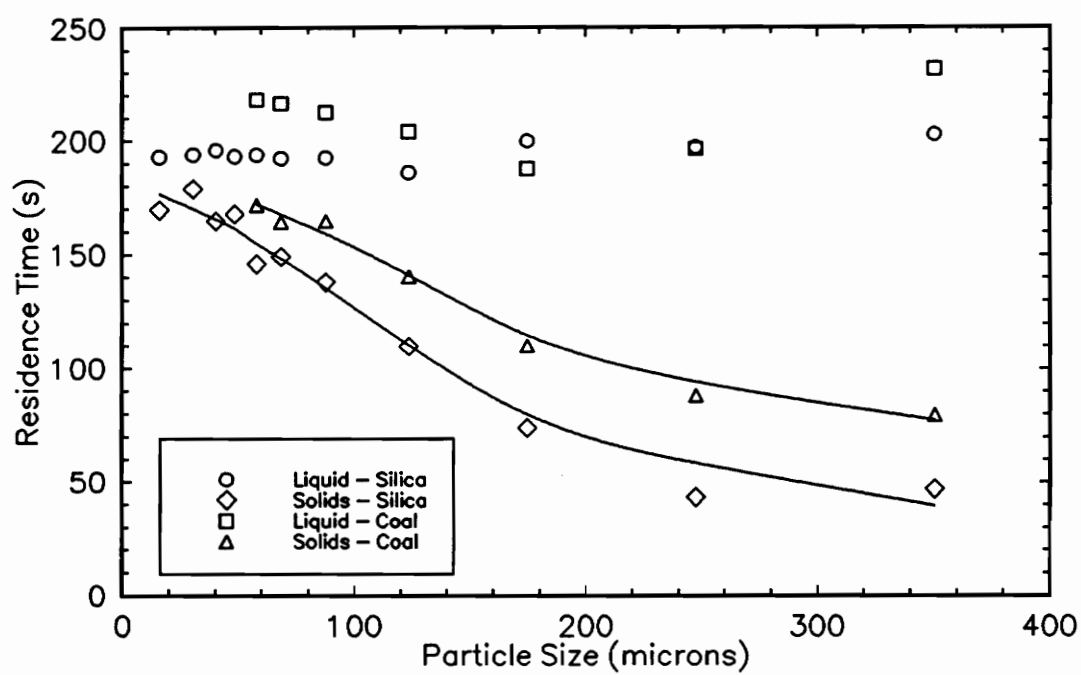


Figure 3.9 Relationship between residence time and particle size for coal and silica samples.

[3.4]). The relationship between solids residence time and particle size for the silica and coal tests is depicted in Figures 3.10 and 3.11. The particle settling velocity, u_s , was calculated from the expression derived by Concha and Almendra (1979), which corrects for hindered settling and nonsphericity of the particles. Figure 3.11 shows that there is a fairly good fit between the experimental and theoretical solids residence time for the silica samples. For the coal, however, the experimental τ_s is seen to fall below the theoretical values predicted by Dobby and Finch's equation. This discrepancy may be due to irregularities in the shape and surface morphology of the coal. The shape factor incorporated into Concha and Almendra's equation may not be accurate for coal. Additional research is required to obtain shape factors applicable to a wider variety of materials.

3.7 Flotation Performance

As mentioned in the chapter 1, the overriding aim of the present research is the formulation of a fundamental flotation model that can be used to predict flotation performance. This involves the determination of the various parameters which are known to impact recovery: the flotation rate constant, the residence time, and the Peclet number. The residence time and the Peclet number can be obtained from tracer tests, as discussed above. The flotation rate constant, k , on the other hand, must be evaluated indirectly with the bubble-particle interaction model developed in chapter 2. This is done by relating the probability of particle collection,

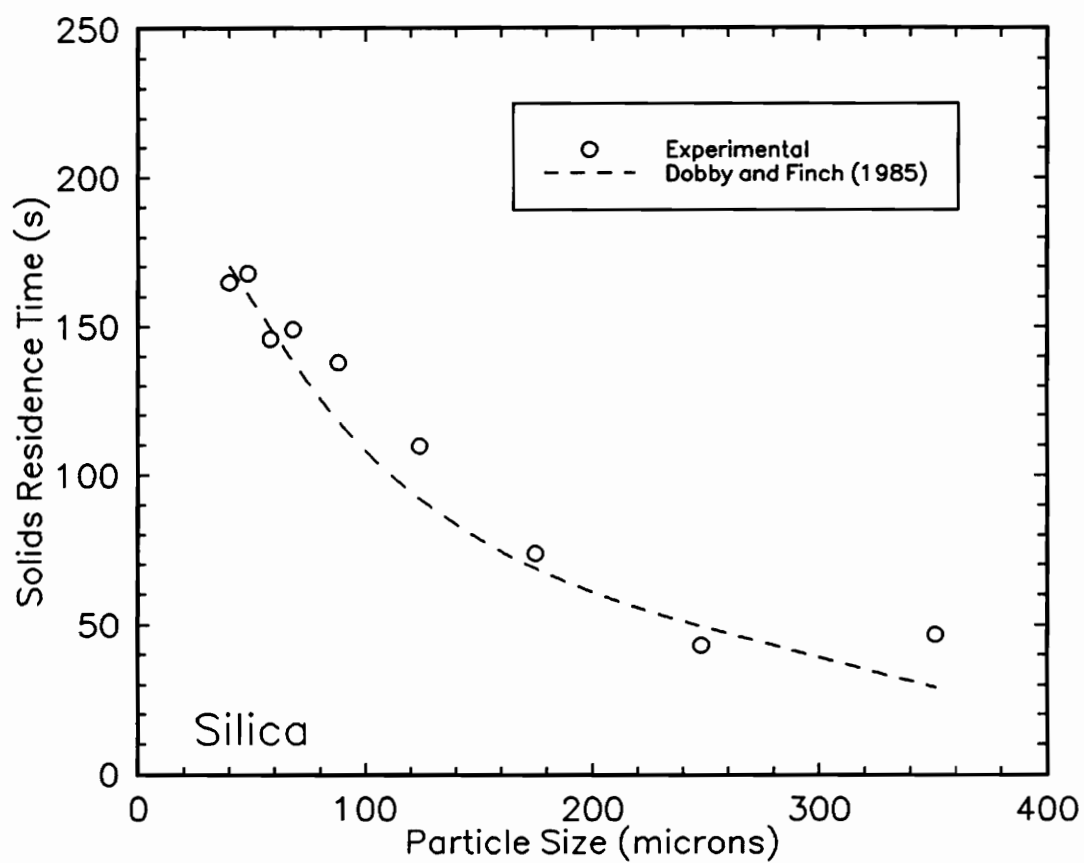


Figure 3.10 Comparison between experimental and theoretical solids residence time for silica.

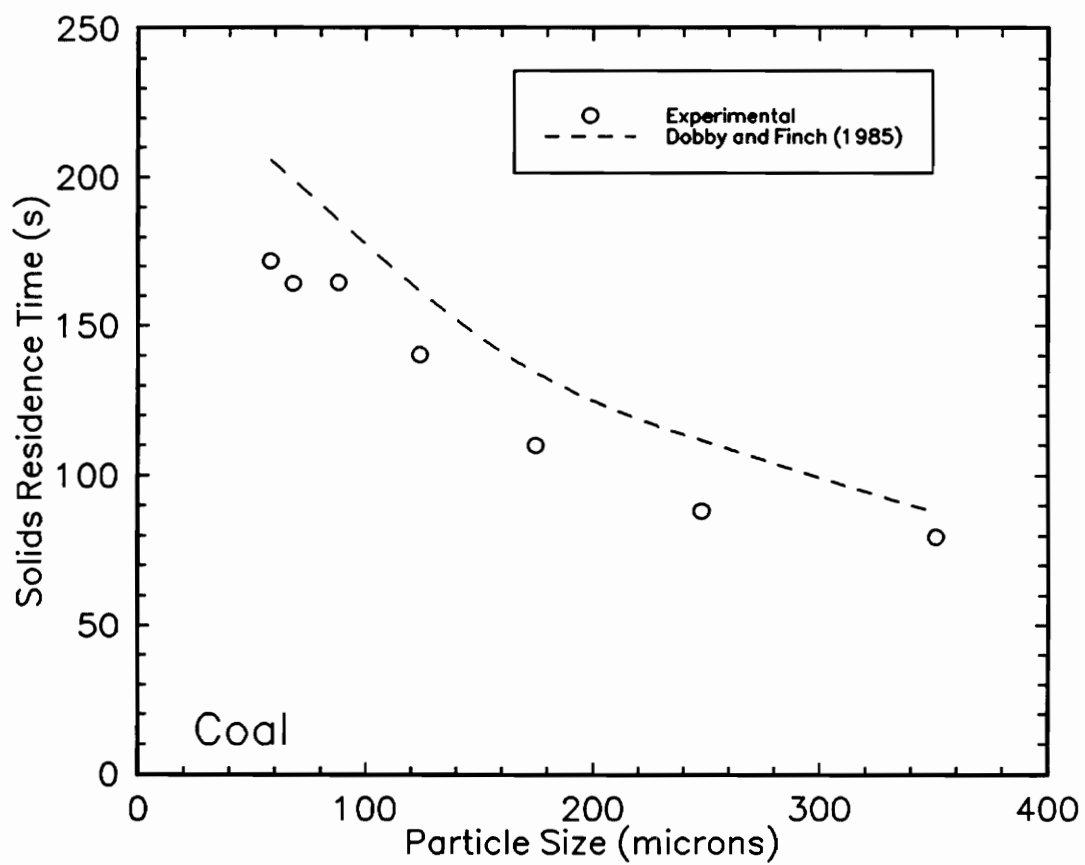


Figure 3.11 Comparison between experimental and theoretical solids residence time for coal.

P, to the flotation rate constant.

If a first-order rate process is assumed to characterize flotation, the following equation represents the removal rate of particles from the cell:

$$\frac{dN_p}{dt} = -kN_p \quad [3.8]$$

where N_p is the total number of particles in the cell, and k is the flotation rate constant. An expression for k can be obtained by analyzing the removal process of particles by rising air bubbles. The number of particles removed from the cell by a single bubble, $N_{p/b}$, is given by:

$$N_{p/b} = \frac{\pi D_b^2 L P N_p}{4 V_c} \quad [3.9]$$

where D_b is the bubble diameter, L is the cell length, P is the probability of collection, and V_c is the volume of the cell. For a given volumetric air flow rate, Q , the number of bubbles in the cell per unit time is expressed as:

$$N_b = \frac{6 Q}{\pi D_b^3} \quad [3.10]$$

Multiplying Equations [3.9] and [3.10] gives the total number of particles removed per unit time:

$$-\frac{dN_p}{dt} = \frac{3 P Q L}{2 D_b V_c} N_p \quad [3.11]$$

Furthermore, since the cell volume, V_c , can be expressed as:

$$V_c = \frac{\pi D_c^2 L}{4} \quad [3.12]$$

where D_c is the cell diameter, and since the superficial gas rate, V_g , is equal to the following:

$$V_g = \frac{4 Q}{\pi D_c^2} \quad [3.13]$$

Equation [3.11] can be rearranged to yield:

$$-\frac{dN_p}{dt} = \frac{3 P V_g}{2 D_b} N_p \quad [3.14]$$

By equating Equations [3.8] and [3.14] results in the following well-known expression for k :

$$k = \frac{3 P}{2 D_b} V_g \quad [3.15]$$

which shows that smaller bubbles and higher gas rates result in higher rate constants.

The rate constant provides an excellent indication of the floatability of a given species. In general, higher k values correspond to faster flotation kinetics and more hydrophobic materials. As stated earlier, however, flotation recovery cannot be directly equated with the rate constant. The cell mixing conditions must be considered as well. The degree of mixing (Pe) and the residence time of the solids (τ_s) in the cell also play significant roles in determining recovery.

As the Peclet number decreases, indicating more mixed conditions, flotation

recovery is hampered. This is because the increased axial mixing disrupts transport of bubble-particle aggregates into the froth, reducing the efficiency of particle collection from the cell. For perfectly plug-flow conditions, on the other hand, material moves through the cell as "plugs", less conducive to disruption, and recovery is maximized. For most operating conditions, the degree of mixing will fall between perfectly mixed and plug flow. The challenge, then, is to approach plug-flow conditions, thereby enhancing recovery without sacrificing grade considerably.

The solids residence time dictates how long a given particle is in the cell, available for flotation. Ideally, an infinite residence time would be utilized to recover all particles capable of attaching to bubbles. Practically, however, infinite residence times are not feasible. Flotation cells must be designed such that fairly high recoveries can be attained within a reasonable amount of time.

The relationship between recovery and k , Pe , and τ_s has been derived by Levenspiel (1972):

$$R = 1 - \frac{4a \exp\left(\frac{Pe}{2}\right)}{(1+a)^2 \exp\left[\left(\frac{a}{2}\right)Pe\right] - (1-a)^2 \exp\left[\left(\frac{-a}{2}\right)Pe\right]} \quad [3.16]$$

where:

$$a = \sqrt{1 + \frac{4k\tau_s}{Pe}} \quad [3.17]$$

Equation [3.16] is seen to be a function of three main variables: the flotation rate

constant, k , the solids residence time, τ_s , and the degree of axial mixing, Pe . The flotation rate constant can be determined with the model derived in chapter 2 and then applying equation [3.15]. The mixing parameters can be obtained either from experimental residence time distributions or from literature expressions relating Pe and τ_s to other operating variables (Field and Davidson, 1980; Dobby and Finch, 1985, 1986; Mankosa, 1990).

Provided the mixing parameters are known, assessing recovery becomes a matter of determining the rate constant, k . Furthermore, if the bubble size and superficial gas rate remain essentially constant, the rate constant is simply a function of the probability of particle collection, P , according to equation [3.15]. The probability of particle collection, as shown in chapter 2, can be obtained from an analysis of the fundamental forces involved in bubble-particle interaction. Therefore, since P is directly related to R , the model developed in this work represents a first principles solution to the prediction of recovery, a lofty objective deemed virtually impossible less than ten years ago (Fuerstenau, 1984). Starting from a set of initial physical and chemical parameters, a value for P can be acquired, which can then be integrated with values for Pe and τ_s to predict recovery.

Equation [3.16] can better be illustrated graphically by plotting R versus the dimensionless quantity $k\tau$ as a function of the axial mixing (Figure 3.12). Recovery is seen to increase as $k\tau$ increases and as the mixing conditions approach plug flow.

The relative importance of Pe and $k\tau$ can also be assessed with figure 3.12.

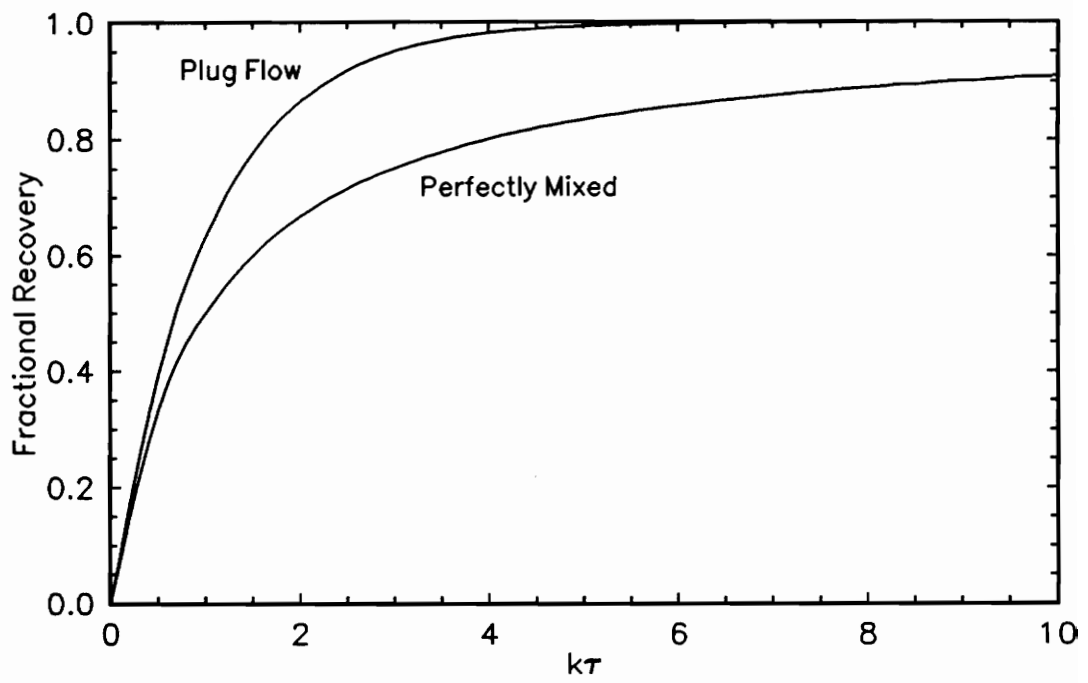


Figure 3.12 Relationship between recovery and $k\tau$ as a function of the mixing conditions.

The distance between the two curves for perfectly mixed and plug flow conditions is fairly small. This indicates that increasing the Peclet number will not provide a substantial improvement in recovery. Also, since the Peclet numbers for industrial flotation column installations span only a small range, between about 1 and 6, little real benefit is possible.

The greatest room for improvement lies in increasing the value of $k\tau$. The initial steepness of the two curves demonstrates the tremendous gains that can be obtained by raising the $k\tau$ value. By simply increasing $k\tau$ one unit, from 0.5 to 1.5, recovery can be increased about 25% under perfectly mixed conditions. Two methods are available to increase $k\tau$: the flotation rate constant can be increased according to equation [3.15] at a fixed τ , or the residence time can be lengthened for a given value of k . Which method is chosen depends on the operator's need and options. If high throughput must be maintained, increasing the residence time is unfeasible, and attention should be focused on the flotation rate constant. Conversely, if k is fixed by physical and chemical restraints, recovery can be maximized by using a longer column and increasing the retention time. The best solution is commonly a middle ground compromise: the residence time is set as high as possible to attain a given capacity, while other attempts are made to increase k , by decreasing bubble size, for example.

3.8 Conclusions

1. Tracer tests have been performed to characterize the mixing behavior of both liquid and solids in column flotation. Residence time distributions have been obtained by using two tracers simultaneously: potassium chloride for the liquid and narrowly-sized, hydrophilic particles of different densities for the solids. The residence time (τ) and Peclet number (Pe) for the solids and liquid have been shown to differ, highlighting the need to consider the mixing behavior of the solids for scale-up purposes.
2. The Peclet number of the solids (Pe_s) and liquid (Pe_l) have been found to be roughly equivalent below about $150\ \mu\text{m}$. This finding agrees with previous investigations that demonstrate the equality of Pe_s and Pe_l at finer sizes. Above $150\ \mu\text{m}$, the deviation between Pe_s and Pe_l increased, indicating that the solids exhibited more plug-flow behavior. In addition, the deviation of Pe_s from Pe_l was more pronounced for the denser particles. This suggests that particles of higher density are less prone to disruption by axial mixing, resulting in a higher Peclet number.
3. The residence time distributions have demonstrated that larger particles are less susceptible to the movements of the fluid flow, resulting in shorter residence times. The expression developed by Dobby and Finch (1985)

relating the residence time for the solid (τ_s) to that of the liquid (τ_l) has been shown to be reasonably accurate over a range of particle sizes and densities. However, experimental data collected in the present work suggests that variations in particle settling velocity, due to irregularities in shape and surface morphology, may not be adequately accounted for in their expression.

4. The results of the mixing studies have been coupled with the bubble-particle interaction model developed in Chapter 2 to formulate a procedure for the prediction of flotation performance. Using Levenspiel's (1972) axially dispersed reactor model, recovery has been related to the solids mixing parameters, Pe_s and τ_s , and to the flotation rate constant, k . A simple kinetic model has been used to relate k to the theoretical probability of particle collection, P . Since P is obtained from the first principles governing bubble-particle interaction, recovery, in turn, can be estimated from first principle considerations.

3.9 References

- Al Taweel, A.M., and Kasireddy, V.K., 1989, "Column Flotation of Aggregated Ultrafine Coal," in *Advances in Coal and Mineral Processing Using Flotation*, S. Chander and R.R. Klimpel, editors, SME, Inc., Littleton, CO., p. 356.
- Boutin, P., and Wheeler, D.A., 1967, "Column Flotation Using an 18 in. Pilot Unit," *Canadian Mining Journal*, Volume 88, Number 3, p. 94.
- "Deister Flotaire Column Flotation Cells, 1989," The Deister Concentrator Company, Inc., P.O. Box 1, 901 Glasgow Avenue, Fort Wayne, IN 46801.
- Dobby, G.S., and Finch, J.A., 1985, "Mixing Characterization of Industrial Flotation Columns," *Chemical Engineering Science*, Volume 40, Number 7, p. 1061.
- Dobby, G.S., and Finch, J.A., 1986, "Flotation Column Scale-up and Modelling," *CIM Bulletin*, Volume 79, Number 889, p. 89.
- Fahim, M.A., and Wakao, N., 1982, "Parameter Estimation from Tracer Response Measurements," *Chemical Engineering Journal*, Volume 25, p. 1.
- Field, R.W., and Davidson, J.F., 1980, "Axial Dispersion in Bubble Columns," *Transactions IChemE*, Volume 32, p. 35.
- Fuerstenau, D.W., 1984, in *The Wark Symposium*.
- Goodall, C.M., and O'Connor, C.T., 1990, "Residence Time Distribution Studies in a Flotation Column. Part 1: The Modelling of Residence Time Distributions in a Laboratory Column Flotation Cell," *International Journal of Mineral Processing*, Volume 31, p. 97.
- Ityokumbul, M.T., Kosaric, N., Bulani, W., 1988, "Parameter Estimation with Simplified Boundary Conditions," *Chemical Engineering Science*, Volume 43, Number 9, p. 2457.
- Kawatra, S.K., and Eisele, T.C., 1987, "Column Flotation of Coal," in *Fine Coal Processing*, S.K. Mishra and R.R. Klimpel, editors, Noyes Publications, Park Ridge, N.J., p. 415.

Kho, C.J., and Sohn, H.J., 1989, "Column Flotation of Talc," *International Journal of Mineral Processing*, Volume 27, p. 157.

Levenspiel, O., 1972, *Chemical Reaction Engineering*, John Wiley & Sons, Inc., New York, N.Y.

Luttrell, G.H., Weber, A.T., Adel, G.T., and Yoon, R.-H., 1988, "Microbubble Flotation of Fine Coal," in *Column Flotation '88*, K.V.S. Sastry, editor, SME, Inc., Littleton, CO, p. 205.

Mankosa, M.J., 1990, *Ph.D. Dissertation*, Virginia Polytechnic Institute and State University, Blacksburg, VA.

Mankosa, M.J., Adel, G.T., Luttrell, G.H., and Yoon, R.-H., 1990, "Modeling of Column Flotation with a View Toward Scale-up and Control," in *Control '90*, R.K. Rajamani and J.A. Herbst, editors, SME, Inc., Littleton, CO., p. 35.

Mathieu, G.I., 1972, "Comparison of Flotation Column with Conventional Flotation for Concentration of a Molybdenum Ore," *CIM Bulletin*, May, p. 41.

Mavros, P., Lazaridis, N.K., and Matis, K.A., 1989, "A Study and Modelling of Liquid-phase Mixing in a Flotation Column," *International Journal of Mineral Processing*, Volume 26, p. 1.

Michelsen, M.L., and Ostergaard, K., 1970, "The Use of Residence Time Distribution Data for Estimation of Parameters in the Axial Dispersion Model," *Chemical Engineering Science*, Volume 25, p. 583.

Ostergaard, K., and Michelsen, M.L., 1969, "On the Use of the Imperfect Tracer Pulse Method for Determination of Hold-up and Axial Mixing," *Canadian Journal of Chemical Engineering*, Volume 47, p. 107.

Reddy, B.S.R., Kumar, S.G., Bhattacharyya, K.K., Sastri, S.R.S., and Narasimhan, K.S., 1988, "Flotation Column for Fine Coal Beneficiation," *International Journal of Mineral Processing*, Volume 24, p. 161.

Rice, R.G., Oliver, A.D., Newman, J.P., and Wiles, R.J., 1974, "Reduced Dispersion Using Baffles in Column Flotation," *Powder Technology*, Volume 10, p. 201.

Rice, R.G, Tupperainen, J.M.I., and Hedge, R.M., 1981, "Dispersion and Hold-up in Bubble Columns: Comparison of Rigid and Flexible Spargers," *Canadian Journal of Chemical Engineering*, Volume 59, p. 677.

Richardson, J.F., and Zaki, W.N., 1954, "Sedimentation and Fluidization: Part I," *Transaction IChemE*, Volume 32, p. 35.

Shah, Y.T., Kelkar, B.G., Godbole, S.P., and Deckwer, W.D., 1982, "Design Parameters Estimations for Bubble Column Reactors," *AIChE Journal*, Volume 28, Number 3, p. 353.

Trigg, R.D., 1984, *M.S. Thesis*, Virginia Polytechnic Institute and State University, Blacksburg, VA.

Xu, M., Finch, J.A., and LaPlante, A.R., 1991, "Numerical Solution to Axial Dispersion Model in Flotation Column Studies," *Canadian Metallurgical Quarterly*, Volme 30, Number 2, p. 71.

Chapter 4 Conclusions

From the results of the present investigation, the following conclusions may be drawn:

1. A fundamental flotation model capable of predicting recovery from first principles has been developed, based on an analysis of bubble-particle interaction. The model combines both the hydrodynamic and surface forces which are known to impact bubble-particle interaction. Hydrodynamic forces include buoyancy, gravity, the streamline pressing force, and the film thinning resistance force. The surface forces considered were the electrostatic, dispersion, and structural forces.
2. The proposed model fundamentally differs from previous bubble-particle interaction models in that the collision and adhesion subprocesses have been addressed together rather than separately. The entire attachment process has been studied by concentrating solely on the forces responsible for bringing the bubble and particle into contact. This enables the theoretical trajectory of the particle to be constructed, which can be used to analyze the likelihood of

attachment for a given set of conditions.

3. The improved flotation results obtained with small bubbles has been confirmed in the present work. A thorough analysis of the elementary components of flotation reveals two reasons for this result. First of all, the bubble-particle interaction model demonstrated a substantial increase in the probability of particle collection as bubble size was reduced. Secondly, the rate at which particles are removed from a flotation cell also exhibited an inverse dependence on bubble size. The combined effect of these two factors provides a tremendous incentive for using small bubbles in flotation.
4. Computer simulations conducted in the present work have been used to examine the effects of various physical and chemical parameters on the bubble-particle interaction. The response of the probability of particle collection, P , to changes in the hydrodynamic and surface force variables have been shown to be consistent with experimental findings. The simulations suggest that the hydrodynamic parameters, such as particle size, bubble size, and particle density, are largely responsible for determining the rate of flotation. The surface force parameters, on the other hand, are primarily responsible for determining whether or not flotation ever occurs. Therefore, the surface force parameters are extremely important in determining flotation

selectivity. These results indicate that the separation of P into P_c and P_a may indeed be valid.

5. Bubble-particle attachment tests have been performed for coal and silica samples using a modified flotation cell. A frothless flotation cell has been utilized in order to conduct a direct investigation of the bubble-particle attachment process. A good agreement between the experimental measurements and theoretical predictions of the probability of bubble-particle attachment (P) has been obtained, lending credence to the model's validity.
6. Since maximum flotation performance is normally possible only under a limited set of conditions, identification of these optimum conditions is desired. The proposed bubble-particle interaction model can be used for this purpose. Preferred regions for flotation can be identified for various combinations of any chosen physical or chemical variables. For example, the model has shown that bubble-particle attachment, and subsequent flotation, for a weakly hydrophobic material is possible only at low values of the particle charge.
7. The effect of mixing on flotation performance has been considered as a function of two characteristic parameters: the residence time, τ , and the Peclet number, Pe . Tracer tests conducted in a flotation column investigated

the relationship between τ , Pe , and the particle size (d_p) and density (ρ_p). The residence time has been shown to possess a strong dependence on d_p and ρ_p , in accord with Dobby and Finch's equation (1985). The Peclet number is relatively independent of particle size and density below a nominal value of d_p , although above this value Pe increases considerably with d_p and ρ_p . These findings emphasize the need for adequate characterization of mixing; correct values for τ and Pe of the solids in a system are required for successful scale-up. Use of the liquid mixing parameters, a common simplification in the past, can lead to erroneous results.

8. The bubble-particle interaction model developed in the present work can be extended to predict recovery (R) of a given component during flotation. This can be accomplished by relating the probability of bubble-particle attachment (P) to the flotation rate constant (k) using a simple kinetic analysis. Once k is known, R can be calculated using Levenspiel's (1972) equation, which is also a function of the residence time (τ_s) and Peclet number (Pe_s) of the solids. These values can be determined using the techniques outlined in Chapter 3. Since P is determined based solely on the physical and chemical characteristics of the system, the model is capable of predicting flotation response from first principles considerations.

Chapter 5 Recommendations for Future Work

Although significant gains have been made in the fundamental analysis of bubble-particle interaction, considerable research is still needed. Based on the present work, the following recommendations for future investigation are suggested:

1. The importance of inertia in flotation has been recognized for some time. Several recent hydrodynamic analyses have included inertia into bubble-particle collision models by using numerical techniques (Jiang and Holtham, 1986; Dobby and Finch, 1987). These efforts, however, did not include the distance-dependent film thinning resistance force (F_r) into the proposed models, which possibly could reduce the effect of inertia. Models incorporating both inertia and the film thinning resistance force are required to fully evaluate their combined effects.
2. Detachment is almost universally neglected when studying bubble-particle interaction. To accurately represent flotation, however, the possibility of particle detachment must be taken into consideration. Some research has been made into this area (Mika and Fuerstenau, 1969; Woodburn et al.,

1971; Schulze, 1977; Jowett, 1980), but the experimental difficulties associated with analyzing detachment have prevented any significant discoveries. Additional scientific concentration is necessary to develop quantitative relationships governing detachment.

3. The present work has considered an extremely simplified flotation system, i.e., single particle-single bubble interaction in a quiescent environment. Actual flotation, of course, consists of particles encountering numerous bubbles. The presence of such a "bubble swarm" is thought to shift streamlines and decrease bubble rise velocity (Flint and Howarth, 1971; Rulev, 1979; LeClair and Hamielec, 1968). This qualitative research now needs to be converted into a quantitative representation of the influence of bubble swarms on particle collection.
4. Schulze (1989) has outlined several other factors which should be considered when examining bubble-particle interaction. These include possible collision in the turbulent wake of the bubble, collision due to turbulent particle motion, and restricted particle motion caused by densely packed bubble zones. None of these effects have been incorporated into the present model. Future work should aim to determine their impact on bubble-particle interaction.

5. Two assumptions made in developing the model were that the particles were spherical and that rotational motion was negligible. The validity of these assumptions for actual flotation systems is questionable. Anfruns and Kitchener (1977), for example, found that angular quartz particles resulted in higher probabilities of collision than spherical beads. Also, Schulze (1989) has postulated that particle rotation on the bubble surface may adversely affect collection rates. A complete phenomenological flotation model must account for these possibilities; therefore, additional research is imperative.
6. The model presented in this work has considered bubble-particle interaction only in the recovery zone, because this is where the elemental flotation subprocesses take place. However, characterization of the froth zone is just as important: achieving maximum grade and recovery requires stable, well-drained froths to support product overflow and prohibit nonselective entrainment. Unfortunately, froth research has lagged behind research into the collision and adhesion mechanisms involved in flotation. Perhaps a force-balance approach, patterned after the model developed in this work, would assist in elucidating the fundamental secrets associated with froth behavior.

References

- Anfruns, J.F., and Kitchener, J.A., 1977, "Rate of Capture of Small Particles in Flotation," *Transactions of the Institute of Mining and Metallurgy*, Volume 86, p. C9.
- Dobby, G.S., and Finch, J.A., 1987, "Particle Size Dependence in Flotation Derived from a Fundamental Model of the Capture Process," *International Journal of Mineral Processing*, Volume 21, p. 241.
- Flint, L.R., and Howarth, W.J., 1971, "The Collision Efficiency of Small Particles with Spherical Air Bubbles," *Chemical Engineering Science*, Volume 26, p. 1155.
- Jiang, Z.W., and Holtham, P.N., 1986, "Theoretical Model of Collision between Particles and Bubbles in Flotation," *Transactions of the Institute of Mining and Metallurgy*, Volume 95, p. C187.
- Jowett, A., 1980, "Formation and Disruption of Particle-Bubble Aggregates in Flotation," in *Fine Particles Processing*, Volume 1, P. Somasundaran, editor, American Institute of Mining Engineering, New York, N.Y., p. 720.
- LeClair, B.F., and Hamielec, A.E., 1968, "Viscous Flow Through Particle Assemblages at Intermediate Reynolds Numbers," *I. and E.C. Fundamentals*, Volume 7, Number 4, p. 542.
- Mika, T.S., and Fuerstenau, D.W., 1969, "A Microscopic Model of the Flotation Process," in *Proceedings*, Eighth International Mineral Processing Congress, Leningrad, Volume II, p. C9.
- Rulev, N.N., 1979, "Efficiency of Particle Capture by Bubble in Non-inertial Flotation," *Colloid Science*, Volume 40, Number 5, p. 747.
- Schulze, H.J., 1977, "New Theoretical and Experimental Investigations of Stability of Particle/Bubble Aggregates in Flotation: A Theory on the Upper Particle Size of Floatability," *International Journal of Mineral Processing*, Volume 4, p. 241.
- Schulze, H.J., 1989, "Hydrodynamics of Bubble-Mineral Particle Collision," in *Frothing in Flotation*, J. Laskowski, editor, Gordon and Breach Science Publishers, New York, N.Y., p. 43.
- Woodburn, E.T., King, R.P., Colburn, R.P., "The Effect of Particle Size Distribution and the Performance of a Phosphate Flotation Process," *Metallurgical Transactions*, Volume 2, p. 3163.

APPENDIX I

Bubble-Particle Interaction Program

```

2 LOCATE 15,5
PRINT "BUBBLE PARTICLE COLLECTION MODEL"
FOR I = 1 TO 10000: NEXT I
REM *****
REM *          BUBBLE-PARTICLE COLLECTION MODEL          *
REM *          Brian K. Schimmoller                      *
REM *          Masters of Science                        *
REM *          Department of Mining and Minerals          *
REM *          Virginia Tech                             *
REM *****
REM
WIDTH 80
SCREEN 0,0
CLS
REM *****
REM *          DEFINE VARIABLES USED                      *
REM *          *
REM *          R: distance between center of particle and bubble *
REM *          ROLD: old value of R in iterative process *
REM *          RB: radius of bubble *
REM *          RP: radius of particle *
REM *          H: film thickness, distance between *
REM *          surfaces of bubble and particle *
REM *          HMIN: minimum film thickness *
REM *          A: initial radial distance from equator to particle *
REM *          TH: angle formed between equatorial *
REM *          line and radial line *
REM *          PROB: probability of collision *
REM *          Z: valency of counterions *
REM *          EC: concentration of indifferent electrolyte *
REM *          EPS: dielectric constant of the medium *
REM *          PSIP: zeta potential of the particle *
REM *          PSIB: zeta potential of the bubble *
REM *          AM: complex Hamaker constant *
REM *          SC: structural constant *
REM *          DL: decay length *
REM *          MU: viscosity of the medium *
REM *          T: time *
REM *          DT: time step *
REM *          K: double layer thickness *
REM *          P,Q: constants related to electrostatic *
REM *          interaction term *
REM *          UB: bubble rise velocity *
REM *          I,COUNTER,CTR,Y: counters *
REM *          START: initial distance between surfaces *
REM *          X,SF: dimensionless variables used *
REM *          to characterize streamlines *
REM *          UT: tangential velocity of streamline *
REM *          UTP: tangential velocity of particle *
REM *          UR: radial velocity of streamline *
REM *          URP: radial velocity of particle *
REM *          URPOLD: old value of URP used in iterative process *
REM *          B: Stokes correction factor for *
REM *          film thinning resistance force *
REM *          URPA: electrostatic component of *
REM *          radial particle velocity *
REM *          FURPA: electrostatic component of *
REM *          total force on particle *
REM *          URPB: dispersion component of *
REM *          radial particle velocity *
REM *          FURPB: dispersion component of *
REM *          total force on particle *
REM *          URPC: structural component of *
REM *          radial particle velocity *

```

```

REM *   FURPC: structural component of          *
REM *   total force on particle                 *
REM *   URPD: streamline pressing component of  *
REM *   radial particle velocity               *
REM *   FURPD: streamline pressing component of *
REM *   total force on particle                 *
REM *   URPE: gravity component of radial particle velocity *
REM *   FURPE: gravity component of total force on particle *
REM *   FURP: total force on particle           *
REM *                                           *
REM *****
REM -----
REM      DEFINE CONSTANT VARIABLES AS DOUBLE PRECISION
REM -----
REM      DEFDBL A,B,D-H,J-X,Z
REM -----
REM      DEFINE PI AND NATURAL LOG
REM -----
REM      PI = 3.1415927
REM      ENLN = 2.7182818
REM -----
REM      INPUT RANGES FOR PARTICLE SIZE,
REM      BUBBLE SIZE, AND PROBABILITY
REM -----
LOCATE 4,3
PRINT "INPUT PARTICLE SIZE RANGE:"
LOCATE 6,5
INPUT "LOWER RADIUS LIMIT, IN MICRONS";RPLO
RPLO = RPLO*10^3
LOCATE 8,5
INPUT "UPPER RADIUS LIMIT, IN MICRONS";RPUP
RPUP = RPUP*10^3
LOCATE 10,5
INPUT "PARTICLE RADIUS STEP, IN MICRONS";RPST
RPST = RPST*10^3
FOR I = 1 TO 2500:NEXT I
CLS
LOCATE 4,3
PRINT "INPUT BUBBLE SIZE RANGE:"
LOCATE 6,5
INPUT "LOWER RADIUS LIMIT";RBLO
RBLO = RBLO*10^3
LOCATE 8,5
INPUT "UPPER RADIUS LIMIT";RBUP
RBUP = RBUP*10^3
LOCATE 10,5
INPUT "BUBBLE RADIUS STEP";RBST
RBST = RBST*10^3
FOR I = 1 TO 2500:NEXT I
CLS
LOCATE 4,3
PRINT "INPUT PROBABILITY RANGE:"
LOCATE 6,5
INPUT "LOWER PROBABILITY LIMIT";PROBLO
LOCATE 8,5
INPUT "UPPER PROBABILITY LIMIT";PROBUP
LOCATE 10,5
INPUT "PROBABILITY STEP";PROBST
FOR I = 1 TO 2500:NEXT I
REM
REM *****
REM *   DEFINE PARAMETERS FOR COMPONENTS OF TOTAL FORCE *
REM *****
REM

```

```

REM -----
REM          1. ELECTROSTATIC FORCE
REM
REM      INPUT VALUES TO DETERMINE CONSTANTS
REM      K,P,Q MUST BE CALCULATED
REM      PSI: SURFACE POTENTIAL, APPROXIMATED BY
REM      ZETA POTENTIAL
REM      EPS: DIELECTRIC CONSTANT
REM      Z: VALENCY OF COUNTERIONS
REM      EC: CONCENTRATION OF THE INDIFFERENT ELECTROLYTE
REM -----
REM
CLS
LOCATE 2,5
PRINT "DEFINITION OF PARAMETERS RELATED TO THE ELECTROSTATIC FORCE"
LOCATE 5,8
INPUT "INPUT THE VALENCY OF THE COUNTERIONS";Z
LOCATE 8,8
PRINT "INPUT THE CONCENTRATION OF THE INDIFFERENT "
LOCATE 9,8
INPUT "ELECTROLYTE IN TERMS OF MOLES PER LITER";EC
LOCATE 12,8
INPUT "INPUT THE DIELECTRIC CONSTANT OF THE MEDIUM";EPS
LOCATE 15,8
INPUT "INPUT THE ZETA POTENTIAL OF THE PARTICLE, AT THE DESIRED pH (mV)";PSIP
PSIP = PSIP * 10^-3
LOCATE 18,8
INPUT "INPUT THE ZETA POTENTIAL OF THE BUBBLE, AT THE
      DESIRED pH (mV)";PSIB
PSIB = PSIB * 10^-3
REM
REM -----
REM          2. DISPERSION FORCE
REM
REM      INPUT VALUE FOR THE COMPLEX HAMAKER CONSTANT
REM      AM: COMPLEX HAMAKER CONSTANT
REM -----
REM
FOR I = 1 TO 2000:NEXT I
CLS
LOCATE 10,5
PRINT "DEFINITION OF PARAMETERS RELATED TO THE DISPERSION FORCE"
LOCATE 14,8
INPUT "INPUT THE COMPLEX HAMAKER CONSTANT, AM (x10^-21)";AM
AM = AM * 10^-12
REM
REM -----
REM          3. STRUCTURAL FORCE
REM
REM      INPUT VALUES FOR SC,DL
REM      SC: STRUCTURAL CONSTANT
REM      DL: DECAY LENGTH
REM -----
REM
FOR I = 1 TO 2000:NEXT I
CLS
LOCATE 8,5
PRINT "DEFINITION OF PARAMETERS RELATED TO THE STRUCTURAL FORCE"
LOCATE 12,8
INPUT "INPUT THE STRUCTURAL CONSTANT (x10^-3)";SC
SC = SC * 10^-12
LOCATE 14,8
INPUT "INPUT THE DECAY LENGTH IN NANOMETERS";DL
REM
REM -----

```

```

REM          4. PRESSING FORCE
REM
REM          INPUT VALUE FOR ABSOLUTE VISCOSITY
REM          MU: ABSOLUTE VISCOSITY
REM -----
REM
FOR I = 1 TO 2000:NEXT I
CLS
LOCATE 8,5
PRINT "DEFINITION OF PARAMETERS RELATED TO THE DRAG AND PUSH FORCES"
LOCATE 10,8
INPUT "INPUT VALUE OF THE ABSOLUTE VISCOSITY (x10^-4)";MU
MU = MU * 10^-22
REM
REM -----
REM          5. FILM RESISTING FORCE
REM
REM          STOKES CORRECTION FACTOR, B
REM          VALUE BASED ON GOREN AND O'NEILL'S DATA
REM          CURVE BROKEN INTO TWO SECTIONS
REM          BELOW H/RP OF 0.3, B=0.377*(H/RP)^-0.811
REM          ABOVE H/RP OF 0.3, B=1
REM -----
REM
REM -----
REM          INPUT TIME STEP
REM -----
CLS
LOCATE 12,8
INPUT "INPUT TIME STEP";DT
II = 0
REM
REM *****
REM *          INITIALIZE LOOPS          *
REM *****
REM
REM -----
REM          1. OUTER PARTICLE RADIUS LOOP
REM -----
FOR RP = RPLO TO RPUP STEP RPST
  II = II+1
  IF II = 1 THEN A$ = "C:C1.DAT"
  IF II = 2 THEN A$ = "C:C2.DAT"
  IF II = 3 THEN A$ = "C:C3.DAT"
  IF II = 4 THEN 500
  OPEN A$ FOR OUTPUT AS #1
REM -----
REM          2. INNER BUBBLE RADIUS LOOP
REM -----
  WRITE #1, RP/500, RB/500
  WRITE #1, PSIP*10^3, PSIB*10^3
  WRITE #1, AM*10^-9, SC*10^9
  FOR RB = RBLO TO RBUP STEP RBST
    REM -----
    REM          CALCULATE K,P,Q
    REM -----
    K = 2*(EC^.5)/3.0*10.0
    P = EPS*4*PI*(8.85*10^-12)*RP*RB*
      (PSIP^2+PSIB^2)/(4*(RP+RB))
    Q = 2*PSIP*PSIB/((PSIP)^2+(PSIB)^2)
    REM -----
    REM          CALCULATE BUBBLE TERMINAL RISE VELOCITY
    REM -----
    UB = 148*10^7*(RB*2*10^-7)^1.14
    RE = 2*RB*10^-7*UB*10^-7*1/.01
  
```

```

CTR = 0
REM -----
REM      3. INNER PROBABILITY LOOP
REM -----
FOR PROB = PROBL0 TO PROBU0 STEP PROBST
PRINT "PD = ";RP/500;"BD = ";RB/500;"PROB = ";10^PROB
PRINT "SC = ";SC*10^9;"ZPP = ";PSIP*10^3
Y = 1
B = 1.0
T = 0.0
REM -----
REM      CALCULATE INITIAL DISTANCE FROM CENTERLINE,
REM      INITIAL ANGLE, INITIAL DISTANCE BETWEEN
REM      CENTERS, AND INITIAL DISTANCE BETWEEN
REM      SURFACES.
REM -----
RPROB = 10^PROB
A = RB*((10^PROB)^0.5)
START = 20*RB
TH = ATN(A/START)
R = A/SIN(TH)
HMIN = R-RP-RB
REM -----
REM      INITIALIZE TIME SEQUENCE
REM -----
10 T = T+DT
ROLD = R
COUNTER = 0
REM *****
REM *      DEFINE EQUATIONS FOR TANGENTIAL      *
REM *      AND RADIAL VELOCITIES                  *
REM *****
REM -----
REM      CALCULATE TANGENTIAL VELOCITY
REM      AND NEW THETA ANGLE
REM -----
URPEI = 2*RP^2*.3*10^-24*9.81/(9*MU)
X = R/RB
SFR = 1-1.5/X+.5/X^3+(2*RE^.72/15)*
      (1/X^4-1/X^3+1/X-1/X^2)
UR = UB*COS(TH)*SFR
SF = 1-.75/X-.25/X^3+(RE^.72/15)*
      (1/X^3-2/X^4+1/X)
UT = UB*SIN(TH)*SF
IF Y = 1 THEN 11 ELSE 12
11 UTP = UB*SIN(TH)*SF+URPEI*SIN(TH)
   URP = UB*COS(TH)*SFR+URPEI*COS(TH)
   GOTO 13
12 UTP = UB*SIN(TH)*SF+URPEI*SIN(TH)
13 TH = TH+UTP*DT/R
REM -----
REM      CALCULATE RADIAL VELOCITY
REM -----
REM -----
REM      FOR FIRST PASS, PARTICLE RADIAL VELOCITY =
REM      RADIAL VELOCITY OF STREAMLINE
REM -----
REM -----
REM      CALCULATE NEW R AND H VALUES
REM -----
20 IF URP < 0 THEN 450
   R = ROLD-URP*DT

```

```

H = R-RP-RB
IF H < 1E-5 THEN 450
REM -----
REM      CALCULATE STOKES CORRECTION FACTOR
REM -----
B = 0.377*(RP/H)^0.811
IF B < 1.0 THEN B = 1.0
REM -----
REM      SET URPOLD = URP FOR ITERATIVE PROCESS
REM -----
URPOLD = URP
REM -----
REM      NEGLECT ELECTROSTATIC AND STRUCTURAL FORCES
REM      FOR LARGE H VALUES SINCE THEIR MAGNITUDES
REM      ARE VERY SMALL.
REM -----
REM *****
REM *      CALCULATE COMPONENTS OF PARTICLE RADIAL      *
REM *      VELOCITY AND COMPONENTS OF TOTAL FORCE      *
REM *      ON PARTICLE                                  *
REM *****
REM -----
REM      1. ELECTROSTATIC COMPONENT
REM -----
IF H < 1.0*10^3 THEN 40
URPA = 0: GOTO 41
40 URPA = 10^18*(P*K*(ENLN^(-2*K*H)-Q*ENLN^(-K*H)))/
(3*PI*MU*10^18*RP*B*(1-ENLN^(-2*K*H)))
41 FURPA = URPA*6*PI*RP*B
REM -----
REM      2. DISPERSION COMPONENT
REM -----
KITCHP = 2*PI*H/100
IF KITCHP <= 0.57 THEN 42 ELSE 43
42 KITCHF = 1/(1+1.77*KITCHP)
GOTO 44
43 KITCHF = 2.45/(5*KITCHP)-2.17/(15*KITCHP^2)
+0.59/(35*KITCHP^3)
44 URPB = AM*KITCHF*RB*10^18/
(36*PI*MU*10^18*B*H*(RP+RB))
FURPB = URPB*6*PI*MU*RP*B
REM -----
REM      3. STRUCTURAL COMPONENT
REM -----
ZT = -H/DL
IF H < 1.0*10^3 THEN 50
URPC = 0: ZV = 0: GOTO 55
50 F = 2.7182818^(ZT)
ZV = -SC*F*RB
ZW = 6.0*PI*MU*10^18*B*(RP+RB)
URPC = ZV*10^18/ZW
55 FURPC = URPC*6*PI*MU*RP*B
REM -----
REM      4. PRESSING COMPONENT
REM -----
REM -----
60 REM IF Y = 1 THEN 61
ARG = (1-1.5/X+.5/X^3+(2*RE^.72/15)*
(1/X^4-1/X^3+1/X-1/X^2))
URPD = UB*COS(TH)*ARG/B
FURPD = URPD*6*PI*MU*RP*B
REM -----

```

```

      REM      5. GRAVITY COMPONENT
      REM -----
61  FURPE = 4/3*PI*(RP^3)*.3*10^-24*9.81*COS(TH)
      URPE = FURPE/(6*PI*MU*RP*B)
      REM -----
      REM      SUM UP ALL CONTRIBUTIONS TO OVERALL RADIAL
      REM      PARTICLE VELOCITY AND CALCULATE TOTAL FORCE
      REM      ACTING ON THE PARTICLE
      REM -----
      URP = URPA+URPB+URPC+URPD+URPE
62  FURP = URP*6*PI*MU*RP*B
      REM
      Y = Y+1
      REM -----
      REM      TEST FOR DYNAMIC EQUILIBRIUM
      REM      INITIALIZE COUNTER
      REM -----
      COUNTER = COUNTER+1
      IF COUNTER = 25 THEN 150
      REM -----
      REM      CRITERIA FOR CONVERGENCE
      REM -----
      IF ABS((URPOLD-URP)/URPOLD) > 0.000001 THEN 20
      REM -----
      REM      DETERMINE MINIMUM APPROACH DISTANCE
      REM -----
150 IF H < HMIN THEN HMIN = H
      REM -----
      REM      PRINT OUT DATA EVERY n ITERATIONS
      REM -----
      CTR = CTR+1
      IF CTR/10000 = INT(CTR/10000) THEN 200 ELSE 300
200 PRINT "H = ";H;"THETA = ";TH*180/PI
      PRINT "B = ";B;"R = ";R
      PRINT "URPA = ";URPA;"URPB = ";URPB
      PRINT "URPC = ";URPC;"URPD = ";URPD
      PRINT "URPE = ";URPE;"URP = ";URP
      PRINT "FE = ";FURPA;"FD = ";FURPB;"FS = ";FURPC
      PRINT "FP = ";FURPD;"FG = ";FURPE
      PRINT "FR = ";FURP
250 GOTO 300
270 WRITE #1,H,URP,FURP
      WRITE #1,H,TH*180/PI,B,R
      WRITE #1,URPA,URPB
      WRITE #1,URPC,URPD
      WRITE #1,URPE,URP
      WRITE #1,FURPA,FURPB
      WRITE #1,FURPC,FURPC
      WRITE #1,FURPE,FURP
      REM -----
      REM      DETERMINE IF PARTICLE HAS GONE BY BUBBLE
      REM -----
300 IF TH < PI/2 THEN 10
      REM -----
      REM      WRITE DATA TO A FILE
      REM      INITIAL DISTANCE FROM CENTERLINE
      REM      AND MINIMUM SEPARATION
      REM -----
450 WRITE #1, RPROB,HMIN,T,TH*180/PI
      NEXT PROB
      CLOSE #1
      NEXT RB
      NEXT RP
500 PRINT "END"
      END

```

VITA

Brian Keith Schimmoller was born on May 15, 1968, in Boise, Idaho. He moved several times growing up, eventually graduating from high school in Concord, New Hampshire in 1986. He continued his education at Virginia Tech that fall, and graduated in 1990 Summa Cum Laude with a B.S. degree in mining and minerals engineering. As an undergraduate, he was active in several honor societies, the Burkhardt Mining Society, and the Student Engineer's Council. During his senior year, he won several awards, including the national Mineral Processing Division Award from the Society of Mining Engineers of AIME, of which he is a student member.

He began his graduate work at Virginia Tech in the Department of Mining and Minerals Engineering in the summer of 1990. He has remained involved in the Burkhardt Mining Society, and has served on the Graduate Student Engineering Committee. His masters thesis research has been presented at a national meeting, and several publications are in press. The author is currently employed by Cargill, Inc. in Tampa, Florida as a mineral processing engineer at a phosphate operation.

Brian K. Schimmoller